

Faculty of Graduate Studies

**Removal of Ibuprofen from aqueous solution by using
ZnO-SiO₂ (CTAB) and Fe₃O₄-SiO₂ (CTAB)
nanoparticles: A kinetic and thermodynamic study**

إزالة الايبوبروفين من المحاليل المائية باستخدام جسيمات ZnO-SiO₂
(CTAB), Fe₃O₄-SiO₂ (CTAB) النانوية : دراسة حركية
وثيرموديناميكية

This Thesis was submitted in partial fulfillment of the
requirements for the
Master's Degree in Applied Chemistry
From the Faculty of Graduate Studies at Birzeit University,
Palestine.

Laila Khalil

1175370

Supervisors:

Dr. Mohammed Al-jabarei & Dr. Saleh Sulaiman

2021

Removal of Ibuprofen from aqueous solution by using (ZnO-SiO₂ (CTAB), Fe₃O₄-SiO₂ (CTAB)) nanoparticles: A kinetic and thermodynamic study

By

Laila Khalil

This thesis was defended successfully on 11 /1/2021 and approved by:

Committee Members

Signature

Dr. Mohammed Al-jabarei

Supervisor

Chemistry Department-Faculty Member

Birzeit University



Dr. Saleh Sulaiman

Supervisor

Chemistry Department-Faculty Member

Birzeit University



Prof. Talal Shahwan

Committee Member

Chemistry Department-Faculty Member

Birzeit University




Dr. Imtiaz Khalid

Committee Member

Chemistry Department-Faculty Member

Birzeit University



الإهداء

إلى مَنْ حصد الأشواك عن دربي ليمهد لي طريق العلم، إلى مَنْ تمنّيته أن يكون

بجانبي لتوثيق نجاحي هذا، إلى روح أبي الطاهرة.

إلى القلب الكبير، إلى مَنْ كانت بوصلتي، وكانت دعواتها ترافقني طيلة مسيرتي

الدراسيّة وسرّ نجاحي، إلى أمّي الغالية.

Acknowledgement

Foremost, I am very grateful to God for being with me in all my steps and giving me the strength and ability to complete this thesis. I would like to sincerely thank my supervisor's Dr. Mohammed Al-jabarei and Dr. Saleh Sulaiman, who provided me with valuable advice and always supported me with their knowledge and experiences. Thanks for continues effort and motivation to complete this work.

I would also like to thank the members of the thesis committee Prof. Talal Shahwan and Dr. Imtiaz Khalid for their efforts in reading and assessing.

I would like to thank the chemistry department members at Birzeit University, and lab technicians: Mr. Asem Mubarak, Mr. Azmi Dudin and Dr. Ibrahim Shalash for facilitating my work in the labs. Many thanks to Mrs. Ghadeer Tayem, Mrs. Lina Jundi and Mrs. Eman Mohammed for their kind help through my years study.

In addition, I would like to thank the Middle East Desalination Research Center (MEDRC) and Palestinian Water Authority for their financial support.

Many thanks to Prof. Atef Qasrawi (at Arab American University) who helped in SEM characterization.

A deep thanks to my brothers (Tawfiq, Rafiq, and Ahmad) and my sister (Suha) for their unlimited help and support.

Special thanks to my dear friends Sabreen, Fatima, Mayes, Nihal, Shuoroq, and Ola for their care and encouragement.

Finally, a special thanks for my friends, colleagues, teachers, and chemistry department members at An-Najah National University.

Table of contents

Acknowledgement	IV
Table of contents	VI
List of Figures	IX
List of Tables.....	XII
Abbreviations.....	XIV
Abstract	XV
المخلص بالعربية	XVIII
1. Introduction.....	1
<i>1.1 Water pollution and pharmaceuticals.....</i>	<i>1</i>
<i>1.2. Methods of pharmaceutical removal</i>	<i>5</i>
<i>1.3 Nanoparticles</i>	<i>13</i>
1.3.1 Iron oxide nanoparticles.....	13
1.3.2. Zinc oxide nanoparticles.....	16
<i>1.4. Adsorption isotherms.....</i>	<i>18</i>
1.4.1. Langmuir isotherm	19

1.4.2. Freundlich isotherm.....	21
1.5. <i>Research objectives</i>	22
2. Experimental	23
2.1. <i>Chemicals and reagents</i>	23
2.2. <i>Synthesis of iron oxide (magnetite; Fe₃O₄) and zinc oxide (ZnO) nanoparticles</i>	24
2.2.1. Synthesis of iron oxide magnetite (Fe ₃ O ₄) nanoparticles ...	24
2.2.2. Synthesis of zinc oxide nanoparticles.....	25
2.2.3. Synthesis of Fe ₃ O ₄ -SiO ₂ (CTAB) nanocomposite.....	26
2.2.4. Synthesis of ZnO-SiO ₂ (CTAB) nanocomposite.....	26
2.3. <i>Standard solutions and calibration curve</i>	27
2.4. <i>IBU removal experiments</i>	28
2.4.1. Effect of initial IBU concentration.....	28
2.4.2. IBU removal kinetics	29
2.4.3. Effect of pH and PZC.....	29
2.4.4. Effect of temperature.....	30
2.5. <i>Characterization</i>	31
3. Results and discussion	33

<i>3.1 Characterization of ZnO and ZnO-SiO₂ (CTAB) NP's</i>	33
<i>3.2 Characterization of Fe₃O₄ and Fe₃O₄-SiO₂ (CTAB) NP's</i>	41
<i>3.3. IBU removal kinetics</i>	51
<i>3.4. Effect of initial IBU concentration</i>	70
<i>3.5 Adsorption isotherms</i>	73
<i>3.6 Effect of pH and PZC on the removal of IBU</i>	88
<i>3.7 Effect of temperature</i>	95
<i>3.8 Adsorption thermodynamics</i>	102
4. Conclusions	106
5. References	108
Appendix	131

List of Figures

Figure 1.1: Structure of Ibuprofen	11
Figure 1.2 : Molecular structures of (S) and (R) of IBU	12
Figure 1.3: Chemical structure of cetyltrimethylammonium bromide (CTAB). ...	15
Figure 1.4: Structure of CTAB coated Fe ₃ O ₄ nanoparticles.	16
Figure 3.1: SEM images (a) of ZnO-SiO ₂ (CTAB) NP's (first batch), and (b) of ZnO-SiO ₂ (CTAB) NP's (second batch).	35
Figure 3.2: TEM images (a) of ZnO NP's and b) of ZnO-SiO ₂ (CTAB) NP's.	36
Figure 3.3: EDS analysis of ZnO-SiO ₂ (CTAB) NP's.....	37
Figure 3.4: FT-IR spectra for a) IBU b) ZnO-SiO ₂ (CTAB) c) ZnO-SiO ₂ (CTAB) and IBU scanning range 400-4000.	40
Figure 3.5: XRD patterns of a) F ₃ O ₄ b) Fe ₃ O ₄ -SiO ₂ (CTAB) NP's. ⁹⁹	42
Figure 3.6: SEM images of (a) and (b) are Fe ₃ O ₄ NP's, (c) and (d) are Fe ₃ O ₄ -SiO ₂ (CTAB) NP's.	44
Figure 3.7: (a) TEM image of Fe ₃ O ₄ -SiO ₂ (CTAB) NP's, and (b) SAED of Fe ₃ O ₄ NP's.	45
Figure 3.8: EDS analysis of Fe ₃ O ₄ NP's.....	47
Figure 3.9: EDS analysis of Fe ₃ O ₄ -SiO ₂ (CTAB) NP's.	48
Figure 3.10: FT-IR spectra for a) IBU b) Fe ₃ O ₄ -SiO ₂ (CTAB) c) Fe ₃ O ₄ -SiO ₂ (CTAB) and IBU.	50

Figure 3.11: Effect of contact time on the concentration of IBU for Fe ₃ O ₄ -SiO ₂ (CTAB) and ZnO-SiO ₂ (CTAB) NP's; (a) 15 mg/L, (b) 25 mg/L, (c) 35 mg/L at 298 K.....	52
Figure 3.12: Effect of contact time on removal efficiency of IBU for ZnO-SiO ₂ (CTAB) and Fe ₃ O ₄ -SiO ₂ (CTAB) NP's, (a) 15 mg/L, (b) 25 mg/L,(c) 35 mg/L at 298 K.....	54
Figure 3.13: The pseudo-first-order model for adsorption of IBU on: a) ZnO-SiO ₂ (CTAB) NP's b) Fe ₃ O ₄ -SiO ₂ (CTAB) NP's at 298 K and 25 mg/L.....	56
Figure 3.14: The pseudo-second-order linear fits for IBU adsorption via a) ZnO-SiO ₂ (CTAB) NP's b) Fe ₃ O ₄ -SiO ₂ (CTAB) NP's at 298 K.	58
Figure 3.15: Nonlinear fits of the kinetic data of IBU removal by ZnO-SiO ₂ (CTAB) NPs; (a) using Ho equation (b) using Shahwan equation at different concentration.....	65
Figure 3.16: Nonlinear fits of the kinetic data of IBU removal by Fe ₃ O ₄ -SiO ₂ (CTAB) NPs; (a) using Ho equation (b) using Shahwan equation at different concentration.....	66
Figure 3.17: Effect of initial IBU concentration on its percentage removal; a) Fe ₃ O ₄ -SiO ₂ (CTAB) b) ZnO-SiO ₂ (CTAB) NP's.....	71
Figure 3.18: Linear plots of Langmuir isotherm model of IBU adsorption on: a) Fe ₃ O ₄ -SiO ₂ (CTAB) NP's b) ZnO-SiO ₂ (CTAB) NP's at 288K.....	76
Figure 3.19: Linear plots of Freundlich isotherm model of IBU adsorption on: a) Fe ₃ O ₄ -SiO ₂ (CTAB) NP's b) ZnO-SiO ₂ (CTAB) NP's at 288K.....	79

Figure 3.20: Nonlinear fits of the kinetic data of IBU removal by Fe₃O₄-SiO₂ (CTAB) NPs; (a) using Langmuir model (b) using Freundlich model at 288 K...85

Figure 3.21: Nonlinear fits of the kinetic data of IBU removal by ZnO-SiO₂ (CTAB) NPs; (a) using Langmuir model (b) using Freundlich model at 288 K...86

Figure 3.22: Evaluation of p*H*_{pzc} for: a) Fe₃O₄-SiO₂ (CTAB) NP's b) ZnO-SiO₂ (CTAB) NP's.....93

Figure 3.23: Effect of pH on the percentage removal of IBU using: a) Fe₃O₄-SiO₂ (CTAB) b) ZnO-SiO₂ (CTAB) NP's at 298 K.94

Figure 3.24: Effect of temperature on the adsorption of IBU onto: a) Fe₃O₄-SiO₂ (CTAB) NP's b) ZnO-SiO₂ (CTAB) NP's at different initial IBU concentration.96

Figure 3.25: Arrhenius equation graph of IBU adsorption on: a) Fe₃O₄-SiO₂ (CTAB) NP's b) ZnO-SiO₂ (CTAB) NP's.99

Figure 3.26: Determination of thermodynamic parameters of IBU adsorbed onto Fe₃O₄-SiO₂ (CTAB) and ZnO-SiO₂ (CTAB) NP's..... 103

List of Tables

Table 3.1: Elements analyzed of ZnO-SiO ₂ (CTAB) NP's.	37
Table 3.2: Kinetic parameters for IBU adsorption on ZnO-SiO ₂ (CTAB) at 298K.	60
Table 3.3: Kinetic parameters for IBU adsorption on Fe ₃ O ₄ -SiO ₂ (CTAB) at 298K.....	60
Table 3.4: The kinetic parameters for adsorption IBU onto ZnO-SiO ₂ (CTAB) NP's of the pseudo second order linear fits using equations 14 and 16 at different concentration at 298K.	62
Table 3.5: The kinetic parameters for adsorption IBU onto Fe ₃ O ₄ -SiO ₂ (CTAB) NP's of the pseudo second order linear fits using equations 14 and 16 at different concentration at 298K.	63
Table 3.6: Values of Q obtained from experiment, values of Q predicted by equations (13 and 15), and the Chi –test values for the sorption systems of ZnO- SiO ₂ (CTAB) NP's at different concentration.	68
Table 3.7: Values of Q obtained from experiment, values of Q predicted by equations (13 and 15), and the Chi –test values for the sorption systems of Fe ₃ O ₄ - SiO ₂ (CTAB) NP's at different concentration.	69
Table 3.8: The calculated Q values of adsorbed IBU onto Fe ₃ O ₄ -SiO ₂ (CTAB) and ZnO-SiO ₂ (CTAB) NP's at different initial concentrations.	72
Table 3.9: correlation coefficients (R ²) values of linear Langmuir forms at 288 K.	74

Table 3.10: Parameters of Langmuir and Freundlich models for IBU adsorption using Fe ₃ O ₄ -SiO ₂ (CTAB) and ZnO-SiO ₂ (CTAB) NP's.....	81
Table 3.11: Maximum adsorption capacities of IBU for different adsorbents.	83
Table 3.12: Values of Q obtained from experiment, values of Q predicted by equations (18 and 20), and the Chi –test values for the sorption systems of Fe ₃ O ₄ -SiO ₂ (CTAB) NP's at 288 K.	87
Table 3.13: Amount of IBU adsorbed via Fe ₃ O ₄ -SiO ₂ (CTAB) and	97
Table 3.14 : Activation energy and rate constant values of adsorbed IBU onto Fe ₃ O ₄ -SiO ₂ (CTAB) and ZnO-SiO ₂ (CTAB) NP at different temperature.....	101
Table 3.15: Thermodynamic parameters of IBU adsorbed using Fe ₃ O ₄ -SiO ₂ (CTAB).	104
Table 3.16: Thermodynamic parameters of IBU adsorbed using ZnO-SiO ₂ (CTAB).	104

Abbreviations

CTAB	Cetyltrimethylammonium bromide
EOCs	Emerging Organic Contaminants
EDS	Energy-Dispersive Spectroscopy
FT-IR	Fourier Transform - Infrared Spectroscopy
IBU	Ibuprofen
NP's	Nanoparticles
NSAID	Nonsteroidal Anti-Inflammatory Drug
PCPs	Personal Care Products
PhACs	Pharmaceutical Compounds
POPs	Persistent Organic Pollutants
PZC	Point of Zero Charge
SEAD	Selected Area Electron Diffraction
SEM	Scanning Electron Microscopy
STP	Sewage Treatment Plant
TEM	Transmission Electron Microscopy
UV-Vis	Ultraviolet-Visible Spectrophotometer
WWTPs	Waste Water Treatment Plants
XRD	X-Ray Diffraction

Abstract

Recently, water pollution has become a global issue, due to the development of industry and the growth of the population. Pharmaceutical residues which are introduced into the environment through wastewater streams, have adverse effects on humans and the environment and are biologically active. Ibuprofen (IBU) is a common nonsteroidal anti-inflammatory non-biodegradable drug used for the treatment of pain and fever which was found to accumulate in environmental compartments.

Recently, nanomaterials have gained a lot of attention as effective substances for removing pharmaceuticals residue from wastewater. Silica nanoparticles $\text{Fe}_3\text{O}_4\text{-SiO}_2$ (CTAB) and ZnO-SiO_2 (CTAB) were prepared by green approaches and characterized using Fourier Transform- Infrared Spectroscopy (FT-IR), X-Ray Diffraction (XRD), Scanning Electron Microscopy (SEM), Transmission Electron Microscopy (TEM), and Energy-dispersive spectroscopy (EDS) techniques.

This study is aimed to investigate the adsorption of IBU via $\text{Fe}_3\text{O}_4\text{-SiO}_2$ (CTAB) and ZnO-SiO_2 (CTAB). The comparative study was performed to evaluate the effectiveness of $\text{Fe}_3\text{O}_4\text{-SiO}_2$ (CTAB) and ZnO-SiO_2 (CTAB) nanoparticles in the removal of IBU from waste water. Moreover, the effect of different parameters which may affect the removal efficiency, such as pH, contact time, initial pollutant's concentration, and temperature, was investigated.

The results showed that the IBU removal process using $\text{Fe}_3\text{O}_4\text{-SiO}_2$ (CTAB) was faster than that of ZnO-SiO_2 (CTAB) NP's. The kinetic models, which were used to explain the adsorption process and the kinetic result showed that IBU adsorption using $\text{Fe}_3\text{O}_4\text{-SiO}_2$ (CTAB) and ZnO-SiO_2 (CTAB) NP's have followed the pseudo-second-order model. The equilibrium experimental data were analyzed using Langmuir and Freundlich isotherm models at different temperatures, and the isotherm studies showed that the maximum adsorption capacity of $\text{Fe}_3\text{O}_4\text{-SiO}_2$ (CTAB) exceeds that of ZnO-SiO_2 (CTAB). The thermodynamic parameters indicated that the adsorption of IBU via both types of adsorbent favors the products and have exothermic nature.

The developed method may be useful for the removal of ibuprofen drug residue from natural water resources at specific pH values with small adsorbent amounts and short agitation time.

الملخص بالعربية

في الآونة الأخيرة، أصبح تلوث المياه مشكلة عالمية، بسبب تطور الصناعة ونمو السكان. حيث ان المخلفات الصيدلانية التي يتم إدخالها إلى البيئة من خلال تيارات المياه العادمة لها تأثيرات ضارة على الإنسان والبيئة كما انها نشطة بيولوجيًا. احدى هذه الملوثات هو مركب الإيبوبروفين (IBU) حيث انه دواء شائع مضاد للالتهابات غير قابل للتحلل الحيوي يستخدم لعلاج الألم والحمى ووجد أنه يتراكم في الأجزاء البيئية.

وفي الفترة الاخيرة اكتسبت المواد النانوية الكثير من الاهتمام كمواد فعالة في إزالة بقايا الأدوية من مياه الصرف الصحي. في هذه الدراسة تم تحضير نوعين من جسيمات السيليكا النانوية $\text{Fe}_3\text{O}_4\text{-SiO}_2$ (CTAB) و ZnO-SiO_2 (CTAB) باستخدام الطرق الخضراء وقد تم تشخيص هذه الجسيمات بتقنيات مثل (FT-IR) و (XRD) و (SEM) و (TEM) و (EDX).

هدفت الدراسة إلى وصف امتزاز IBU باستخدام $\text{Fe}_3\text{O}_4\text{-SiO}_2$ (CTAB) و

ZnO-SiO_2 (CTAB) حيث أجريت دراسة مقارنة لتقييم فعالية

$\text{Fe}_3\text{O}_4\text{-SiO}_2$ (CTAB) و ZnO-SiO_2 (CTAB) النانوية في إزالة IBU من

محاليل مائية . علاوة على ذلك، تم دراسة تأثير العوامل المختلفة التي قد تؤثر على كفاءة الإزالة، مثل درجة الحموضة، وقت الامتصاص، تركيز الملوثات الأولية، ودرجة الحرارة.

أظهرت النتائج أن عملية إزالة IBU باستخدام جسيمات $\text{Fe}_3\text{O}_4\text{@SiO}_2$ (CTAB) كانت أسرع من تلك الخاصة بـ ZnO-SiO_2 (CTAB) كما تم استخدام النماذج الحركية لشرح عملية الامتزاز وأظهرت النتيجة الحركية أن امتزاز IBU باستخدام جسيمات

(ZnO-SiO₂ (CTAB) و Fe₃O₄-SiO₂ (CTAB) قد اتبعت نموذج معادلة الدرجة الثانية. كما تم تحليل البيانات التجريبية للتوازن باستخدام نموذجي Langmuir و Freundlich عند تساوي الحرارة و عند درجات حرارة مختلفة وتظهر الدراسة عند تساوي الحرارة أن أقصى سعة امتزاز لجسيمات Fe₃O₄-SiO₂ (CTAB) أكثر من جسيمات ZnO-SiO₂ (CTAB).

كما أشارت النتائج الديناميكية الحرارية إلى أن امتزاز IBU عبر كلا النوعين من الممتزات هو عملية مائلة نحو النواتج وطاردة للحرارة.

قد تكون هذه الطريقة المطورة مفيدة لإزالة بقايا عقار الإيبوبروفين من موارد المياه الطبيعية عند درجة حموضة معينة مع كمية منخفضة من الامتصاص.

1. Introduction

1.1 Water pollution and pharmaceuticals

Exponential population growth and the increase in industrial facilities have led to negative impacts on the environment and human beings.¹⁻² Consequently, the demand for water supplies increases in parallel with depletion and pollution of water resources like streams, lakes, rivers, and oceans.³ Pollution causes pressure on the quality and quantity of water resources available and leads to many infectious diseases, which affect the human health causing illness, such as typhoid fever, diarrhea, vomiting, and kidney problem.³⁻⁴

As a result, alternative water sources are being explored, and water reuse will play an important role in this matter. Therefore, the removal of trace organic pollutants from contaminated water resources destined for reuse application is a goal for many researchers in the water sector.

Different examples of trace organic pollutants like surfactants, pesticides, fertilizers, plastics, polythene bags, pharmaceuticals, and many other chemicals reach environmental water resources causing water pollution, which is dangerous to human health.⁵

Also, the continuous production and development of new chemicals without knowing their impact on the environment may contribute to the spreading of environmental pollution. As a result, more emerging organic contaminants has been detected in wastewater, which could affect the surface and groundwater.⁶

Recently, water treatment has become one of the most important topics, and people are paying great attention to the problems related to environmental pollution that affect their health.

Most conventional wastewater treatment methods such as activated sludge, sand filtration, and coagulation-flocculation are inefficient in the removal of the chemical pollutants and are recalcitrant to emerging contaminants. These conventional methods are ineffective to eliminate the majority of the polluting compounds, which leads to the accumulation of the remaining quantities in water.^{1,6} Therefore, new techniques are needed to be developed for waste water treatment in order to face the problem of increasing water pollution and to provide improved sanitation and safe drinking water.⁷

Emerging organic contaminants (EOCs) detected in the aquatic environment have adverse effects on human health and the environment, since it includes a wide range of different pollutants like pharmaceuticals, pesticides, personal care products (PCPs), and veterinary products, so several studies have focused on EOCs.⁸

Pharmaceutical compounds are produced and used in large quantities, which lead to the uncontrolled continuous release of these contaminants to the water environment; therefore, the presence of pharmaceutical residues in the environment is an emerging issue.⁹⁻¹⁰

EOCs can alter the endocrine system of humans and wildlife at very low concentrations. Therefore, it is necessary to investigate treatment alternatives that effectively remove EOCs and pharmaceutical compounds (PhACs) from wastewater treatment plant discharges and drinking water sources. The increased consumption of pharmaceuticals leads to concerns about its presence in the environment, because it is not possible to assimilate these large quantities of such therapeutic compounds. The main sources of pharmaceuticals to the environment are hospitals, research activities

using therapeutic compounds, disposing of expired drugs to the environment, and pharmaceutical industries.¹¹⁻¹³

Pharmaceutical compounds have been found to be more abundant in sewage treatment plant (STP) effluents and surface waters, and less available in drinking water and groundwater.¹⁴⁻¹⁵

Increased levels of trace active pharmaceutical ingredients, which are present in water in the range of ng/L to $\mu\text{g/L}$ attracts researchers attention to investigate the fate and occurrence of such compounds in the aquatic environment.¹⁶⁻²⁰

Low volatility, upraised polarity, and the partial metabolization of consuming drugs are factors that allow easy movement of pharmaceuticals to environment compartments. Pharmaceutical compounds in the aquatic environment are classified into beta-blockers, hormones, antibiotics, anti-inflammatory, and analgesics.²¹

A combination of microbial metabolites and parent compounds resulting from the complete or partial degradation of pharmaceuticals and their metabolites, enter the surface and groundwater through effluent discharge. As a result, pharmaceutical pollutants can be transferred to sewage sludge by the sorption process that occurs

during the treatment in WWTPs. The continuous infusion of pharmaceuticals effluents from WWTPs is one of the persistent pollutants in the aqueous environment.²²⁻²³

Anti-inflammatory drugs are used for the relief of pain, inflammation and fever. But they are the most resistant compounds in wastewater treatment effluents, that have adverse effects on humans and the environment together, so it is necessary to investigate and develop new methods, which have the capability to eliminate such pollutants from the aqueous environment.²¹

1.2. Methods of pharmaceutical removal

Conventional wastewater treatment processes like activated sludge, sand filtration, and coagulation-flocculation are unable to eliminate recalcitrant pharmaceuticals from polluted water; however, the advanced treatment technologies are designed to achieve this.²⁴⁻²⁸

The aim of the coagulation-flocculation process is to aggregate the fine particles into larger particles to reduce suspended pollutants in wastewater. The coagulation process is done by adding a coagulant, followed by flocculation to increase the size of particles. This process

leads to unstable pollutant particles causing sedimentation. These techniques involve pH adjustment and additions of some materials such as coagulants to increase the amount of precipitated materials.²⁹⁻

31

Recently, advanced treatment technologies such as advanced oxidation and adsorption by activated carbon have received much attention, however the results showed incomplete removal and expensive cost.³²⁻³³

The oxidation technique was successfully applied to convert the organic pollutant residues in the wastewater. Remediation of trace organic pollutants with oxidizers has the ability to eliminate the organic contaminant, but oxidizing intermediates during the oxidation process are preventing complete elimination. Mineralization of trace organic contaminants is the main target in choosing the type of technique used in the treatment process, to increase the possibility of reuse of treated wastewater in various applications. The Ozonation process is another technique used for pharmaceutical pollutants mineralization in wastewater, the advanced oxidation processes based on the hydroxyl radicals ($\bullet\text{OH}$) as a primary oxidant. However, this method is not sufficiently

effective in some cases because of the presence of some natural organic compounds such as bicarbonate, carbonate, and chloride ions in the wastewater. These compounds act as radical scavengers, competing with pollutants for hydroxyl root consumption, as well as a relatively energy-intensive and high cost. Therefore, its presence increases the requirements for oxidation and reduces treatment efficiency. In addition, the pharmaceutical compounds are present in wastewater at very low concentration and this leads to an increase in the cost of processing treatment per unit mass.³⁴⁻³⁷

Membrane filtration is a separation technique, which has the ability to remove organic and inorganic pollutants as well as suspended solids. In these techniques, different types of membranes can be used for treatment of wastewater depending on the size of particles that will be attached to it.³⁸

Three types of membrane filtration were commonly used, the first type of these membranes is ultrafiltration, in which a permeable membrane is used to separate the suspended solid and macromolecules from wastewater. The second type is nanofiltration, where the membrane contains small pores and surface charge. These

two properties give the membrane an advantage to reject charged solutes that are smaller than the membrane pores, and neutral solutes that are bigger than the pores. The third type of membrane filtration is reverse osmosis. The removal efficiency of these membranes depends on pressure difference across the membrane. Therefore, the higher the pressure, the higher the removal efficiency of pollutants in wastewater, which requires high energy.³⁹⁻⁴¹

Membrane water treatment technology was found to be more effective in removing metals than organic contaminants such as pharmaceuticals. On the other hand, membrane fouling makes the operating cost of this method expensive.⁴²

One of the alternative methods that has been used for the wastewater treatment is the adsorption technique. It is a surface phenomenon, which involves transferring substances from the liquid phase (adsorbent) to the solid surface (absorbent). Contaminants adhere to the solid surface through physical adhesion. However, a weak chemical bonding force sometimes occurs. It is a surface phenomenon, and it is the process of transferring the mass which a substance is transported from the liquid (adsorbate) phase to the surface of a solid (absorbent), and the contaminant compounds adhere

at the surface of a solid by physical bonds, but sometimes weak chemical bonding forces take place. The adsorption process is affected by different parameters such as the nature of adsorbate, type of adsorbent, temperature, presence of other pollutants, and the experimental conditions (contact time, the concentration of pollutant, the particles size of adsorbent, pH, and temperature). Due to its ability to remove biological, soluble and insoluble pollutants, adsorption technique has received extensive attention and wide range of applications.^{39, 43}

Activated carbon has good adsorption performance, due to its characteristics as an adsorbent including developed microspores, large surface area, and strong adsorption capacity, so it is widely used as a good adsorbent in water treatment. However, the widespread use of this technology has many limitations and is expensive. The filters used to separate contaminated activated carbon from the treated solution have a short service life, so these filters need to be replaced regularly, otherwise, the surface of these filters will be saturated and cannot be used for further purification.⁴⁴⁻⁴⁷

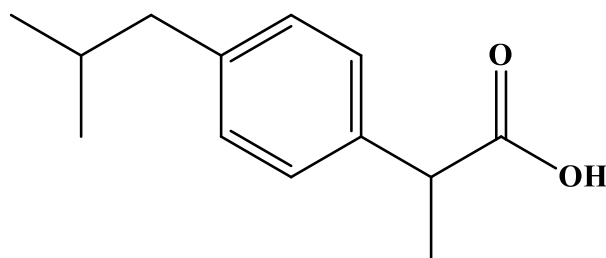
With the continuous spreading of the pharmaceutical residuals in the aquatic environment, the development of a cost-effective method and high capacity for removing the pharmaceutical contaminants from the aquatic environment has become an urgent necessity.⁴⁸

Nanotechnology is applied to produce an effective nanomaterial for wastewater treatment. These nanomaterials have gained a lot of attention as eco-friendly and effective substances for removing pharmaceutical residues from wastewater. Because of their extraordinary properties such as high surface area, antimicrobial activity, magnetic properties, and photosensitivity, they have been used effectively for many applications.⁴⁹⁻⁵¹

Ibuprofen (IBU) is a nonsteroidal anti-inflammatory drug (NSAID) introduced initially in the UK by 1969. Ibuprofen is chemically named 2-(4-(2-Methylpropyl) phenyl) propanoic acid and is used to relieve acute pain, antipyretic and anti-inflammatory. Ibuprofen is one of the persistent organic pollutants (POPs) which has an adverse effect on human health and the environment.⁵²⁻⁵⁵

The structural formula of Ibuprofen is shown in Figure 1.1. The chemical formula of IBU is $C_{13}H_{18}O_2$, molecular weight 206.28 g/mol,

and its density is 1.03 g/cm^3 . Ibuprofen is soluble in organic solvents and is practically insoluble in water 21 mg/L at $25 \text{ }^\circ\text{C}$.



2-(4-(2-Methylpropyl) phenyl) propanoic acid

Figure 1.1: Structure of Ibuprofen

Ibuprofen is weak acid has acid dissociation constant $K_a = 1.2 \times 10^{-5}$ at $25 \text{ }^\circ\text{C}$, therefore most ibuprofen molecules present in aqueous solution as undissociated ibuprofen molecules. Although Ibuprofen contains

polar carboxyl group COOH, the presence of benzene ring and non-polar alkyl group reduce its polarity.⁵⁶⁻⁵⁷

Ibuprofen has S and R enantiomer molecules present in two chemical chiral structures. Ibuprofen S and R, which have similar physical properties, such as solubility, boiling point, and melting point, but have different biological effects and metabolism in the body. As a results only S enantiomer has anti-inflammatory effect in human body.⁵⁸⁻⁶⁰ Molecular structures of (S) and (R) of IBU are shown in Figure 1.2

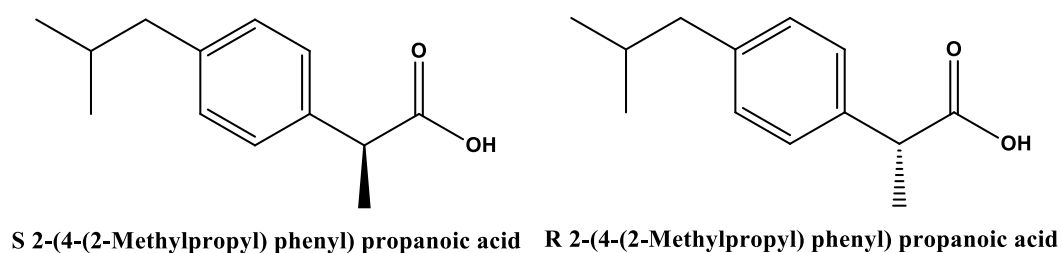


Figure 1.2 : Molecular structures of (S) and (R) of IBU

1.3 Nanoparticles

Nanoparticles has been used as nano adsorbents because of its distinctive properties that enable it to be functionalize, and enhance the selectivity for eliminating specific contaminants such as residual drugs.⁴⁹

Nanoparticles (NP's) can be prepared in two ways: top-down process (e.g., lithographic, machining) or bottom-up synthesis (e.g., sol-gel, colloidal). Metal oxides NPs have receiving noticeable attention for nanoparticles adsorbent synthesis; previous studies show that the metal oxides NPs have the ability to alter the surface structure and properties which increase the active adsorption sites (edges, corners, and vacancies), which improve the adsorption for removing the pharmaceuticals from wastewater.^{49, 61}

1.3.1 Iron oxide nanoparticles

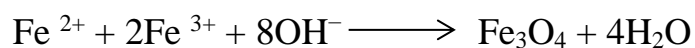
Iron oxide is present in several forms, like maghemite ($\gamma\text{-Fe}_2\text{O}_3$), hematite ($\alpha\text{-Fe}_2\text{O}_3$), and magnetite (Fe_3O_4). Numerous previous researches have been applied magnetic nanocomposites in many fields because of their magnetic properties, large specific surface area, high

adsorption capacity, super-paramagnetic properties, specific functionality, and short adsorption equilibrium time. These characteristics make it possible to eliminate pollutants in a short time.⁶²⁻⁶⁶

The magnetic Fe₃O₄ nanoparticles are synthesized using several methods such as hydrothermal, microemulsion, colloidal chemistry and, co-precipitation. The preferred approach for preparing Fe₃O₄ is the co-precipitation method because of simplicity, ability to use water as a solvent, reproducibility, and short-time reaction.⁶⁷⁻⁶⁹

Iron has two oxidation states; iron (II) and iron (III), while Fe₃O₄ nanoparticles are synthesized by co-precipitation of ferric (Fe³⁺) and ferrous (Fe²⁺) ions in an alkaline media.⁶²

The following equation shows the formation mechanism of Fe₃O₄ magnetic nanoparticles with ferric and ferrous salts at the ratio of 2 to 1.



The magnetic dipole attractions between magnetic nanoparticles reduce their stability in aqueous solutions and limits their efficiency in various applications. Surface modification of Fe_3O_4 nanoparticles has been used with different biocompatible and biodegradable polymers to enhance stability and dispersibility of Fe_3O_4 nanoparticles, such as surfactants or xerogels. The cetyltrimethylammonium bromide (CTAB) binds strongly with pharmaceuticals pollutants by electrostatic forces or dipole-dipole attractions. CTAB surfactant was used as a template or to modify the surface and morphology of NPs.⁷⁰⁻

⁷¹ Figure 1.3 shows the chemical structure of CTAB.

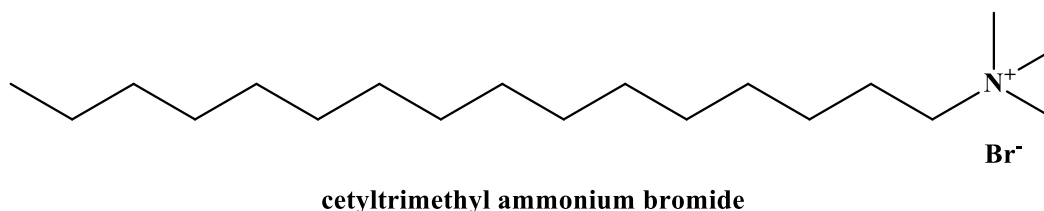


Figure 1.3: Chemical structure of cetyltrimethylammonium bromide (CTAB).

Figure 1.4 clarifies how positively charged CTAB surfactant was used as a coating layer for Fe_3O_4 nanoparticles.

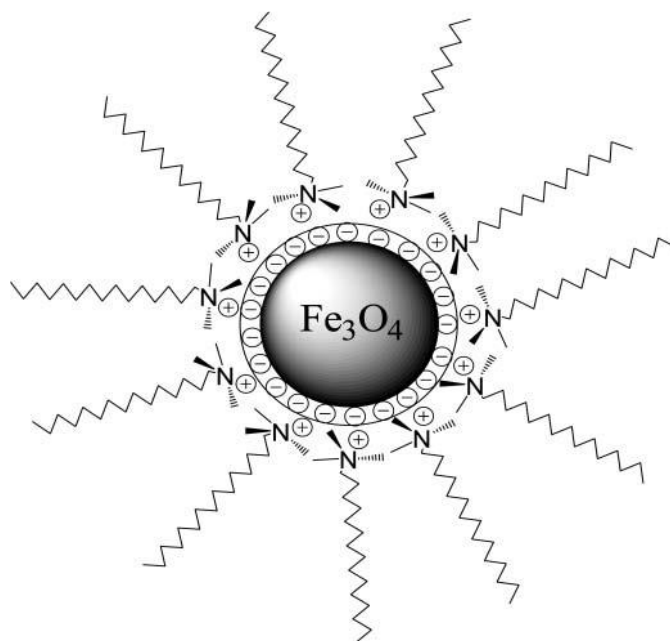


Figure 1.4: Structure of CTAB coated Fe₃O₄ nanoparticles.

1.3.2. Zinc oxide nanoparticles

Zinc oxide (ZnO) is a semiconductor material in group II-VI with a band gap energy of 3.2 eV, and possesses a high quantum efficiency, therefore the effective band gap of the semiconductor is large.⁷²

ZnO nanoparticles are known as a luminescent material and are one of the metal oxides that have been given attention due to their distinctive characteristics like optical properties, low cost, low toxicity, a wide range of UV absorption, and was used as a photocatalyst for the degradation of pollutants in water. ZnO

nanoparticles have different chemical and physical properties from the bulk ZnO material. The activity of ZnO changes when its size is reduced to nanometer scale because of its high surface area and the changes of the surface properties.⁷³⁻⁷⁶

Several methods have been used to synthesize ZnO nanoparticles, such as the sol-gel method, hydrothermal reaction, and chemical precipitation. The chemical precipitation method is commonly used to synthesize ZnO NPs because of its low cost, low temperature, and the ability to control size.⁷⁷

Zinc oxide nanoparticles have a broad fluorescence emission spectrum in the blue-yellow region. The color emission of ZnO NPs are affected through the surface modifications as indicated in previous works which found that the visible emission of ZnO is mainly affected by the surface oxygen vacancies, which can be optimized by pH adjustment. ZnO NPs are not stable and tend to agglomerate without surface modification, while coating the surface of ZnO NPs with suitable materials such as silica or polymers enhance the stability and increase the ability to control their size.⁷⁸⁻⁸⁰

Silica (SiO_2) was used to increase the surface area and stability of ZnO and Fe_3O_4 nanoparticles. The nanoparticles were distributed within silica layers using the sol-gel method. Using silica is highly considered in recently advanced research because of its compatibility, chemical stability, high surface area, porosity, and functionalization of the silica surface. Polymerization using alkoxides precursors was generally used for SiO_2 synthesis in two steps: hydrolysis and condensation.⁸¹⁻⁸⁵

1.4. Adsorption isotherms

The adsorption isotherm is a mathematical model which is used to describe the equilibrium distribution of the adsorbate between the solution and the adsorbent, at a specific temperature. Equilibrium of adsorption occurs when the chemical potential of the solute that is adsorbed on adsorbent is equal to the chemical potential of the solute in the solution.

The adsorption isotherm is usually applied to interpret the experimental data obtained by batch adsorption tests. The experimental data can be analyzed by different isotherm equations,

which relate the amounts of adsorbate (mg) adsorbed per gram of adsorbent at equilibrium (Q_e) and the equilibrium concentration of solution (C_e). Several isotherm models were applied to study the mechanism of the adsorption process, and the most common models are Langmuir and Freundlich isotherm. The following mass balance equations relate the amount of adsorbate on the solid to its amount in solution: ⁸⁶⁻⁸⁸

$$Q_e = (C_0 - C_e) \frac{V}{m} \quad (1)$$

$$Q_t = (C_0 - C_t) \frac{V}{m} \quad (2)$$

Where C_0 , C_e , C_t are adsorbate concentrations at initial, equilibrium, and at any time respectively, whereas the $V(L)$ and $m(g)$ are volume of solution and adsorbent dosage, respectively.

1.4.1. Langmuir isotherm

The Langmuir isotherm assumes a monolayer surface adsorption of adsorbate, and a homogenous coverage for adsorbent, which means that all sites on the adsorbent surface are identical and have the same affinity for the adsorbate molecules. The Langmuir adsorption isotherm model is represented by the following equation: ⁸⁹⁻⁹¹

$$Q_e = \frac{Q_m K_L C_e}{1 + K_L C_e} \quad (3)$$

The linear Langmuir forms:

$$\frac{C_e}{Q_e} = \frac{1}{Q_m} k_L + \frac{C_e}{Q_m} \quad (4)$$

$$\frac{1}{Q_e} = \frac{1}{Q_m} + \frac{1}{Q_m k_L C_e} \quad (5)$$

$$Q_e = Q_m - \frac{Q_e}{k_L C_e} \quad (6)$$

$$\frac{Q_e}{C_e} = k_L Q_m - k_L Q_e \quad (7)$$

Where:

Q_e = the amount of adsorbate per gram of the adsorbent at equilibrium (mg/g).

Q_m = maximum monolayer coverage capacity (mg/g)

K_L = Langmuir isotherm constant (L/mg).

C_e = the equilibrium concentration of adsorbate (mg/L)

1.4.2. Freundlich isotherm

The Freundlich isotherm assumes that the surface of adsorbent is heterogeneous, which means that the active sites on the surface have different affinities. The Freundlich equation is given by: ⁹²⁻⁹⁴

$$Q_e = k_f C_e^{\frac{1}{n}} \quad (8)$$

The linear Freundlich form:

$$\ln Q_e = \ln k_f + \frac{1}{n} \ln C_e \quad (9)$$

Where k_f and $1/n$ are the Freundlich constants, Q_e is the amount of adsorbate per gram of the adsorbent at equilibrium (mg/g), C_e is the equilibrium concentration of adsorbate (mg/L).

1.5. Research objectives

The main objective of this research was to develop new advanced materials for water/wastewater treatment. These materials ZnO-SiO₂ (CTAB) and Fe₃O₄-SiO₂ (CTAB) nanoparticles will work against the entry of Ibuprofen from aqueous solutions to drinking water or surface water.

The framework of this research is based on studying the removal efficiency of ibuprofen from aqueous solutions using the synthesized nanoparticles. In addition, the effect of different parameters was investigated that may affect the removal efficiency, such as (pH, contact time, initial pollutant's concentration, and temperature). Batch-type experiments are established to study the adsorption process by measuring the concentration of pollutant in an aqueous solution using UV Spectrophotometry (UV-Vis). The synthesized nanoparticles were characterized using Scanning Electron Microscopy (SEM), Transmission Electron Microscopy (TEM), X-Ray powder diffraction (XRD), and Fourier-transform infrared spectroscopy (FT-IR).

2. Experimental

2.1. Chemicals and reagents

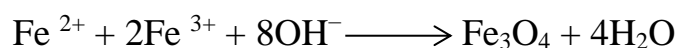
All chemicals were of analytical grade and utilized as received without any further purification. The chemicals are: Ibuprofen ($C_{13}H_{18}O_2$), ferric chloride ($FeCl_3$, $\geq 99\%$), ferrous chloride tetrahydrate ($FeCl_2 \cdot 4H_2O$, $\geq 99\%$), sodium hydroxide ($NaOH$, $\geq 98\%$), ammonium hydroxide (28% NH_3 in H_2O), ethyl acetate ($EtAc$, $\geq 99\%$), tetraethyl orthosilicate (TEOS, $\geq 99\%$), ethanol ($\geq 99\%$), cetyltrimethylammonium bromide (CTAB, $\geq 98\%$), Lithium hydroxide ($LiOH$, 99%), sodium chloride ($NaCl$, $\geq 99\%$), hydrochloric acid and zinc acetate dihydrate ($Zn(CH_3CO_2)_2 \cdot 2H_2O$, 99% pure). All chemicals were purchased from Sigma-Aldrich Chemical Company. Aqueous solutions were prepared using Milli-Q water having resistivity 18.2 $M\Omega \cdot cm$.

2.2. Synthesis of iron oxide (magnetite; Fe₃O₄) and zinc oxide (ZnO) nanoparticles

Iron oxide (magnetite) nanoparticles and zinc oxide nanoparticles were prepared via co-precipitation and precipitation method respectively. Two batches of NP's were synthesized.

2.2.1. Synthesis of iron oxide magnetite (Fe₃O₄) nanoparticles

Magnetite nanoparticles were synthesized via Fe²⁺ and Fe³⁺ at the ratio 1 to 2. According to the following chemical equation: ⁶²



For each batch, 12.5 mLs of ammonium hydroxide were added to 150 mL of Milli-Q water and kept under continuous stirring. The solution was heated to 60°C under nitrogen gas bubbling to keep inert condition. Then, 0.596 g of FeCl₂·4H₂O and 0.973 g of FeCl₃ were dissolved into two separate beakers each of which containing 10 ml of de-aerated MQ water. The iron solution mixture was added to the

ammonium solution with continuous vigorous stirring and the reaction was heated to 70 °C for 2h. The color of the solution changed to black, indicating Fe₃O₄ magnetic nanoparticles formation. After that, the Fe₃O₄ nanoparticles were collected by an external magnet and washed with distilled water to keep the pH value at 7, and was then washed with ethanol. Finally, the synthesized Fe₃O₄ nanoparticles were dried in the oven at 70 °C for 24 h and transferred to a tightly closed bottle under an ethanol environment to prevent oxidation.⁹⁵

2.2.2. Synthesis of zinc oxide nanoparticles

ZnO nanoparticles were synthesized using a precipitation method. In each batch, 0.0439g of Zn(CH₃CO₂)₂·2H₂O was dissolved completely in 40 ml of absolute ethanol with stirring for 30 min at room temperature. Then 5.5 mg of LiOH was added to the zinc/ethanol solution under continuous stirring at room temperature for 2h. Finally, ZnO was prepared and kept in tightly closed bottles.

The pH of this reaction was 6.0. The ZnO nanoparticles were precipitated at different pH values, adjustable by controlling the quantities of LiOH added.⁹⁶

2.2.3. Synthesis of Fe₃O₄-SiO₂ (CTAB) nanocomposite

To prepare a batch of Fe₃O₄-SiO₂ (CTAB) nanoparticles, 0.1g of CTAB was completely dissolved in 5.0 ml of MQ water. Then 0.5 ml of Fe₃O₄/ethanol mixture was added to the surfactant solution with continuous vigorous stirring for 10 min and 40 ml of NaOH (13 mM) was added to the resulting solution. Then, 3.0 ml and 0.5 ml of TEOS, respectively, were added to the solution with continuous stirring for 1h. Finally, 0.1 g of NaOH was added to the solution with continuous stirring for 1hr. The Fe₃O₄-SiO₂ (CTAB) nanoparticles were synthesized and washed with ethanol and MQ water then dried in the oven.⁹⁵

2.2.4. Synthesis of ZnO-SiO₂ (CTAB) nanocomposite

For each batch, 0.1g of CTAB was completely dissolved in 5.0 ml of MQ water. Then 0.5 ml of ZnO/ethanol mixture was added to the

surfactant solution with continuous vigorous stirring for 10 min and 40 ml of NaOH (13 mM) was added to the resulting solution. Then, 3.0 ml and 0.5 ml of TEOS, respectively, were added to the solution with continuous stirring for 1h. Finally, 0.1 g of NaOH was added to the solution with continuous stirring for 1hr. The ZnO-SiO₂ (CTAB) nanoparticles were synthesized and washed with ethanol and MQ water then dried in the oven.⁹⁷

2.3. Standard solutions and calibration curve

1000-ppm IBU stock solution was prepared by dissolving 100.0 mg of IBU in a mixture of (1:1) absolute ethanol: MQ water, and diluted to 100 ml with the same solvent.

Different initial concentrations were prepared using stock solution through serial dilutions to obtain the following solution: 35.0, 30.0, 25.0, 15.0, 10.0, 5.0 mg/L.

IBU calibration curve was constructed in the range 5.0-35.0 mg/L. The absorbance was measured at λ_{\max} (222 nm) for the standard solutions using UV-Visible spectrophotometer. The stock solution was scanned in the range of 200 to 800 to determine the wavelength of maximum absorption (λ_{\max}).

2.4. IBU removal experiments

In order to study the removal efficiency of IBU, various parameters were studied including contact time between material and IBU (kinetic experiments), initial IBU concentration, temperature, and pH. All IBU removal experiments were performed under atmospheric pressure. UV-Vis spectrophotometer was used for determined IBU concentration by measuring the absorbance during each step.

2.4.1. Effect of initial IBU concentration

To determine the optimum concentration of IBU, different initial IBU concentrations were studied at different temperatures.

Batch experiments were performed by adding 50 mg of ZnO-SiO₂ (CTAB), Fe₃O₄-SiO₂ (CTAB) NP's to 75 ml of IBU solution at variable concentration: 15.0, 25.0, and 35.0 mg/L. The solutions were shaken at 150 rpm for 3 hours. Each solution was then double filtered through the syringe filter 0.45 μm and the IBU concentration was

determined by measuring the absorbance using a UV-Vis spectrophotometer at a fixed wavelength of 222 nm.

2.4.2. IBU removal kinetics

The removal of IBU was investigated as a function of shaking time at initial concentration of 25 mg/L IBU at different temperatures 298, 288, and 318 K.

A 50mg of ZnO-SiO₂ (CTAB), Fe₃O₄-SiO₂ (CTAB) nanoparticles samples were added separately to 75 ml of IBU solution. Then the solutions were shaken in a thermostat shaker at 150 rpm for 3 hrs.

Finally, the solutions were filtered through the syringe filter 0.45 μm, and the absorbance of each solution was measured at λ_{\max} (222 nm) using a UV-Vis spectrophotometer.

2.4.3. Effect of pH and PZC

The effect of pH on IBU adsorption was investigated for pH values ranging from 2-8.

The pH of 75 ml of 25 mg/L IBU solution was adjusted using 0.1M of NaOH and HCl solutions to reach the corresponding pH. Then 50 mg of adsorbent was added to the solution and placed in a shaking water bath at a constant temperature.

The point of zero charge (PZC) for both type of NP's Fe₃O₄-SiO₂ (CTAB) and ZnO-SiO₂ (CTAB) were determined by a simple electrochemical method by adding 40 ml of sodium chloride (0.01M) to a series of beakers, and the pH was adjusted at 2, 3, 4, 5, 6, 7, 8, 9, 10, and 11 by using 0.1 M NaOH or 0.1 M HCl solution. Then 50 mg of NP's were added into all beakers and agitated on shaker for 24 hours at 25°C. Then the final pH values were recorded.

2.4.4.Effect of temperature

Temperature affect was studied for the adsorption process. 50 mg of adsorbent was added to 75 ml of 25 mg/L IBU solution. The mixture was shaken in a thermostat shaker at 150 rpm at the following temperatures: 288, 298, and 318 K. Final IBU concentration was determined after filtering by measuring the absorbance at a fixed wavelength of 222 nm using a UV-Vis spectrophotometer.

2.5. Characterization

Different techniques were used to characterize $\text{Fe}_3\text{O}_4\text{-SiO}_2$ (CTAB) and ZnO-SiO_2 (CTAB) NP's. They are described below.

The absorption spectra of the solutions were measured using an Agilent 8453 UV-Vis spectrophotometer which uses deuterium lamps and a photodiode array detector.

The Powder X-Ray Diffraction (XRD) patterns of Fe_3O_4 and $\text{Fe}_3\text{O}_4\text{-SiO}_2$ (CTAB) nanoparticles were obtained by Mini-XRD, Rigaku X-ray diffractometer with a diffraction angle (2θ) ranged from 15° to 80° .

Scanning Electron Microscopy (SEM) was used to characterize the surface morphology, shape, and size of the nanoparticles using a Lyra3, Tescan field emission scanning electron microscope.

Transmission Electron Microscopy (TEM) images were recorded with a JEM-2100F instrument. The samples were prepared by diluting the nanoparticles in ethanol, sonicating for 30 min, and drying on carbon-coated Cu grids under vacuum.

Fourier Transform Infrared Spectroscopy (FT-IR) spectra of nanoparticles samples were obtained using a Bruker TENSOR II Spectrometer. The spectra were recorded using KBr pellets in the range of 4000-200 cm^{-1} .

3. Results and discussion

3.1 Characterization of ZnO and ZnO-SiO₂ (CTAB) NP's

The ZnO and ZnO-SiO₂ (CTAB) NP's synthesized in this study were characterized by SEM, TEM, EDS, and FT-IR.

The surface morphology of ZnO and ZnO-SiO₂ (CTAB) NP's was studied using SEM and TEM techniques as shown in Figure 3.1 and Figure 3.2 respectively. The morphology of ZnO and ZnO-SiO₂ (CTAB) appears as a spherical-like structure, while the birefringence of ZnO Quantum dots and their particle size ranged from 2 to 6.5 nm is clearly shown in Figure 3.2(a). The average diameter of ZnO-SiO₂ (CTAB) NP's from 50-90 nm as shown in Figure 3.1(a) first batch and Figure 3.1(b) second batch. The TEM image in Figure 3.2(b) shows the ZnO NP's as black dots distributed on the surface of SiO₂ and between its layers.⁹⁷

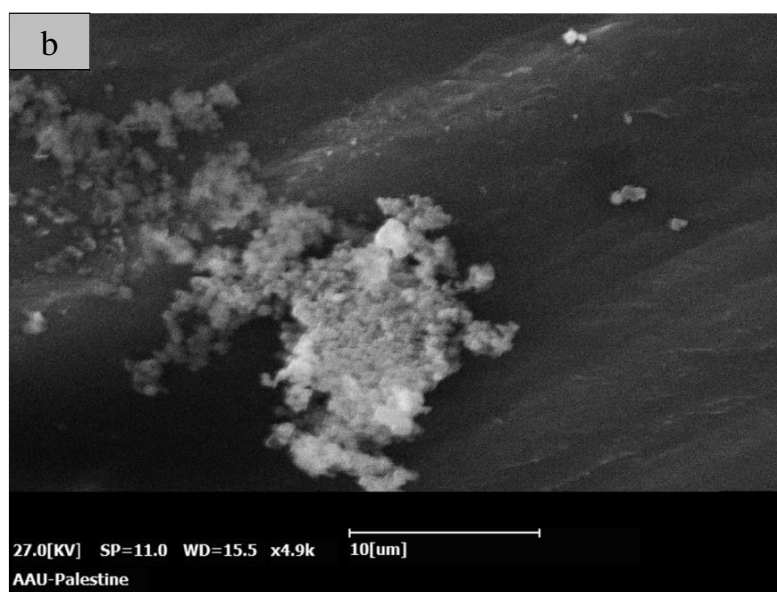
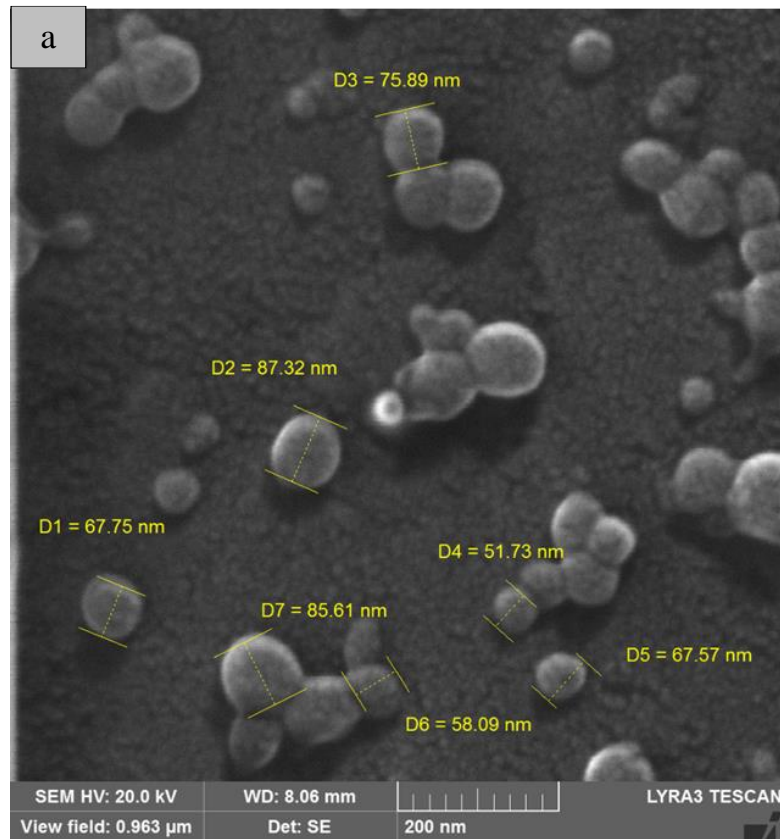


Figure 3.1: SEM images (a) of ZnO-SiO₂ (CTAB) NP's (first batch), and (b) of ZnO-SiO₂ (CTAB) NP's (second batch).

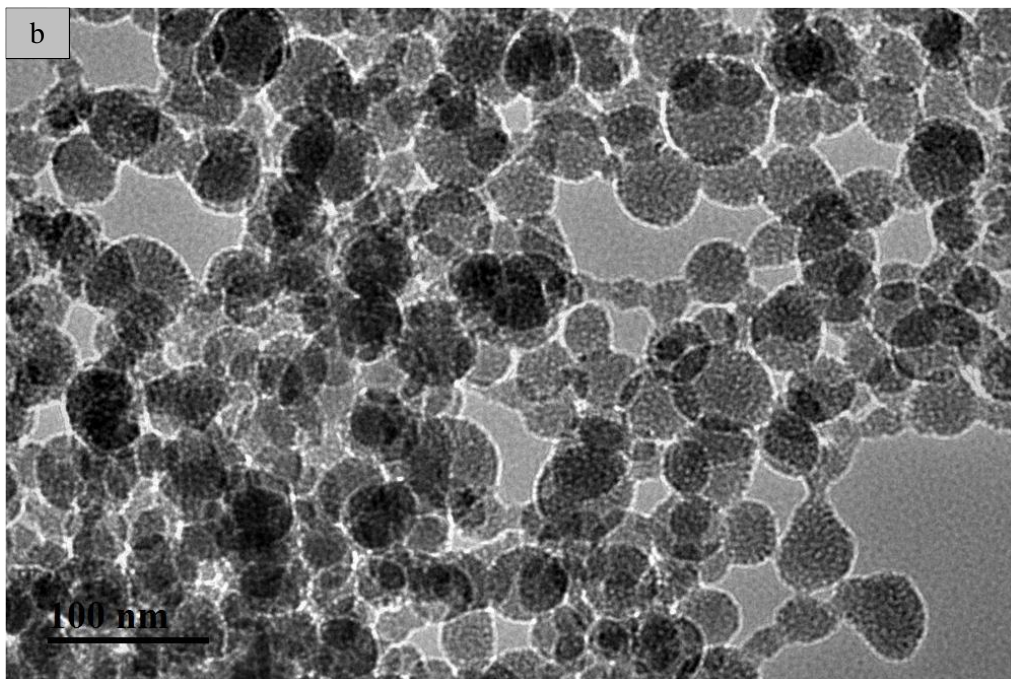
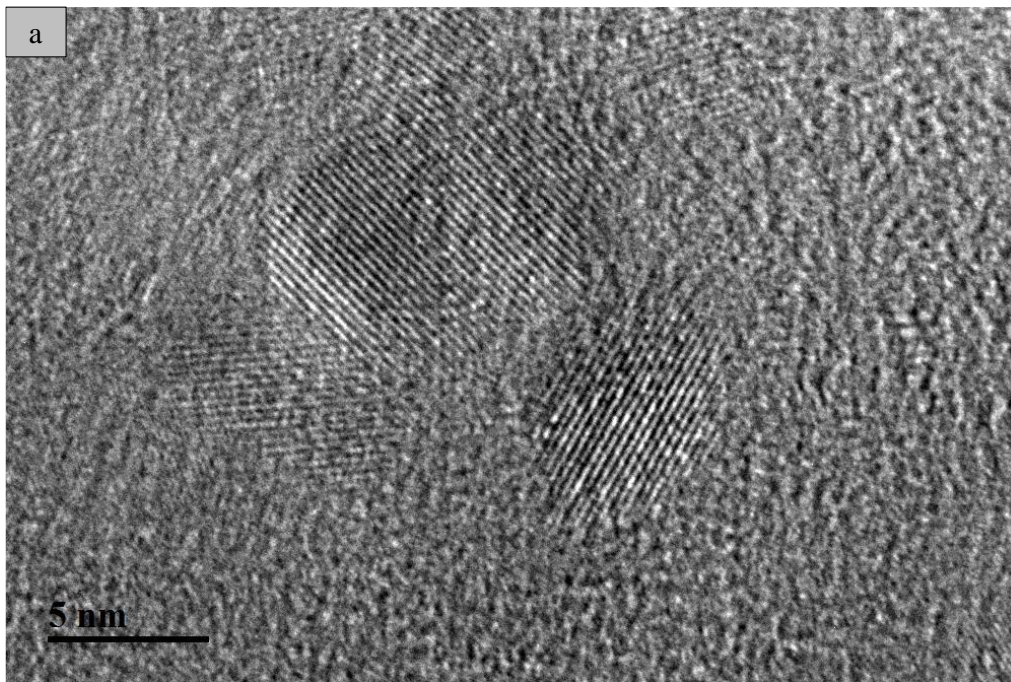


Figure 3.2: TEM images (a) of ZnO NP's and b) of ZnO-SiO₂ (CTAB) NP's. In addition, the Energy-dispersive spectroscopy (EDS) of ZnO-SiO₂ (CTAB) was studied. It is clear from the EDS Weight % analysis that the Zn, Si, and O are the main constituents of adsorbent (Table 3.1) and the area was analyzed are shown in Figure 3.3. Also, the SEM sample holder-Pin stub is the source of Mg and Al elements shown in the results.

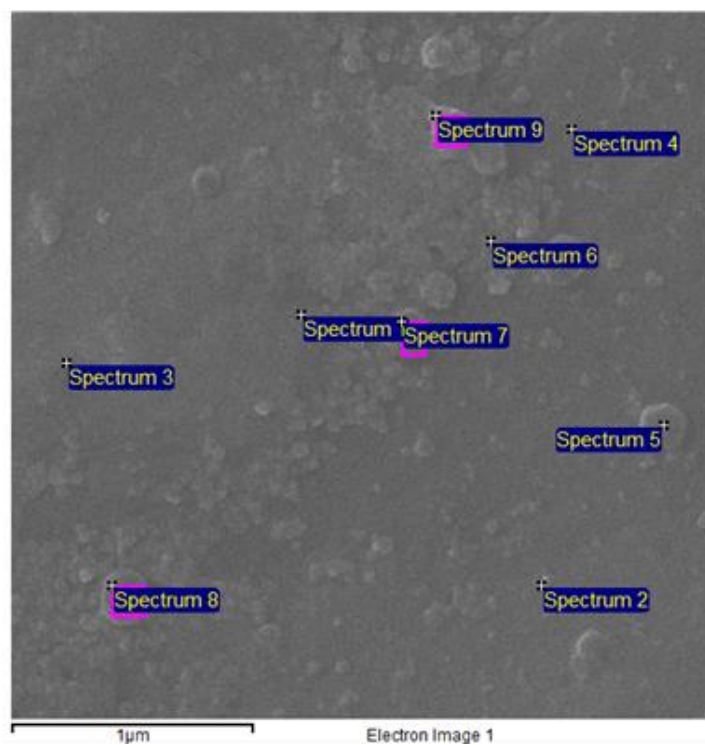


Figure 3.3: EDS analysis of ZnO-SiO₂ (CTAB) NP's.

Table 3.1: Elements analyzed of ZnO-SiO₂ (CTAB) NP's.

Spectrum	In stats.	C	O	Mg	Al	Si	Zn	Total
Spectrum 1	Yes	46.26	9.83	2.41	39.73		1.76	100.00
Spectrum 2	Yes	39.25	13.36	2.51	38.93		5.95	100.00
Spectrum 3	Yes	40.12	14.47	2.45	36.11		6.84	100.00
Spectrum 4	Yes	47.04	5.87	2.60	43.97		0.52	100.00
Spectrum 5	Yes	47.34	6.46	2.51	43.33	0.36		100.00
Spectrum 6	Yes	47.75	4.29	2.50	44.82		0.65	100.00
Spectrum 7	Yes	39.82	7.27	2.95	49.97			100.00
Spectrum 8	Yes	33.75	7.98	3.18	53.88	0.56	0.65	100.00
Spectrum 9	Yes	38.70	7.80	2.86	49.81	0.45	0.39	100.00

FT-IR spectroscopy was carried out to identify the surface functional groups before and after IBU adsorption. The FT-IR spectra of IBU and ZnO-SiO₂ (CTAB) NP's before and after adsorption are shown in Figure 3.4. In spectra of Figure 3.4(a) the peaks in the range 500 – 1500 cm⁻¹ are the fingerprint region of vibration bands of the aromatic ring. The spectrum of IBU shows two characteristic peaks, one of them is at 1709 cm⁻¹ which is attributed to C=O asymmetric stretching vibration, and the other is at 2951 cm⁻¹ which refers to O-H stretching vibration. In spectra of Figure 3.4(b) for ZnO-SiO₂ (CTAB) NP's before adsorption show the characteristics peaks of the corresponding bending vibrational mode at 440 cm⁻¹ which indicate the presence of Si-O and stretching vibrational mode at 578 cm⁻¹ which indicate the presence of ZnO. The intense peaks observed at 1037 and 789 cm⁻¹ are attributed to the asymmetric stretching vibrational mode of the Si-O-Si bridge of the siloxane group and symmetric stretching of the Si-O-Si group. The vibration adsorption peak of the silanol Si-OH bond, which was originally located at 1479 cm⁻¹. The shoulder peak at 963 cm⁻¹ is attributed to Zn-O-Si vibration mode and this peak confirmed that the ZnO is present on the surface of SiO₂.

In Figure 3.4 (c) the intensity after adsorption decrease and show the corresponding bending and stretching vibrational mode at 442 cm^{-1} and at 576 cm^{-1} which indicate the presence of Si-O and ZnO respectively. The intense peaks observed at 1039 and 790 cm^{-1} are attributed to the asymmetric stretching vibrational mode of the Si-O-Si bridge of the siloxane group and symmetric stretching of the Si-O-Si group respectively. The peak in the region 1478 cm^{-1} is attributed to Si-OH vibration mode. The shoulder peaks at 962 cm^{-1} is attributed to Zn-O-Si asymmetric stretching vibrational mode. The peak appeared in the region 1643 cm^{-1} can be attributed to C=O vibration mode which indicated that ibuprofen still at the surface of ZnO-SiO₂ (CTAB) after adsorption. The peaks observed at 2852 and 2922 are attributed to C-H methyl bands symmetric and asymmetric stretching vibrations. ⁹⁸

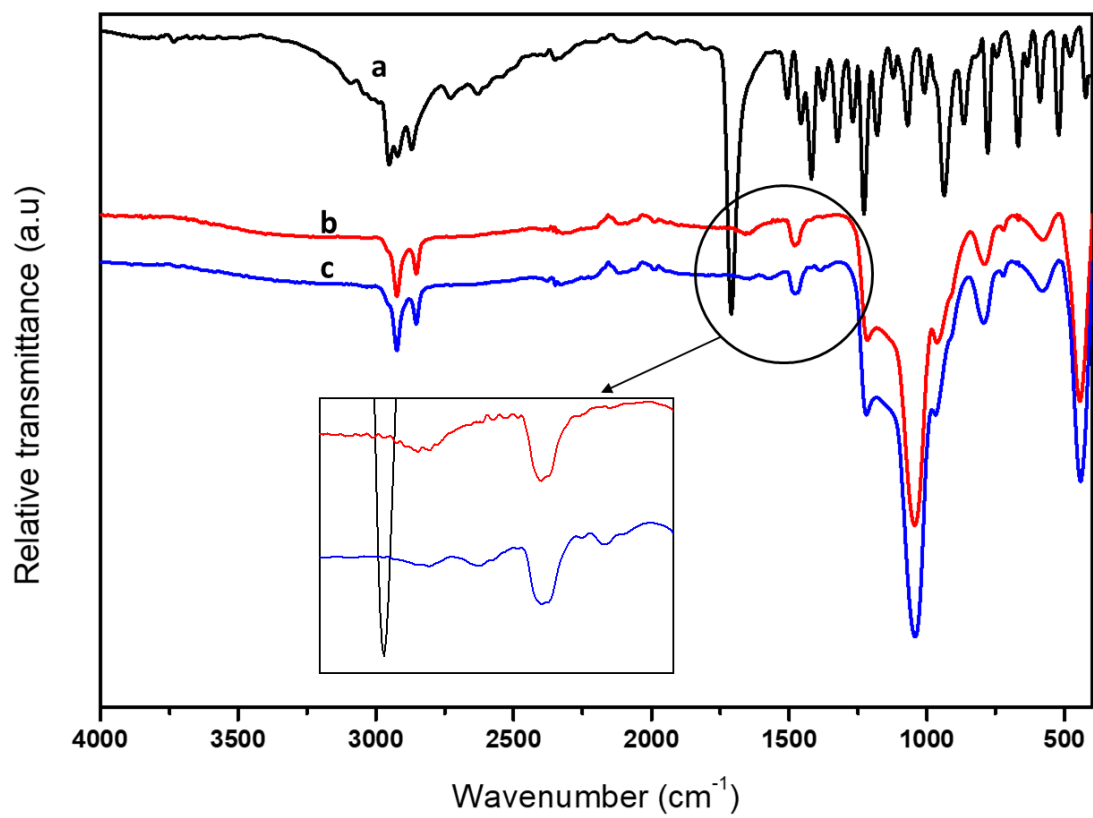


Figure 3.4: FT-IR spectra for a) IBU b) ZnO-SiO₂ (CTAB) c) ZnO-SiO₂ (CTAB) and IBU scanning range 400-4000.

3.2 Characterization of Fe₃O₄ and Fe₃O₄-SiO₂ (CTAB) NP's

The XRD of Fe₃O₄ and Fe₃O₄-SiO₂ (CTAB) NP's was studied in previous work by Al-jabrie.⁹⁵ XRD was used to determine structure and crystalline morphology of Fe₃O₄ and Fe₃O₄-SiO₂ (CTAB) NP's are shown in Figure 3.5. The crystallographic planes (220), (311), (400),(422), (511) and (440) correspond to the peaks at 2θ values of about 30.24°, 35.62°, 43.16°, 53.65°, 57.20°, and 62.88°. After the surface of Fe₃O₄ encapsulation with silica, the weaker and broader bands of amorphous silica located at 2θ values 23° are found in Fe₃O₄-SiO₂ (CTAB) sample. The crystalline morphology shows that the peak intensities of magnetite NPs decrease after surface encapsulation due to the amorphous nature of silica.⁹⁹

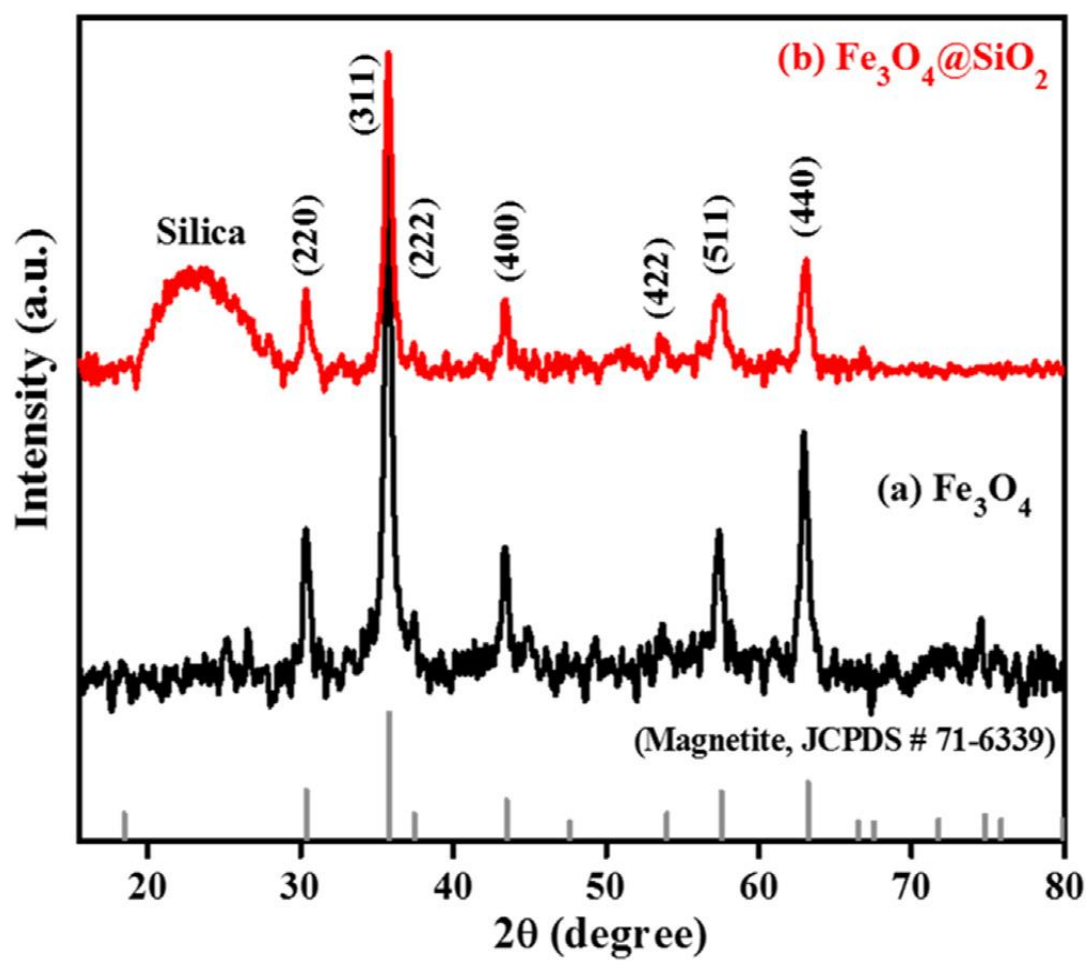


Figure 3.5: XRD patterns of a) Fe_3O_4 b) $\text{Fe}_3\text{O}_4\text{-SiO}_2$ (CTAB) NP's.⁹⁹

The SEM and TEM images of Fe_3O_4 and $\text{Fe}_3\text{O}_4\text{-SiO}_2$ (CTAB) NP's are shown in Figure 3.6 and Figure 3.7 respectively. The magnetite of NP's show as aggregated due to the magnetic properties of Fe_3O_4 NP's. The magnetite has a spherical shape with an average diameter of 10 nm as shown in Figure 3.6(a) and Figure 3.6(b). The selected area was analyzed using selected area electron diffraction pattern (SAED) as presented in Figure 3.7(b), and it reveals a high degree of crystallinity of Fe_3O_4 NP's. The SEM of $\text{Fe}_3\text{O}_4\text{-SiO}_2$ (CTAB) NP's as presented in Figure 3.6(c), and Figure 3.6(d) show a spherical shape with an approximate diameter range of 100 nm. TEM image of $\text{Fe}_3\text{O}_4\text{-SiO}_2$ (CTAB) NP's as presented in Figure 3.7(a) show the Fe_3O_4 NPs are distributed on the surface of the silica and between its layers in an irregular way, so the thickness of SiO_2 is not fixed and this mean that the NP's is not monodispersed.⁹⁵

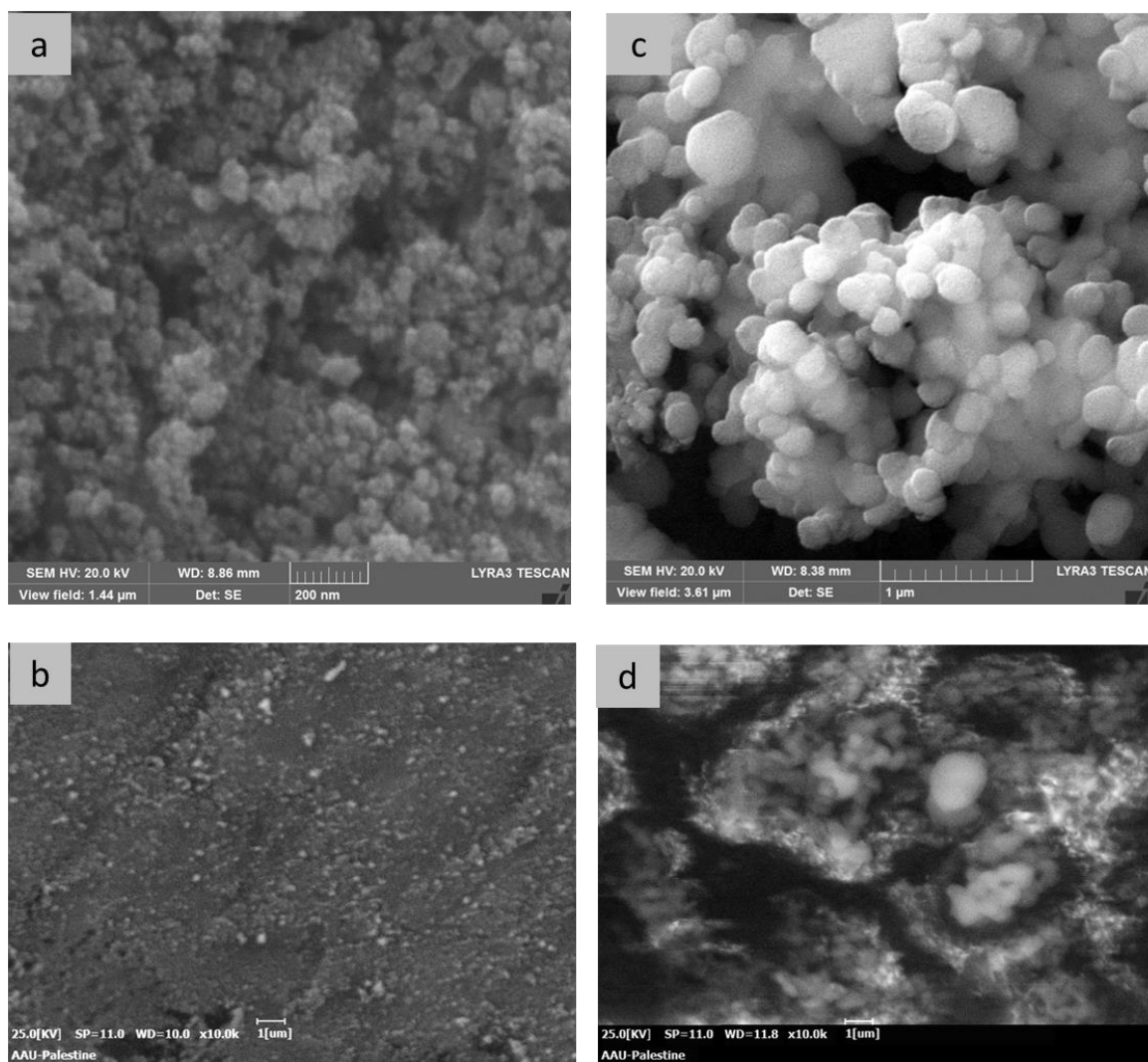


Figure 3.6: SEM images of (a) and (b) are Fe_3O_4 NP's, (c) and (d) are $\text{Fe}_3\text{O}_4\text{-SiO}_2$ (CTAB) NP's.

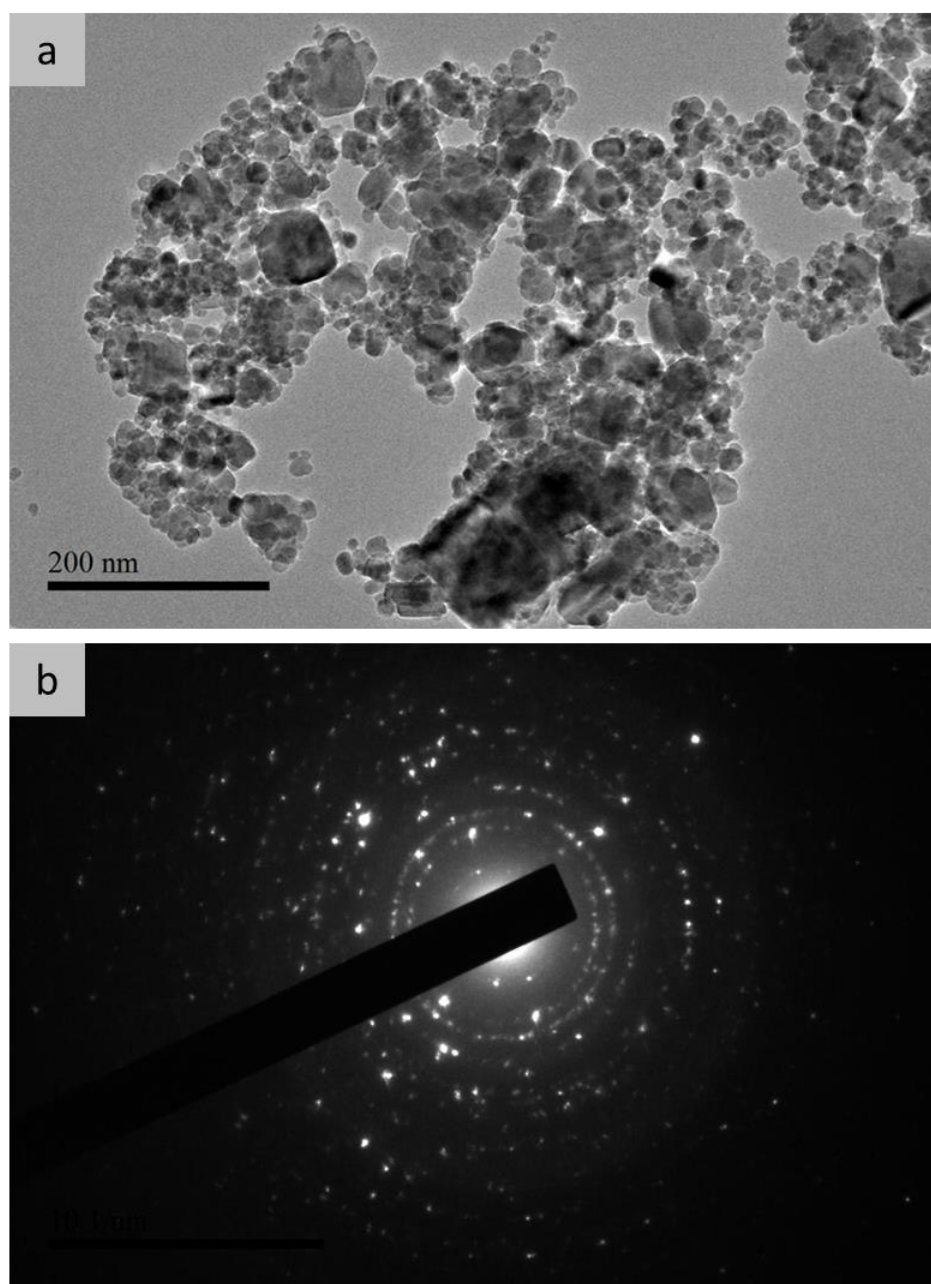


Figure 3.7: (a) TEM image of $\text{Fe}_3\text{O}_4\text{-SiO}_2$ (CTAB) NP's, and (b) SAED of Fe_3O_4 NP's.

The EDS spectra of Fe_3O_4 and $\text{Fe}_3\text{O}_4\text{-SiO}_2$ (CTAB) NP's are shown in Figure 3.8, and Figure 3.9 respectively. Figure 3.8(a) and Figure 3.9(b) shows the areas were analyzed. Figure 3.8(b) shows the EDS pattern imputed to the peaks of O and Fe. Figure 3.9(b) indicates the presence of Si and O and Fe. The EDS results confirm the presence of the expected elements, consisting of iron, oxygen, and silicon.

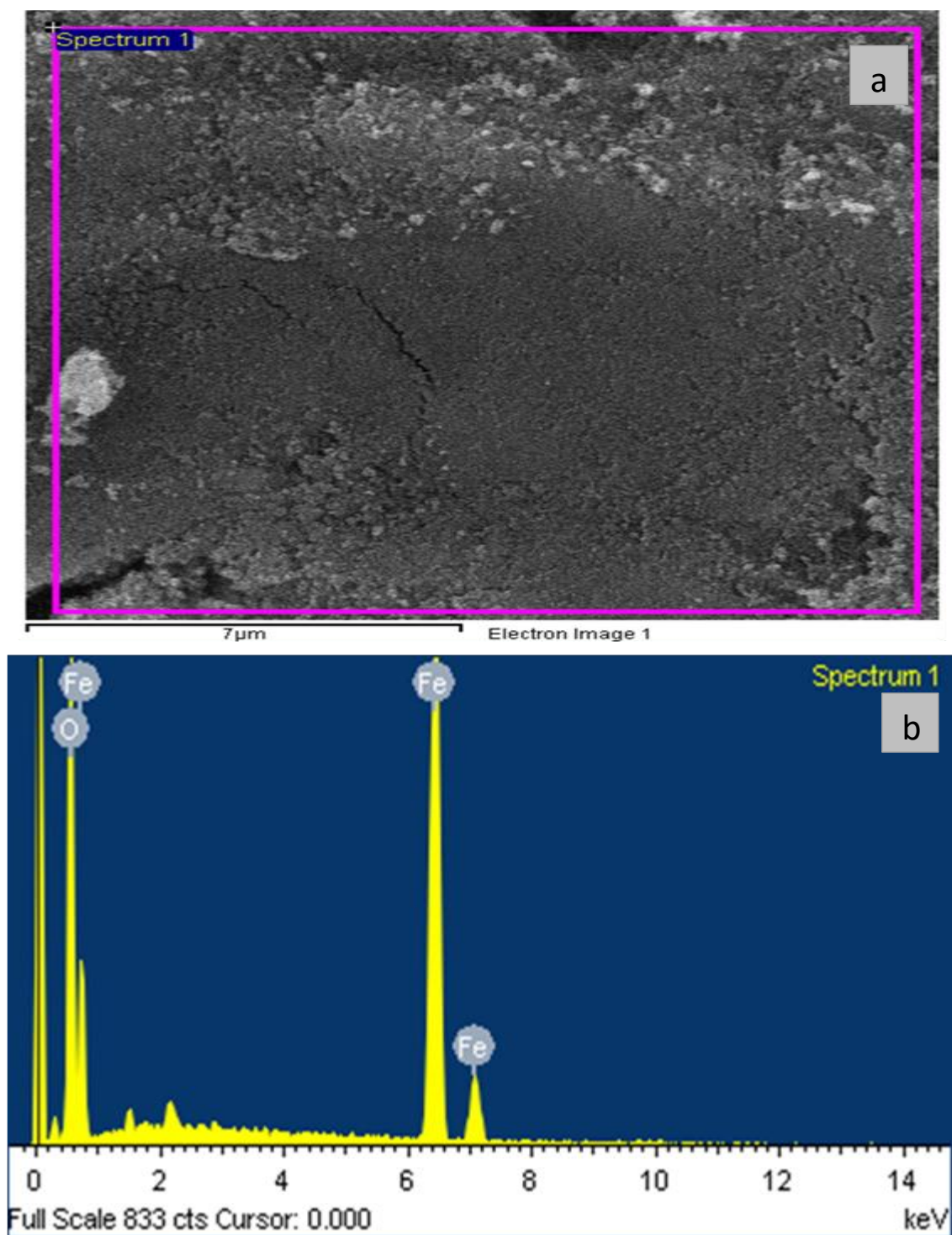


Figure 3.8: EDS analysis of Fe_3O_4 NP's.

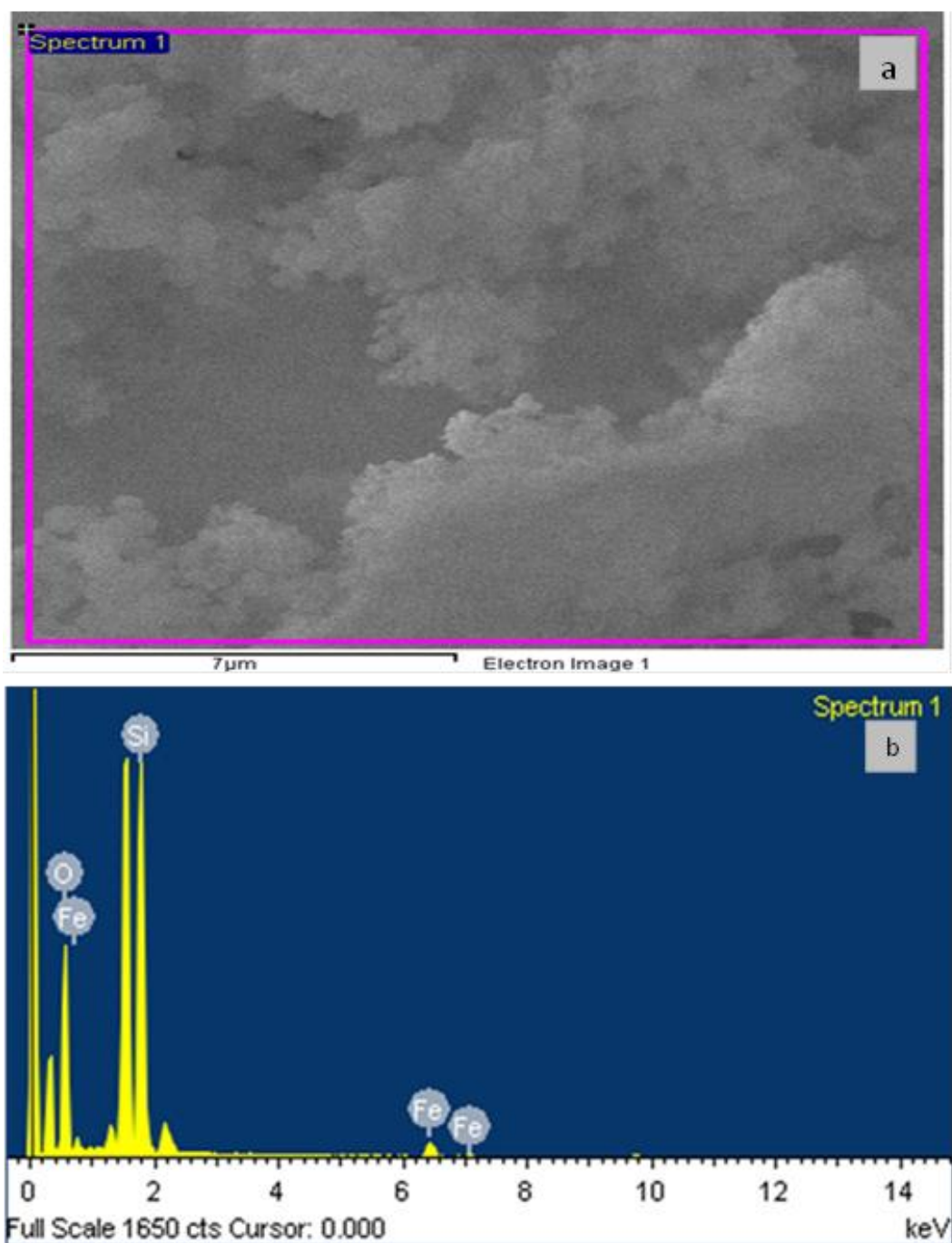


Figure 3.9: EDS analysis of $\text{Fe}_3\text{O}_4\text{-SiO}_2$ (CTAB) NP's.

FT-IR characterization of IBU and Fe₃O₄-SiO₂ (CTAB) NP's before and after adsorption was investigated are shown in Figure 3.10. The spectrum of IBU in Figure 3.10(a) show two characteristic peaks, one of them is at 1709 cm⁻¹ which is attributed to C=O asymmetric stretching vibration, and the other is at 2951 cm⁻¹ which refers to O-H stretching vibration. And peaks in the range 500–1500 cm⁻¹ are the fingerprint region of vibration bands of the aromatic ring. Figure 3.10(b) show the strong peak at 442 cm⁻¹ is due to the stretching vibration of the Si-O bond. The peak around 577 cm⁻¹ is attributed to Fe-O stretching vibration. The intense peaks at 1039 cm⁻¹ and 789 cm⁻¹ are assigned to the asymmetric Si-O-Si stretching vibrational mode and symmetric stretching of the Si-O-Si group, while the shoulder peak at 962 cm⁻¹ is attributed to Fe-O-Si vibration. The peak at 1478 cm⁻¹ is corresponded to silanol Si-OH vibrational mode. The spectra after adsorption in Figure 3.10(c) show the corresponding bending and stretching vibrational mode at 441 cm⁻¹ and at 580 cm⁻¹ which indicate the presence of Si-O and Fe-O respectively. The peak at 790 cm⁻¹ is attributed to symmetric stretching of the Si-O-Si group, while the intense peak at 1042 cm⁻¹ is assigned to the asymmetric Si-O-Si stretching vibrational mode. The peak at 1475 is assigned to silanol

Si-OH vibrational mode. The shoulder peak at 962 cm^{-1} is attributed to Fe-O-Si vibration vibrational mode. After adsorption, the peak observed in the region of 1642 cm^{-1} correspond to C=O vibrational mode. The peaks observed at 2852 cm^{-1} and 2922 cm^{-1} can be attributed to C-H methyl bands symmetric and asymmetric stretching vibrations⁹⁹.

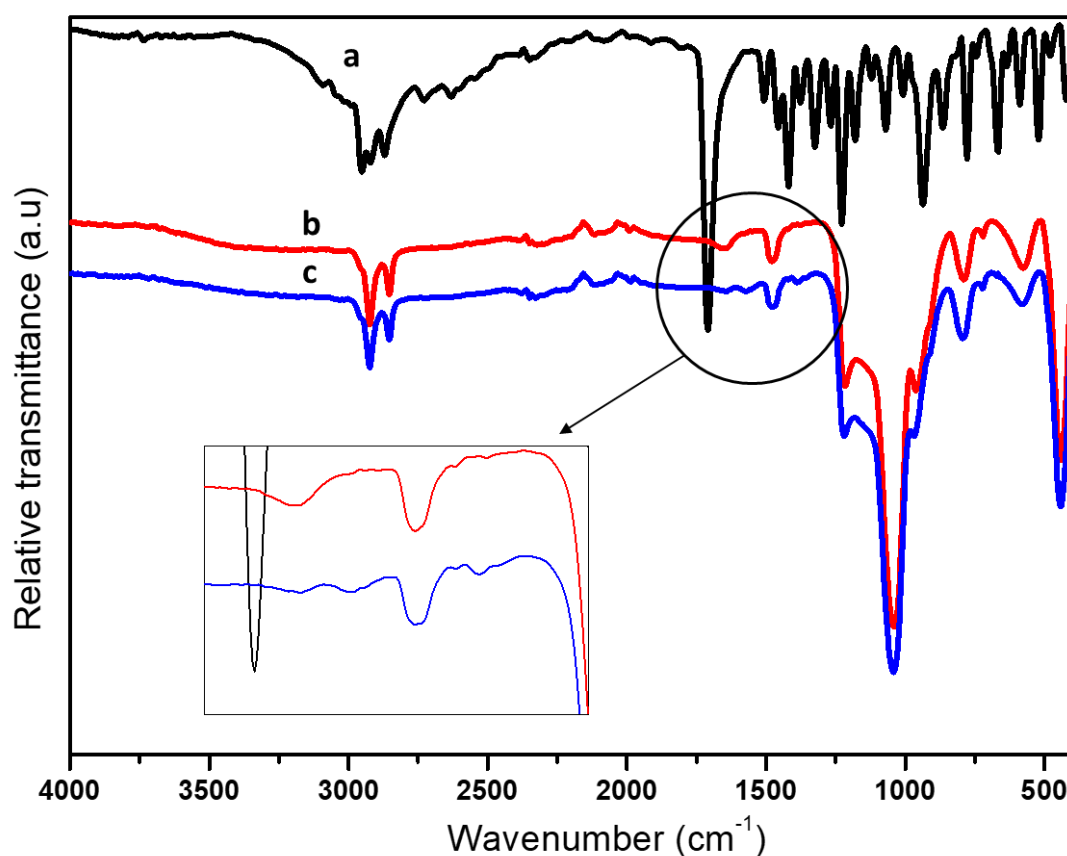


Figure 3.10: FT-IR spectra for a) IBU b) $\text{Fe}_3\text{O}_4\text{-SiO}_2$ (CTAB) c) $\text{Fe}_3\text{O}_4\text{-SiO}_2$ (CTAB) and IBU.

3.3. IBU removal kinetics

The kinetics experiments were performed to study the adsorption rate and to describe the kinetics of IBU adsorption process. The adsorption of IBU adsorbed onto Fe₃O₄-SiO₂ (CTAB) and ZnO-SiO₂ (CTAB) NP's were performed at an initial concentration of 25 mg/L of IBU for a period of time. The amount of IBU adsorbed on the surface of Fe₃O₄-SiO₂ (CTAB) and ZnO-SiO₂ (CTAB) NP's was calculated using a mass balance equation:⁸⁶

$$Q = (C_0 - C) \frac{V}{m} \dots\dots\dots (10)$$

Where Q is the concentration of IBU on the adsorbent (mg/g),

C₀ is the initial concentration of IBU (mg/L),

C is the IBU concentration in solution given at the time,

V is the volume of solution (L),

m is the mass of adsorbent (mg) .

The effects of contact time on the concentration of IBU for the two types of nanoparticles are shown in Figure 3.11.

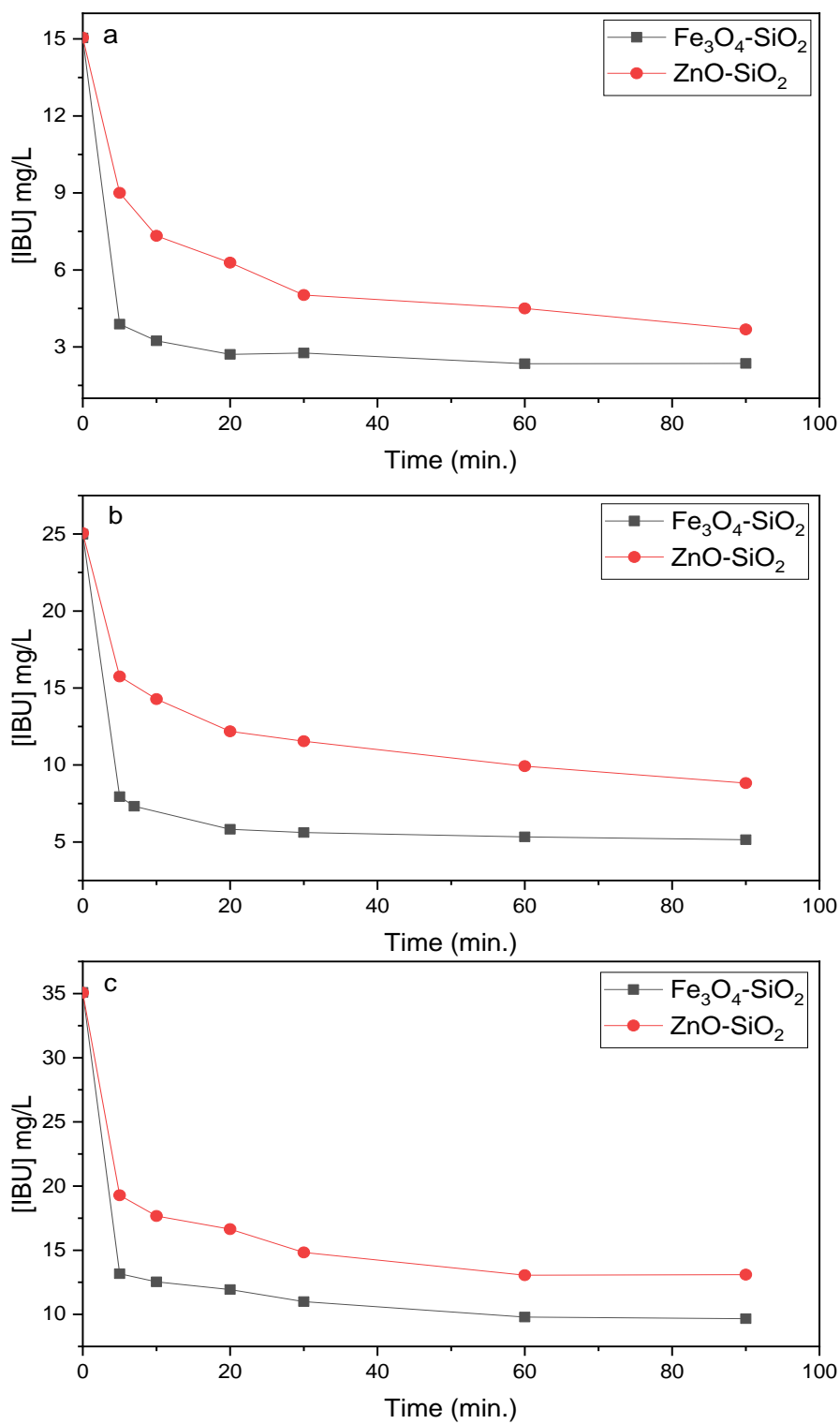


Figure 3.11: Effect of contact time on the concentration of IBU for Fe₃O₄-SiO₂ (CTAB) and ZnO-SiO₂ (CTAB) NP's; (a) 15 mg/L, (b) 25 mg/L, (c) 35 mg/L at 298 K.

The IBU removal percentage was calculated using the following equation: ¹⁰⁰

$$\% \text{ Removal} = \frac{C_0 - C_e}{C_0} * 100\% \dots \dots \dots (11)$$

Where C_0 is the initial concentration of IBU in the solution (mg/L),

C_e is the equilibrium concentration of IBU in the solution (mg/L).

The effects of contact time on the removal efficiency of IBU for the two types of nanoparticles at different concentration are shown in Figure 3.12.

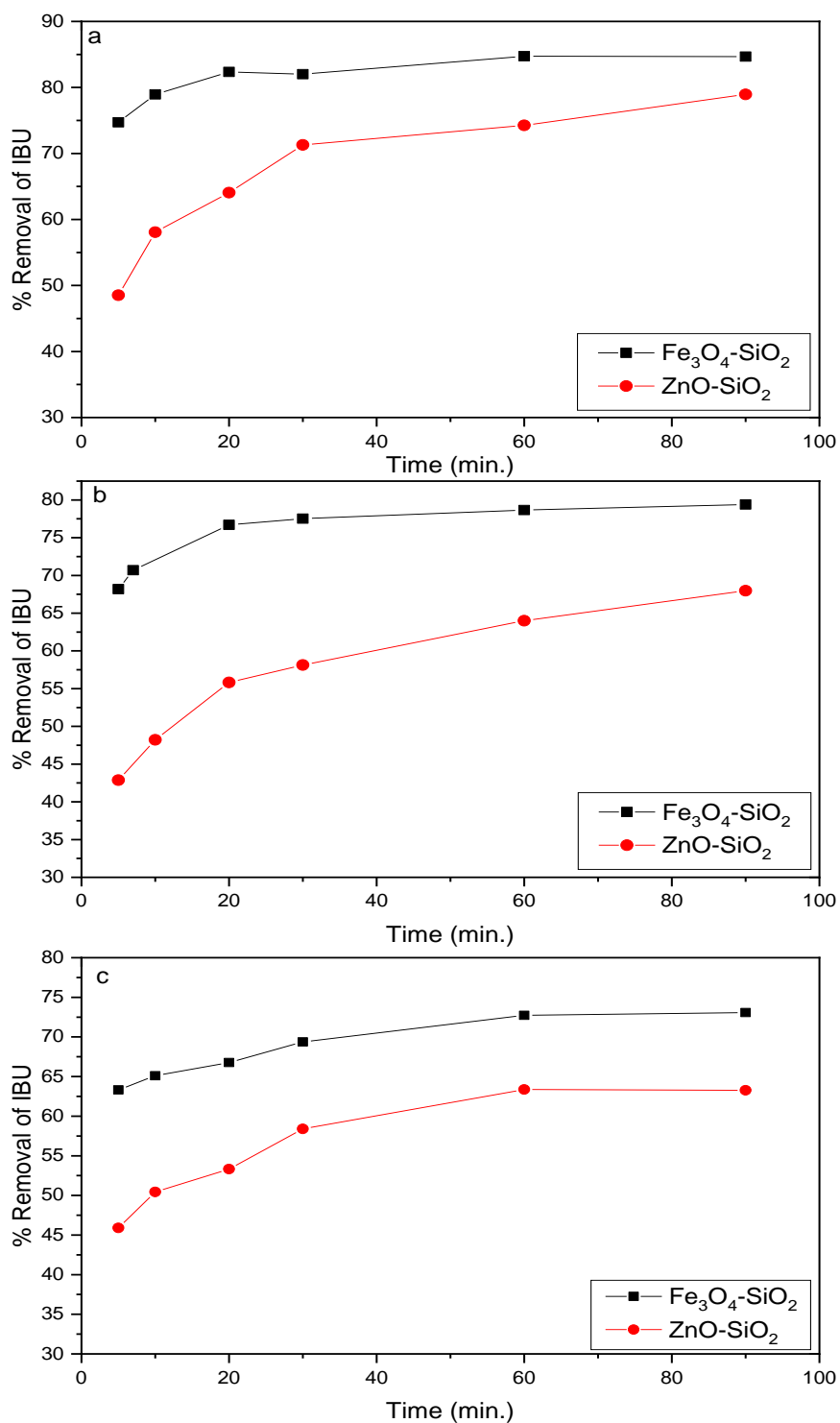


Figure 3.12: Effect of contact time on removal efficiency of IBU for ZnO-SiO_2 (CTAB) and $\text{Fe}_3\text{O}_4\text{-SiO}_2$ (CTAB) NP's, (a) 15 mg/L, (b) 25 mg/L, (c) 35 mg/L at 298 K.

As seen in Figure 3.11 and Figure 3.12 , the concentration of IBU in aqueous solution decreases with time, and the adsorption of IBU on two types of NP's increase with time so in the first period of time, the removal efficiency of IBU increase, then it almost invariant when equilibrium is approached.

The experimental data for the adsorption of IBU onto Fe₃O₄-SiO₂ (CTAB) and ZnO-SiO₂ (CTAB) NP's shown in Fig. 3.11 were tested by Lagergren pseudo-first-order and pseudo-second-order models.⁸⁷⁻⁸⁸

The linear Lagergren pseudo-first-order model represented as:

$$\ln(Q_e - Q) = \ln Q_e - k_1 t \dots\dots\dots (12)$$

Where Q_e and Q are the amounts of IBU (mg/g) adsorbed onto the adsorbent at equilibrium, and at any time, respectively, and k_1 is the first-order rate constant (min^{-1}), and t is the time (min). Linear relationship is obtained by plotting $\ln(Q_e - Q)$ versus time. A resulting figure of this relationship is plotted in Figure 3.13 where the values of k_1 and Q_e are obtained from the slope and intercept, respectively.

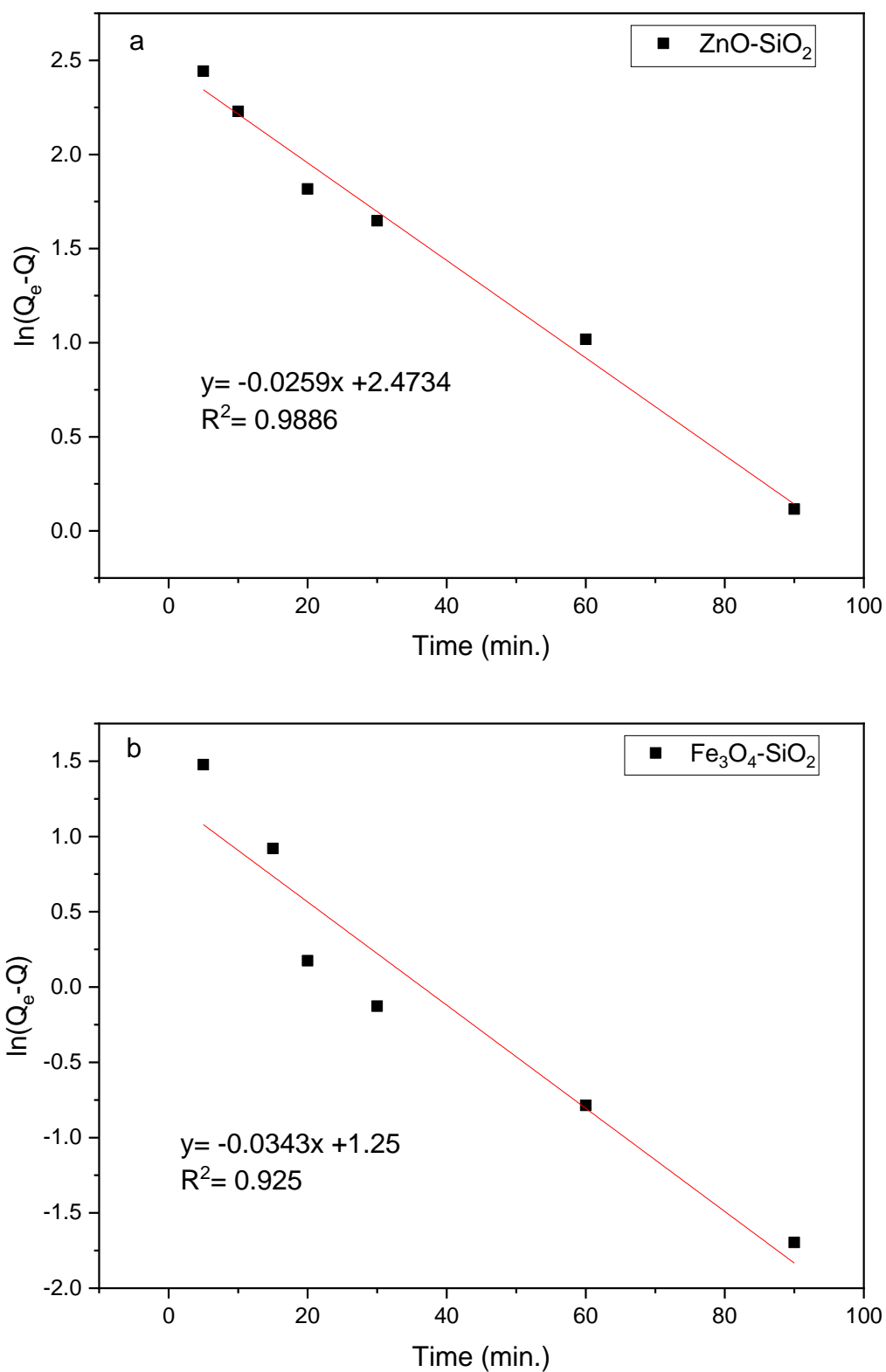


Figure 3.13: The pseudo-first-order model for adsorption of IBU on: a) ZnO-SiO₂ (CTAB) NP's b) Fe₃O₄-SiO₂ (CTAB) NP's at 298 K and 25 mg/L.

As Figure 3.13 shows, the correlation coefficient (R^2) has low value and the data is not fitted with pseudo-first-order model. So another kinetic model was studied to fit with the experimental data.

The linear fits obtained by pseudo-second-order kinetics are shown in Figure 3.14.

The nonlinear pseudo-second-order form of Ho equation is given as:

$$Q = \frac{k \cdot t \cdot Q_e^2}{1 + k \cdot Q_e \cdot t} \dots \dots \dots (13)$$

The linearized pseudo-second-order model as given by Ho: ¹⁰¹

$$\frac{t}{Q} = \frac{1}{k_2 Q_e^2} + \frac{1}{Q_e} t \dots \dots \dots (14)$$

Where Q is the amount of the IBU adsorbed on the adsorbent (mg/g).

Q_e is the amount of the IBU adsorbed on the adsorbent at equilibrium (mg/g).

k_2 is the rate constant of the pseudo-second-order adsorption ($\text{g mg}^{-1} \text{min}^{-1}$).

t is the time (min).

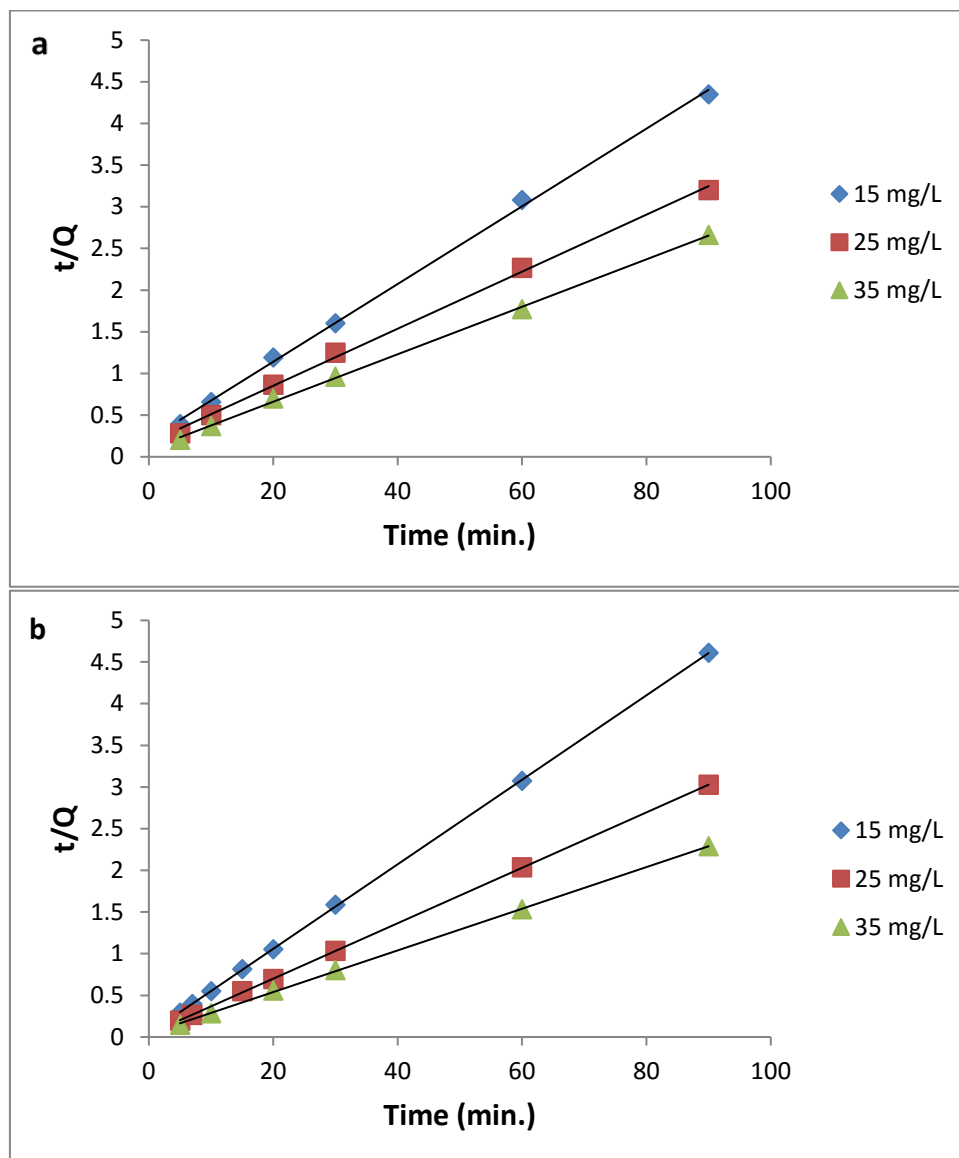


Figure 3.14: The pseudo-second-order linear fits for IBU adsorption via a) ZnO-SiO₂ (CTAB) NP's b) Fe₃O₄-SiO₂ (CTAB) NP's at 298 K.

The kinetic parameters for two kinetic models for two types of NP's are given in Table 3.2 and Table 3.3. The data seems to fit well to the pseudo-second-order kinetics, and Table 3.2 and Table 3.3 show that the values of R^2 are larger than 0.99. Moreover, in pseudo second order kinetics, the calculated values of adsorption capacity ($Q_{e,(cal)}$) are very close to the experimental value of adsorption capacity ($Q_{e,(exp)}$) but large differences exist between $Q_{e,(exp)}$ and $Q_{e,(cal)}$ for pseudo-first-order model. Moreover, it can be indicated that the highest adsorption capacity (Q) was obtained at the greatest ibuprofen concentration.

This indicates that the adsorption of IBU on ZnO-SiO₂ (CTAB) and Fe₃O₄-SiO₂ (CTAB) NP's are well described by the pseudo-second-order model.

Table 3.2: Kinetic parameters for IBU adsorption on ZnO-SiO₂ (CTAB) at 298K.

Pseudo-first order Kinetics					Pseudo-second order kinetics			
C ₀ (mg/L)	Q _{e, exp} (mg g ⁻¹)	Q _{e, cal} (mg g ⁻¹)	k ₁ (min ⁻¹)	R ²	Q _{e, exp} (mg g ⁻¹)	Q _{e, cal} (mg g ⁻¹)	k ₂ (g mg ⁻¹ min ⁻¹)	R ²
15	20.70	8.197	0.0263	0.9606	20.70	21.45	0.01041	0.9988
25	28.11	11.86	0.0259	0.9886	28.11	29.24	0.00697	0.9983
35	33.81	10.19	0.0298	0.9012	33.81	34.84	0.01058	0.9990

Table 3.3: Kinetic parameters for IBU adsorption on Fe₃O₄-SiO₂ (CTAB) at 298K.

Pseudo-first order Kinetics					Pseudo-second order kinetics			
C ₀ (mg/L)	Q _{e, exp} (mg g ⁻¹)	Q _{e, cal} (mg g ⁻¹)	k ₁ (min ⁻¹)	R ²	Q _{e,exp} (mg g ⁻¹)	Q _{e, cal} (mg g ⁻¹)	k ₂ (g mg ⁻¹ min ⁻¹)	R ²
15	19.52	2.058	0.0332	0.8859	19.52	19.68	0.0577	0.9999
25	29.75	3.490	0.0343	0.926	29.75	29.94	0.0316	0.9999
35	39.35	6.402	0.028	0.9561	39.35	40.00	0.01598	0.9997

On the other hand, the relation between Q and t can be illustrated using other models. The pseudo second order rate equations represented by Shahwan equation, as shown in Figure 3.14.

Shahwan model differs than Ho model in the method of determination of the rate constant and its unit, and the interpretation of Q_m .¹⁰²

The nonlinear form of Shahwan equation is given as:

$$Q = \frac{Q_m C_0 k_2 t}{C_0 k_2 t + 1} \dots \dots \dots (15)$$

The linearized equation of this model is given in the following form:

$$\frac{t}{Q} = \frac{1}{Q_m C_0 k_2} + \frac{1}{Q_m} t \dots \dots \dots (16)$$

Where; Q is the amount of IBU adsorbed on the adsorbent (mg/g).

Q_m is the amount of IBU that would be sorbed if the sorption reaction approaches completion (equals to V/ m multiplied by C_0).

C_0 is the initial concentration of the IBU (mg/L).

k_2 is the rate constant ($L \text{ mg}^{-1} \text{ min}^{-1}$).

t is the time (min.).

The linear plots of t/Q vs. t are shown in Figure 3.14.

The calculated Q values, and the calculated kinetic rate constants of pseudo second order obtained using the linearized equations (14 and 16), for two types of NP's are given in Table 3.4 and Table 3.5.

Table 3.4: The kinetic parameters for adsorption IBU onto ZnO-SiO₂ (CTAB) NP's of the pseudo second order linear fits using equations 14 and 16 at different concentration at 298K.

Ho Equation	15 mg/L	25 mg/L	35 mg/L
Slope	0.0466	0.0342	0.0285
R ²	0.9988	0.9983	0.9992
Intercept	0.2086	0.1678	0.0912
k ₂ (g.mg ⁻¹ .min ⁻¹)	0.0104	0.00697	0.0106
Q _{e (cal)} (mg/g)	21.5	29.2	34.8
Q _{e (exp)} (mg/g)	20.7	28.1	35
Shahwan Equation			
Slope	0.0466	0.0342	0.0285
R ²	0.9988	0.9983	0.9992
Intercept	0.2086	0.1678	0.0912
k ₂ (L.mg ⁻¹ .min ⁻¹)	0.0128	0.0363	0.0282
Q _{m (cal)} (mg/g)	21.5	29.2	34.8
Q _{m (exp)} (mg/g)	20.7	28.1	35

Table 3.5: The kinetic parameters for adsorption IBU onto Fe₃O₄-SiO₂ (CTAB) NP's of the pseudo second order linear fits using equations 14 and 16 at different concentration at 298K.

Ho Equation	15 mg/L	25 mg/L	35 mg/L
Slope	0.0508	0.0334	0.025
R ²	0.9999	0.9999	0.9997
intercept	0.0383	0.0287	0.0391
k ₂ (g.mg ⁻¹ .min ⁻¹)	0.0673	0.0388	0.0159
Q _{e (cal)} (mg/g)	19.7	29.9	40
Q _{e (exp)} (mg/g)	19.5	29.7	39.3
Shahwan Equation			
Slope	0.0508	0.0334	0.025
R ²	0.9999	0.9999	0.9997
intercept	0.0383	0.0287	0.0391
k ₂ (L.mg ⁻¹ .min ⁻¹)	0.0862	0.0465	0.0178
Q _{m (cal)} (mg/g)	19.7	29.9	40
Q _{m (exp)} (mg/g)	19.5	29.7	39.3

Table 3.4 and Table 3.5 show that the rate constant of IBU removal by Fe₃O₄-SiO₂ (CTAB) is higher than the rate constant of ZnO-SiO₂ (CTAB), so the removal process by Fe₃O₄-SiO₂ (CTAB) is faster than ZnO-SiO₂ (CTAB) and the calculated Q_m values are close to the experimental Q_m values.

In order to check which of the two equations provide closer correlation with the experimental results the calculated k_2 and Q values were inserted in the nonlinear equations (13 and 15) then from the calculated Q values the model prediction was obtained. The experimental and predicted data of Q for two types of NP's were plotted as shown in the Figure 3.15 and Figure 3.16.

In Figure 3.15(a), for ZnO-SiO₂ (CTAB) NP's the correlation are preferable at all concentrations while Figure 3.15(b) show that best correlation at lower concentration 15 mg/L.

On the other hand, Figure 3.16(a &b), for ZnO-SiO₂ (CTAB) NP's the two models showed similar correlation, both models fitted to the experimental data at all concentrations.

The results indicate that the Shahwan equation (15) is better valid when the sorption reaction is driven far towards the products.

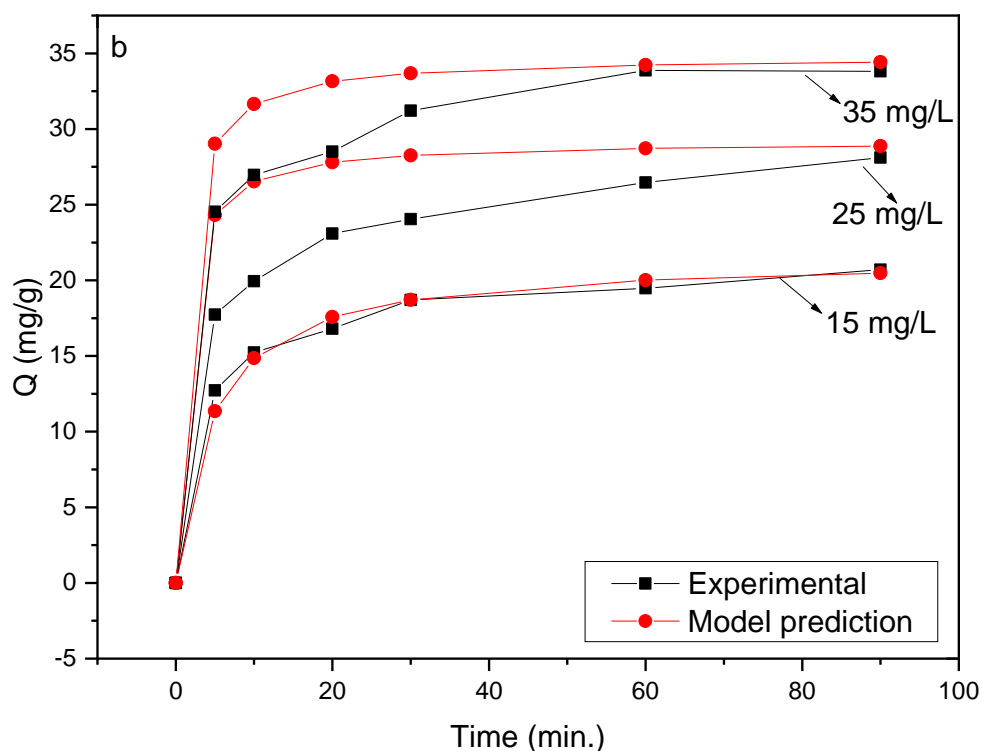
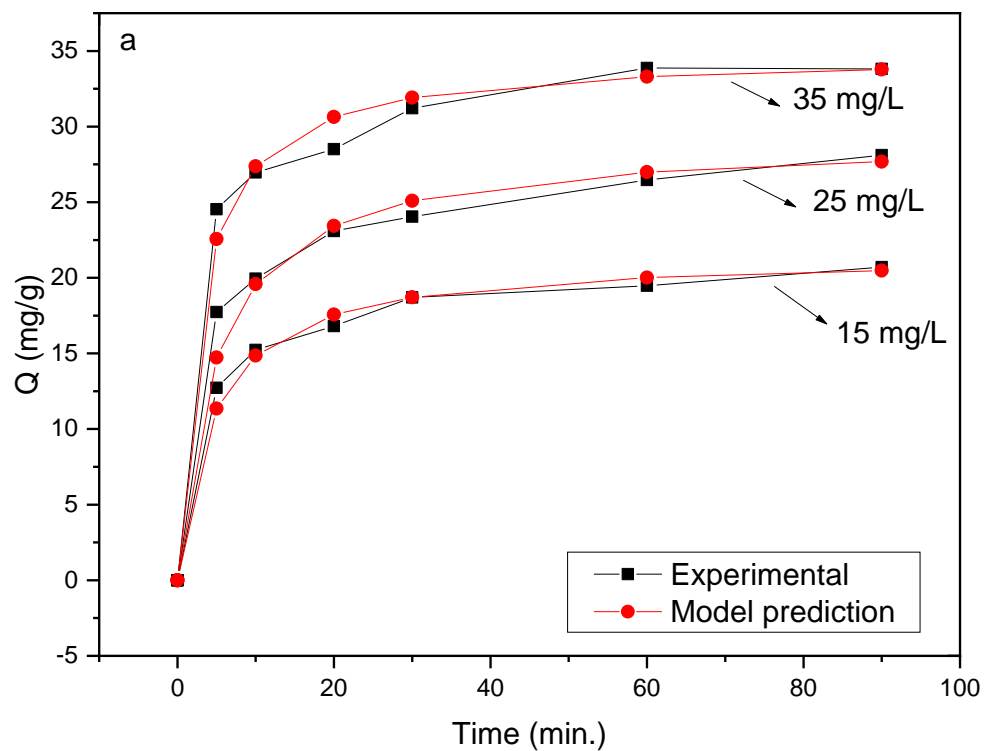


Figure 3.15: Nonlinear fits of the kinetic data of IBU removal by ZnO-SiO₂ (CTAB) NPs; (a) using Ho equation (b) using Shahwan equation at different concentration.

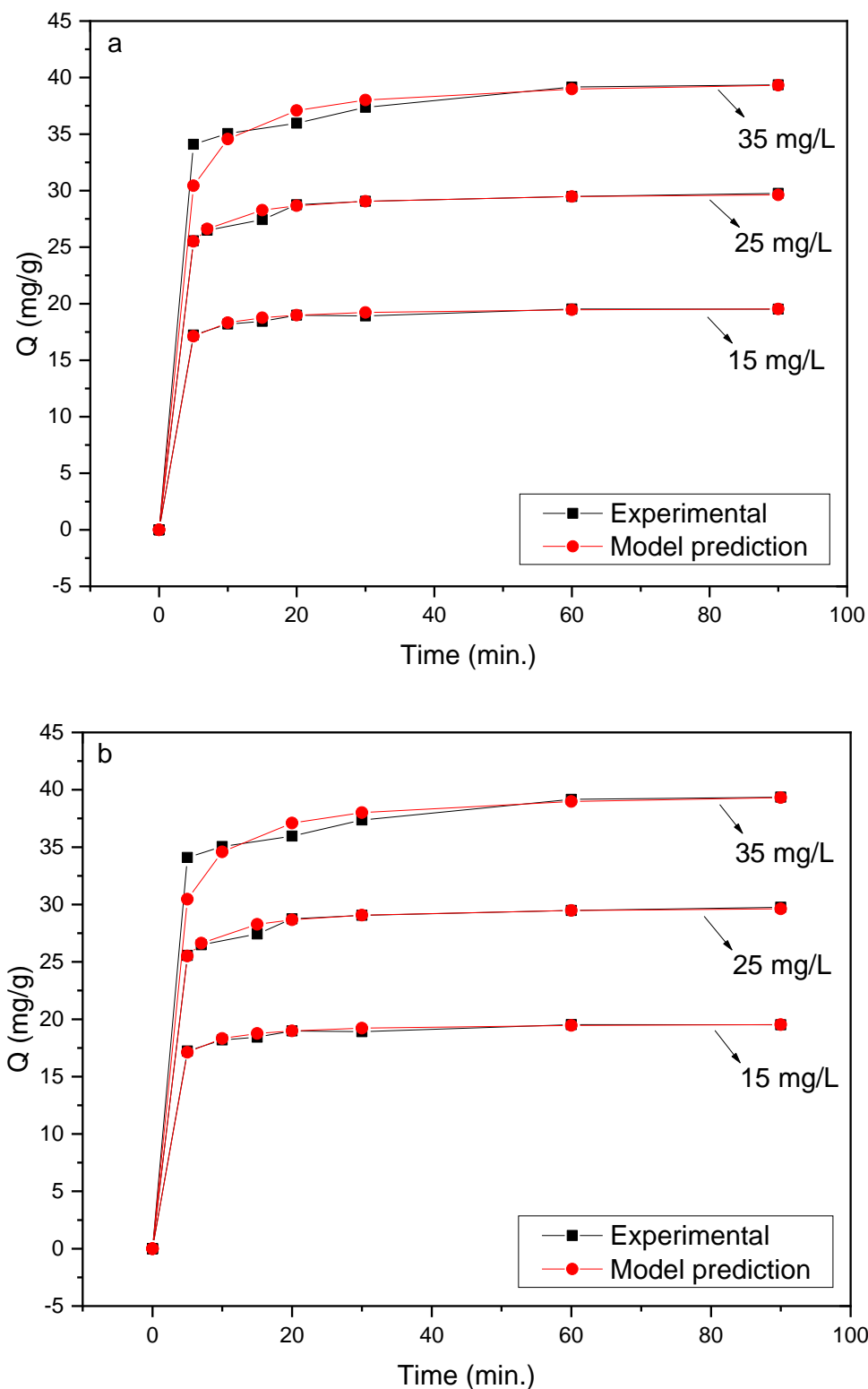


Figure 3.16: Nonlinear fits of the kinetic data of IBU removal by $\text{Fe}_3\text{O}_4\text{-SiO}_2$ (CTAB) NPs; (a) using Ho equation (b) using Shahwan equation at different concentration.

As a further test of the correlation, the Chi test was performed to estimate the difference between experimental values and predicted values also was used to compare the sufficiency of the two kinetic equations (14 and 16). The following equation was used to calculate the Chi square values:

$$\chi^2 = \sum_1^n \frac{(Q_{exp} - Q_{model})^2}{Q_{model}} \dots \dots \dots (17)$$

The smaller the value of χ^2 means that the difference between experimental and predicted values is smaller. As Table 3.6 shows the values of χ^2 for two models of Ho and Shahwan using ZnO-SiO₂ (CTAB) NP's, at the concentration 15 mg/L the Shahwan equation and Ho equation provides similar Q values to the experimental values, while at 25 and 35 mg/L the Ho equation provides closer Q values to the experimental values. But Table 3.7, for Fe₃O₄-SiO₂ (CTAB) NP's, shows that the Chi test provide similar values at all concentration.

Table 3.6: Values of Q obtained from experiment, values of Q predicted by equations (13 and 15), and the Chi –test values for the sorption systems of ZnO-SiO₂ (CTAB) NP's at different concentration.

Time (min.)	Q _{exp} (mg/g)	Q _{model} (mg/g)	Chi test (Ho model)	Q _{model} (mg/g)	Chi test (Shahwan model)
at 15 mg/L					
5	12.7	11.3	0.167	11.35	0.164
10	15.2	14.8	0.0095	14.9	0.0091
20	16.8	17.6	0.0336	17.6	0.0341
30	18.7	18.7	0.00	18.7	0.00
60	19.5	20.0	0.0142	20.01	0.0144
90	20.70	20.5	0.00234	20.5	0.0023
		χ^2	0.227	χ^2	0.224
at 25 mg/L					
5	17.7	14.7	0.614	24.3	1.8
10	19.9	19.6	0.0068	26.5	1.63
20	23.1	23.4	0.0054	27.80	0.801
30	24.0	25.09	0.044	28.3	0.628
60	26.5	26.98	0.0099	28.7	0.176
90	28.1	27.7	0.0066	28.9	0.0201
		χ^2	0.70	χ^2	5.05
at 35 mg/L					
5	24.5	22.6	0.171	29.03	0.697
10	26.9	27.4	0.00627	31.7	0.696
20	28.5	30.6	0.149	33.2	0.652
30	31.2	31.9	0.0152	33.7	0.181
60	33.9	33.3	0.010	34.2	0.0038
90	33.8	33.8	0.00	34.4	0.0105
		χ^2	0.353	χ^2	2.24

Table 3.7: Values of Q obtained from experiment, values of Q predicted by equations (13 and 15), and the Chi –test values for the sorption systems of Fe₃O₄-SiO₂ (CTAB) NP's at different concentration.

Time (min.)	Q _{exp} (mg/g)	Q _{model} (mg/g)	Chi test (Ho model)	Q _{model} (mg/g)	Chi test (Shahwan model)
at 15 mg/L					
5	17.2	17.1	0.0007	17.1	0.00063
10	18.2	18.3	0.00075	18.3	0.0008
20	18.98	18.98	0.00	18.98	0.00
30	18.9	19.2	0.005	19.2	0.0049
60	19.5	19.4	0.000305	19.4	0.0003
90	19.5	19.5	0.00	19.5	0.00
		χ^2	0.0067	χ^2	0.0067
at 25 mg/L					
5	25.6	25.5	0.00013	25.5	0.000102
10	26.5	26.6	0.00059	26.6	0.00064
20	28.7	28.7	0.00025	28.7	0.00024
30	29.06	29.06	0.00	29.06	0.00
60	29.5	29.5	0.00	29.5	0.00
90	29.8	29.6	0.00066	29.6	0.000661
		χ^2	0.00164	χ^2	0.00164
at 35 mg/L					
5	34.01	30.4	0.441	30.5	0.43
10	35.06	34.6	0.0069	34.6	0.0064
20	35.9	37.08	0.034	37.1	0.035
30	37.4	38.00	0.011	38.02	0.011
60	39.2	38.98	0.0009	38.98	0.00084
90	39.3	39.3	0.00	39.3	0.00
		χ^2	0.494	χ^2	0.486

3.4. Effect of initial IBU concentration

The effect of adsorbate concentration was studied at different initial concentrations of IBU 15, 25, 35 mg/L for the two types of silica NP's at 298 K. The percentage removal of IBU was calculated using % removal equation is illustrated in Figure 3.17.

The results indicate that IBU was adsorbed at low and at high concentration until the adsorbent sites approached saturation as time elapsed. So, the extent of removal did not increase further with increasing IBU initial concentration due to the limited number of active sites on the surface of $\text{Fe}_3\text{O}_4\text{-SiO}_2$ (CTAB) and ZnO-SiO_2 (CTAB) NP's.

Therefore, the percentage removal of IBU is observed to decrease as its concentration increases, so at 35 mg/L the removal percent of $\text{Fe}_3\text{O}_4\text{-SiO}_2$ (CTAB) and ZnO-SiO_2 (CTAB) NP's were reached to 73.07% and 63.26% respectively, as shown in Figure 3.17.

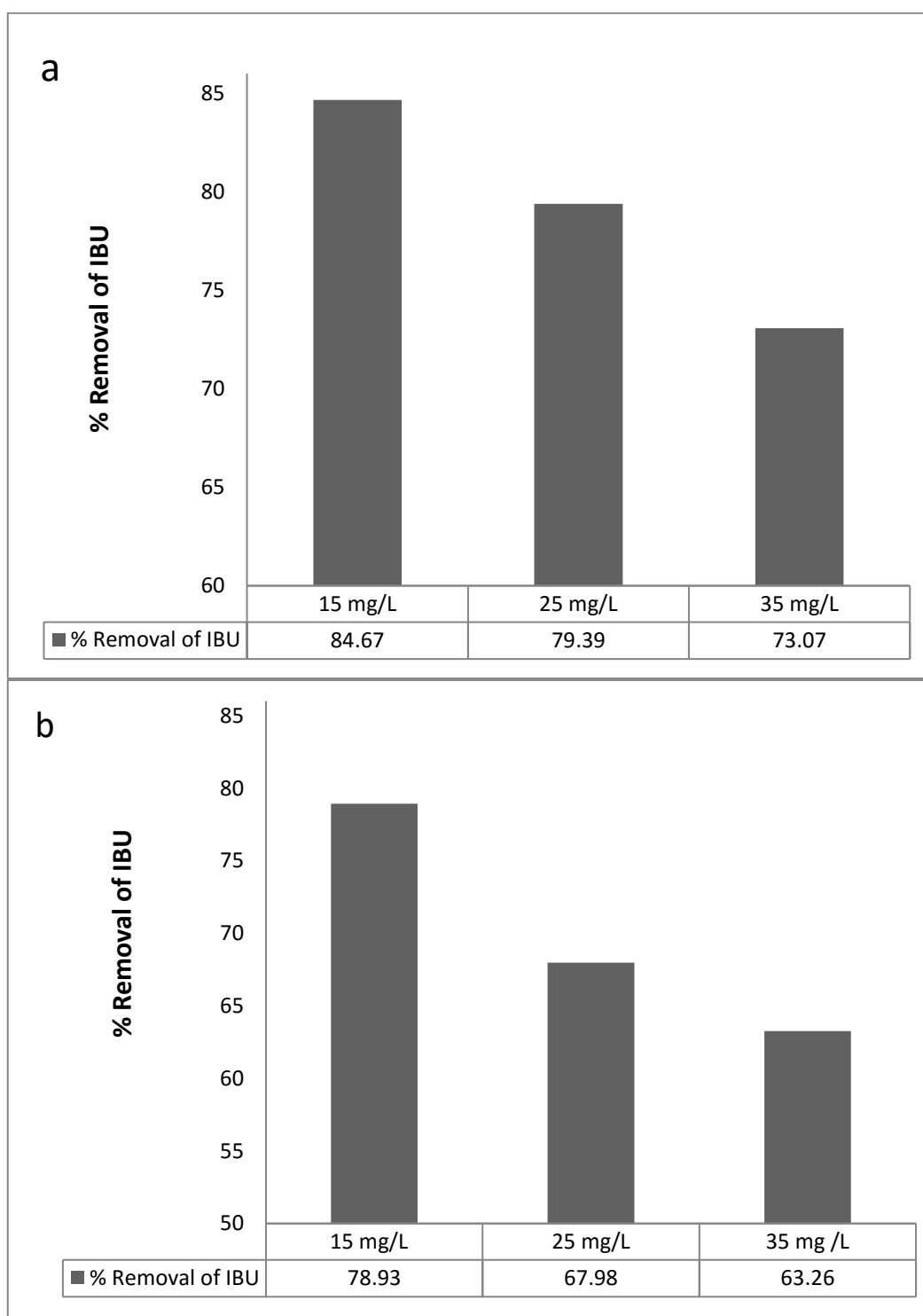


Figure 3.17: Effect of initial IBU concentration on its percentage removal; a) $\text{Fe}_3\text{O}_4\text{-SiO}_2$ (CTAB) b) ZnO-SiO_2 (CTAB) NP's.

In addition, the concentration of IBU on the sorbent surface (Q , mg/g) was also calculated. It can be seen from Table 3.8 that there is an increase in Q value with increasing initial IBU concentration for the two types of silica nanoparticles. So the highest adsorption capacity was obtained at the greatest IBU concentration.

Table 3.8: The calculated Q values of adsorbed IBU onto $\text{Fe}_3\text{O}_4\text{-SiO}_2$ (CTAB) and ZnO-SiO_2 (CTAB) NP's at different initial concentrations.

C_0 (mg/L)	Q (mg/g)	
	$\text{Fe}_3\text{O}_4\text{-SiO}_2$ (CTAB) NP's	ZnO-SiO_2 (CTAB) NP's
15	19.5	20.7
25	29.7	28.1
35	39.3	33.8

3.5 Adsorption isotherms

The adsorption isotherms are used to model the partitioning of IBU between the liquid and solid phases, when equilibrium is attained. The data of adsorption of IBU on to Fe₃O₄-SiO₂ (CTAB) and ZnO-SiO₂ (CTAB) NP's were fitted to Langmuir and Freundlich isotherms. The adsorbed amount of IBU at equilibrium, q_e (mg/g) was calculated by mass balance equation as given in equation 10.

The nonlinear Langmuir adsorption isotherm is given as:

$$Q_e = \frac{Q_m K_L C_e}{1 + K_L C_e} \dots \dots \dots (18)$$

Where C_e is the equilibrium concentration of the IBU solution (mg/L).

Q_e is the amount of IBU adsorbed per gram of the adsorbent at equilibrium (mg/g).

Q_m is the maximum amount of IBU (mg) adsorbed per gram of adsorbents for complete monolayer coverage.

k_L is the Langmuir constant related to the energy of adsorption (L/mg).

The experimental data of adsorption of IBU on to Fe₃O₄-SiO₂ (CTAB) and ZnO-SiO₂ (CTAB) NP's were fitted to four models of Langmuir isotherm. Table 3.9 shows the values of R² for four linear Langmuir forms using ZnO-SiO₂ (CTAB) and Fe₃O₄-SiO₂ (CTAB), and according to the R² values the R² in linear Langmuir form (I) is higher than that obtained by another linear Langmuir forms. These indicate that the linear Langmuir form (I) fitted to the experimental data.

Table 3.9: correlation coefficients (R²) values of linear Langmuir forms at 288 K.

Number	Linear Langmuir forms	R ² ZnO-SiO ₂ (CTAB)	R ² Fe ₃ O ₄ -SiO ₂ (CTAB)
I	$\frac{C_e}{Q_e} = \frac{1}{Q_m} k_L + \frac{C_e}{Q_m}$	0.9905	0.9971
II	$\frac{1}{Q_e} = \frac{1}{Q_m} + \frac{1}{Q_m k_L C_e}$	0.9195	0.9962
III	$Q_e = Q_m - \frac{Q_e}{k_L C_e}$	0.7611	0.9801
IV	$\frac{Q_e}{C_e} = k_L Q_m - k_L Q_e$	0.7611	0.9801

The linear Langmuir adsorption isotherm was used to fit the experimental data is given in the following form:

$$\frac{C_e}{Q_e} = \frac{1}{Q_m K_L} + \frac{C_e}{Q_m} \dots \dots \dots (19)$$

Where C_e is the equilibrium concentration of the IBU solution (mg/L), and Q_e is the amount of IBU adsorbed per gram of the adsorbent at equilibrium (mg/g). Q_m is the maximum amount of IBU (mg) adsorbed per gram of adsorbents for complete monolayer coverage. k_L is the Langmuir constant related to the energy of adsorption (L/mg).

The adsorption parameters Q_m and k_L were obtained from the slope and intercept of the linear plot of C_e/q_e Vs. C_e as shown in Figure 3.18.

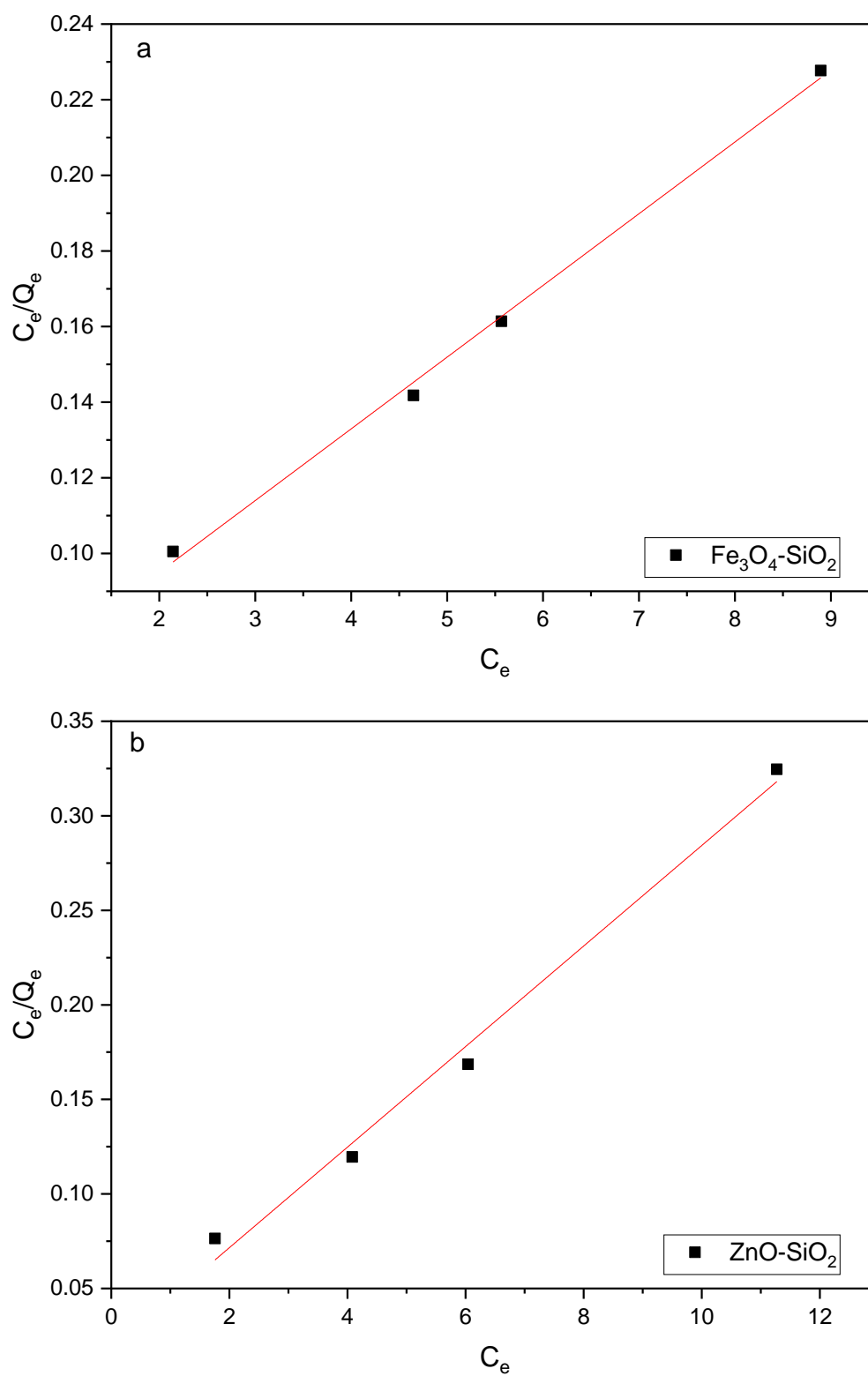


Figure 3.18: Linear plots of Langmuir isotherm model of IBU adsorption on: a) $\text{Fe}_3\text{O}_4\text{-SiO}_2$ (CTAB) NP's b) ZnO-SiO_2 (CTAB) NP's at 288K.

The Freundlich isotherm is another widely applied adsorption model, which allows for multilayer adsorption, and can be used for heterogeneous adsorbent surfaces having different sites with varying adsorption energy.^{100, 103}

The experimental data of adsorption IBU onto the two adsorbents were analyzed using Freundlich isotherm model.

The nonlinear form of Freundlich isotherm model is given as:

$$Q_e = k_f C_e^{\frac{1}{n}} \dots \dots \dots (20)$$

The linearized form of the Freundlich isotherm model represented by this equation:

$$\ln Q_e = \ln k_f + \left(\frac{1}{n}\right) \ln C_e \dots \dots \dots (21)$$

Where C_e is the equilibrium concentration of the IBU solution (mg/L), and Q_e is the amount of IBU adsorbed per gram of the adsorbent at equilibrium (mg/g). k_f is Freundlich constant, which reflects the adsorption affinity, and n is the Freundlich constant related to the adsorption linearity.

The isotherm parameters k_f and $1/n$ of Freundlich for adsorption of IBU onto $\text{Fe}_3\text{O}_4\text{-SiO}_2$ (CTAB) and ZnO-SiO_2 (CTAB) NP's can be calculated from the intercept and slope of the linear plot of $\ln Q_e$ vs. $\ln C_e$ as the corresponding plots are shown in Figure 3.19.

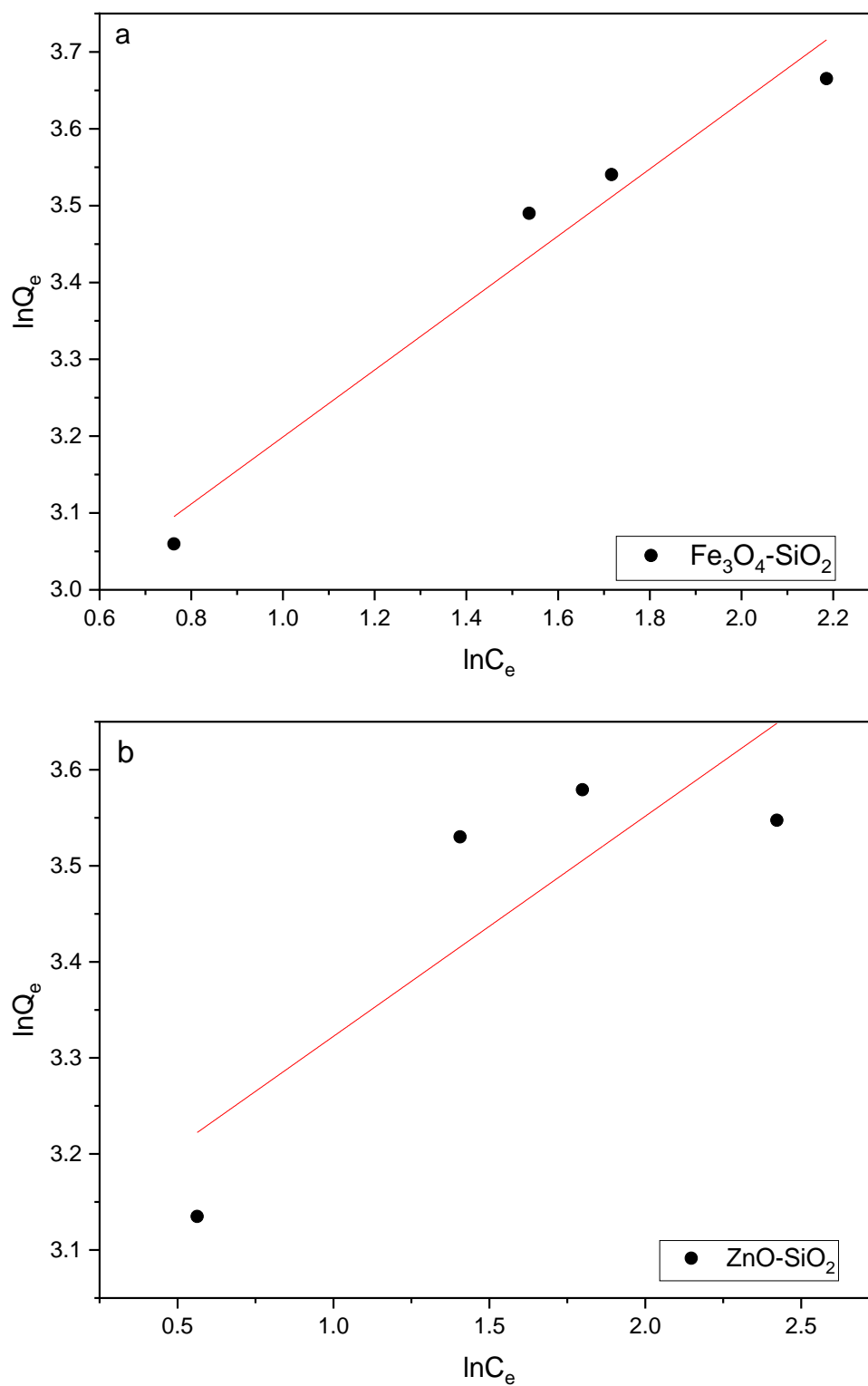


Figure 3.19: Linear plots of Freundlich isotherm model of IBU adsorption on: a) $\text{Fe}_3\text{O}_4\text{-SiO}_2$ (CTAB) NP's b) ZnO-SiO_2 (CTAB) NP's at 288K.

The parameters for the Langmuir and Freundlich models of Fe₃O₄-SiO₂ (CTAB) and ZnO-SiO₂ (CTAB) NP's were calculated at 288, 298, and 318K, the obtained results are listed in Table 3.10.

From the R² values of the two models in Table 3.10, we can conclude that the adsorption of IBU on ZnO-SiO₂ (CTAB) NP's at 288 and 318K is better described by the Langmuir isotherm model, while at 298 K are fitted with both Langmuir and Freundlich isotherm. But in the adsorption of IBU via Fe₃O₄-SiO₂ (CTAB) were fitted by both Langmuir and Freundlich models with a variation of temperature. The R² values for Langmuir at 288, 298, and 318 K were 0.9971, 0.996, and 0.9608 while for Freundlich were found to be 0.9619, 0.9988, and 0.4741 respectively. Therefore, the adsorption of ibuprofen by Fe₃O₄-SiO₂ (CTAB) fitted with Freundlich at 298 K, and at 288 K and 318 K it changed to Langmuir. This indicated that the adsorption of IBU on the surface of ZnO-SiO₂ (CTAB) and Fe₃O₄-SiO₂ (CTAB) surface looks to be both homogeneous and heterogeneous toward IBU molecules.¹⁰⁴

The values of maximum adsorption capacity Q_{\max} (mg/g) for the adsorption of IBU via $\text{Fe}_3\text{O}_4\text{-SiO}_2$ (CTAB) NP's were 52.6, 59.9 and 33.3 at 288, 298 and 318 K, temperatures. While for ZnO-SiO_2 (CTAB) NP's they were found to be 37.59, 44.24 and 35.08 at 288, 298 and 318 K respectively. So, the maximum adsorption capacity of the IBU using $\text{Fe}_3\text{O}_4\text{-SiO}_2$ (CTAB) is more than ZnO-SiO_2 (CTAB) NP's.

Table 3.10: Parameters of Langmuir and Freundlich models for IBU adsorption using $\text{Fe}_3\text{O}_4\text{-SiO}_2$ (CTAB) and ZnO-SiO_2 (CTAB) NP's.

Experimental condition	Langmuir			Freundlich		
	Q_{\max} (mg/g)	k_L (L/mg)	R^2	k_f (L/mg)	n	R^2
$\text{Fe}_3\text{O}_4\text{-SiO}_2$ (CTAB) at pH4						
288 K	52.6	0.332	0.9971	15.8	2.29	0.9619
298 K	59.9	0.214	0.996	13.3	2.01	0.9988
318 K	33.3	0.450	0.9608	14.2	3.62	0.4741
ZnO-SiO_2 (CTAB) at pH4						
288 K	37.6	1.44	0.9905	22.05	4.36	0.7239
298 K	44.2	0.276	0.9905	14.2	2.84	0.9973
318 K	35.01	0.809	0.9961	17.6	4.02	0.8266

The maximum adsorption capacity of IBU using $\text{Fe}_3\text{O}_4\text{-SiO}_2$ (CTAB) and ZnO-SiO_2 (CTAB) NP's were compared with previous studies to evaluate the utility of $\text{Fe}_3\text{O}_4\text{-SiO}_2$ (CTAB) and ZnO-SiO_2 (CTAB) NPs as a remover for IBU.

Table 3.11 summarizes a comparison of the maximum capacities of IBU by different adsorbents including $\text{Fe}_3\text{O}_4\text{-SiO}_2$ (CTAB) and ZnO-SiO_2 (CTAB) NP's for the present study. The comparison indicating that the suitability and applicability of the $\text{Fe}_3\text{O}_4\text{-SiO}_2$ (CTAB) and ZnO-SiO_2 (CTAB) NP's used as an efficient adsorbent for removal of the IBU.

Table 3.11: Maximum adsorption capacities of IBU for different adsorbents.

Adsorbents	Adsorption capacity (mg/g)	References
Copper nanoparticles	33.9	(105)
Activated carbon impregnated with TiO ₂	16.68	(106)
Graphene oxide nanoplatelets	3.72	(107)
Nanographene	11.9	(108)
Natural clay	50	(109)
molecularly imprinted polymer (MIP)	3.5	(110)
ZnO-SiO ₂ (CTAB) NP's	44.24	This study
Fe ₃ O ₄ -SiO ₂ (CTAB) NP's	59.88	This study

In order to check which of the two isotherm models provide closer correlation with the experimental results the calculated Q_m and k_L values were inserted in the nonlinear equation (18) and the calculated k_f and n values were inserted in the nonlinear equation (20) then from the calculated Q values the model prediction was obtained. The experimental and predicted data of Q for two types of NP's were plotted as shown in the Figure 3.20 and Figure 3.21.

As shown in Figure 3.20, for $Fe_3O_4-SiO_2$ (CTAB) NP's, the nonlinear fit using Langmuir isotherm model is better fit to the experimental data than Freundlich isotherm model. While for $ZnO-SiO_2$ (CTAB) NP's as shown in Figure 3.21, the two models showed similar correlation.

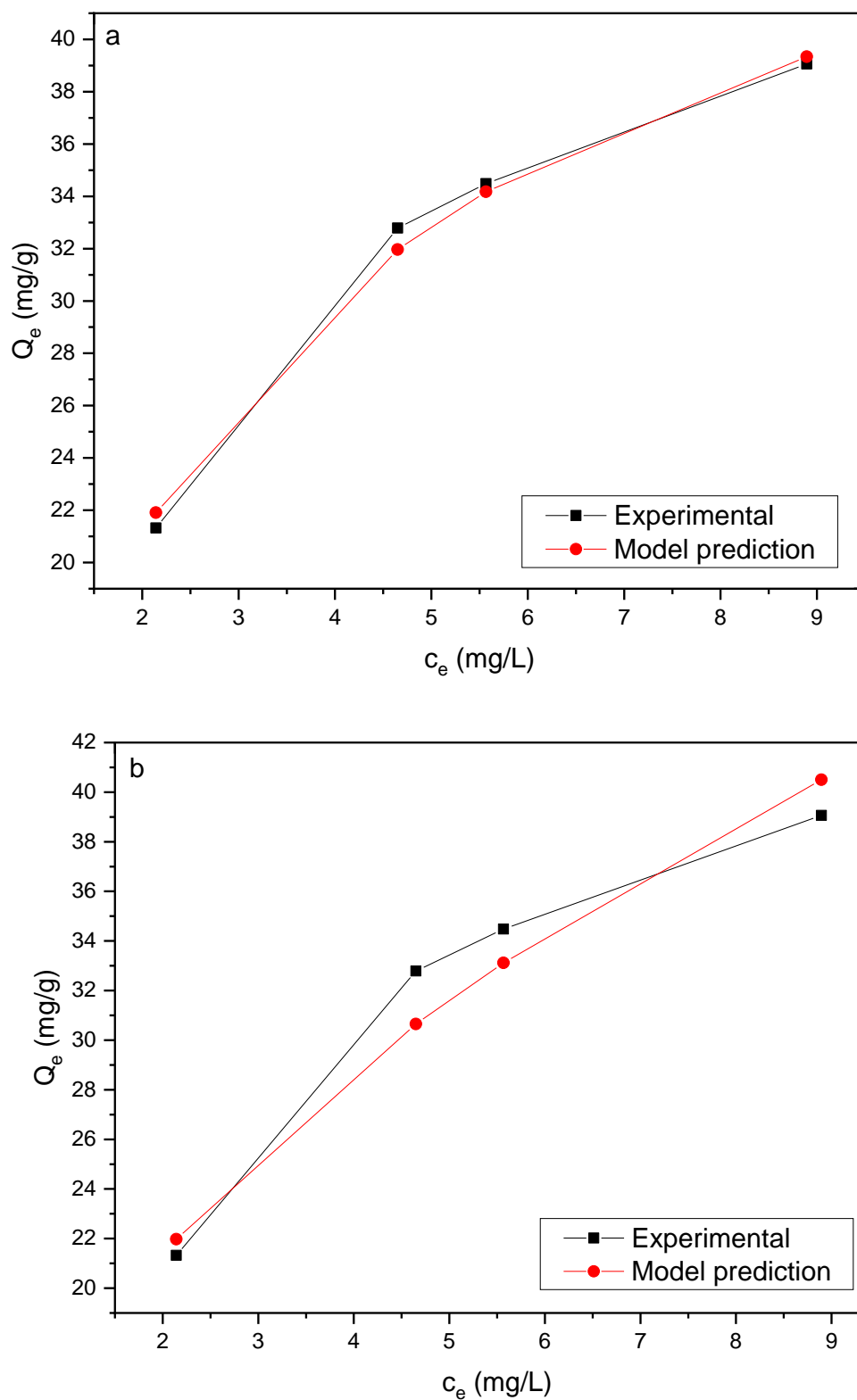


Figure 3.20: Nonlinear fits of the kinetic data of IBU removal by $\text{Fe}_3\text{O}_4\text{-SiO}_2$ (CTAB) NPs; (a) using Langmuir model (b) using Freundlich model at 288 K.

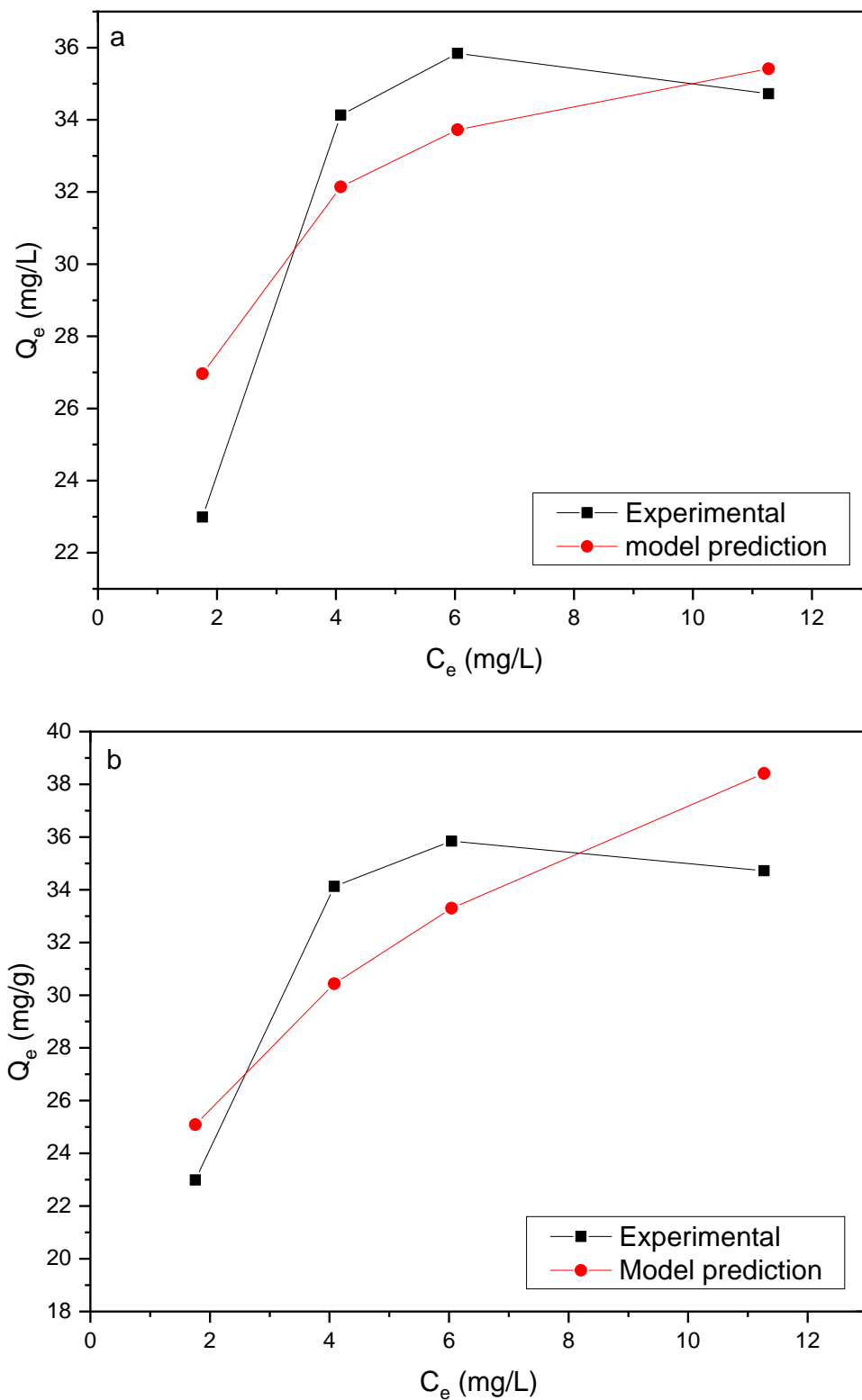


Figure 3.21: Nonlinear fits of the kinetic data of IBU removal by ZnO-SiO₂ (CTAB) NPs; (a) using Langmuir model (b) using Freundlich model at 288 K.

In addition to, the Chi test was performed to test of the correlation and to study the compatibility between the experimental and predicted value of Q by using equation 17.

Table 3.12 shows the values of χ^2 for two models of Langmuir and Freundlich using ZnO-SiO₂ (CTAB) and Fe₃O₄-SiO₂ (CTAB) NPs. the Chi test results for both ZnO-SiO₂ (CTAB) and Fe₃O₄-SiO₂ (CTAB) NPs indicate that the Q values predicted by Langmuir model are closer to the experimental value more than Q values predicted by Freundlich model.

Table 3.12: Values of Q obtained from experiment, values of Q predicted by equations (18 and 20), and the Chi –test values for the sorption systems of Fe₃O₄-SiO₂ (CTAB) NP's at 288 K.

C _e (mg/L)	Q _{exp} (mg/g)	Q _{model} (mg/g)	Chi test (Langmuir model)	Q _{model} (mg/g)	Chi test (Freundlich model)
ZnO-SiO₂					
1.76	22.98	26.96	0.59	25.1	0.176
4.08	34.13	32.1	0.123	30.4	0.448
6.043	35.8	33.7	0.133	33.3	0.194
11.3	34.7	35.4	0.0136	38.4	0.355
		χ^2	0.856	χ^2	1.17
Fe₃O₄-SiO₂					
2.14	21.3	21.9	0.0156	21.97	0.0195
4.65	32.8	31.96	0.0210	30.6	0.148
5.57	34.5	34.2	0.0028	33.1	0.0563
8.89	39.06	39.3	0.00190	40.5	0.0512
		χ^2	0.0413	χ^2	0.276

3.6 Effect of pH and PZC on the removal of IBU

The pH value is an important parameter that affects the adsorption of IBU onto ZnO-SiO₂ (CTAB) and Fe₃O₄-SiO₂ (CTAB) NP's. The extent removal of IBU was studied at initial pH values 2, 4, 6, and 8 using 50 mg portions of adsorbent, with shaking speed 150 rpm for 90 min. The pH of the solution was altered by using 0.1M NaOH and HCl solutions.

The point of zero charge (pH_{pzc}) is an important factor that indicates the adsorption ability of the surface and the type of surface active centers. The PZC was determined by salt addition method by adding 40 ml of sodium chloride (0.01 M) to a series of beakers, the pH of each was adjusted at 2, 3, 4,5, 6, 7, 8, 9, 10, and 11 by addition of hydrochloric acid (0.1 M) or sodium hydroxide (0.1M), then 50 mg of adsorbent was added to each beaker, with shaking speed 150 rpm at 25°C for 24 h, in order to determine the final pH_f .

The PZC corresponds to the intersection of the curve and the pH value for which the net charge of the adsorbent surface is zero.

The difference between initial and final pH values (ΔpH) was plotted versus initial pH values, PZC value was identified at the pH when ΔpH was zero Figure 3.22.

In general, the adsorbent surface is positively charged when $\text{pH} < \text{pH}_{\text{pzc}}$ while when $\text{pH} > \text{pH}_{\text{PZC}}$ the surface is negatively charged. For $\text{Fe}_3\text{O}_4\text{-SiO}_2$ (CTAB) NP's, the pH_{PZC} value is 9 as shown in Figure 3.22(a), so the surface charge of $\text{Fe}_3\text{O}_4\text{-SiO}_2$ (CTAB) is negative at pH above 9, and positive at pH below 9.

The electrical charge of the adsorbent's surface which affected by the value of pH, at $\text{pH} < \text{pH}_{\text{PZC}}$ the protonation reaction of the surface hydroxyl group ($-\text{OH} + \text{H}^+ \longrightarrow -\text{OH}^{2+}$), so the surface of $\text{Fe}_3\text{O}_4\text{-SiO}_2$ (CTAB) is positively charged, which is favorable for the negatively charged IBU to be adsorbed. While at $\text{pH} > \text{pH}_{\text{pzc}}$, the surface charge of $\text{Fe}_3\text{O}_4\text{-SiO}_2$ (CTAB) is negative because of deprotonation reaction ($-\text{OH} \longrightarrow -\text{O}^- + \text{H}^+$).

Figure 3.23 show that the pH affects the removal of IBU significantly, in the case of iron oxide. The adsorption of IBU decreases slowly and then decreases quickly as pH increases from 6 to 8, as shown in Figure 3.23(a), large increases in the adsorption

efficiency of IBU from 39.5% to 95.8 %, when the pH of the solution decreases from 8 to 2. But at pH = 4 and pH = 6, the percentage decrease is still observed but at lower rate. The IBU is a weak acid ($pK_a = 4.91$) and exists as a neutral at $pH < pK_a$, coexists as neutral and anionic species at $pH \cong pK_a$, and exists as anion at $pH > pK_a$. The reasons for the decrease in the % removal of IBU with increasing pH values are attributed to the pK_a value (4.91) for IBU. The IBU molecule has one H-bond donor and two acceptor sites. The mechanism for the adsorption of IBU over Fe_3O_4 - SiO_2 (CTAB) NP's can be explained by H-bonding, considering the electronegative O in IBU, and the functional groups ($-OH$) on Fe_3O_4 - SiO_2 (CTAB) NP's. The increase in the removal of IBU at lower pH can be explained by the H-bond considering the free $-OH$ group on the adsorbent. The decreasing in the removal of IBU by the Fe_3O_4 - SiO_2 (CTAB) at pH higher than 4.0 can be explained by successive deprotonation leading to repulsion between the negatively charged of IBU and the negatively charged Fe_3O_4 - SiO_2 (CTAB) surface. As shown in Figure 3.23(a) when pH increases from 6 to 8, the deprotonation velocity of Fe_3O_4 - SiO_2 (CTAB) is faster than IBU and the electrostatic repulsion between Fe_3O_4 - SiO_2 (CTAB) and IBU increases quickly, therefore it

was found that the decrease of IBU adsorption quickly with pH increasing from 6 to 8.

Similarly, in the case of zinc oxide NP's as shown in Figure 3.23(b) the removal efficiency of IBU decreases at high pH value but increases at low pH value. When the pH of the solution increases from 2 to 8, removal efficiency of IBU decreases from 85.7% to 72.2%. Therefore, at acidic pH values, the adsorption capacity of the IBU onto ZnO-SiO₂ (CTAB) was increased, while at basic pH values the adsorption capacity decreased.

The PZC of the ZnO-SiO₂ (CTAB) adsorbent is 9.13 (Figure 3.22(b)), which means that the adsorbent surface is positively charged at pH below 9.13, and negatively charged at a pH above 9.13.

H-bonding may be the main driving forces for IBU adsorption over ZnO-SiO₂ (CTAB) NP's. The interact IBU with the ZnO-SiO₂ (CTAB) surface through H-bond formation will be very low when the pH is greater than the pKa of IBP, the hydrogen of the carboxylic group of IBU can be removed at pH > 4.9, since IBU does not have any H-donor under these conditions. The more the pH increases towards PZC, the surface of the adsorbent ZnO-SiO₂ (CTAB) is

negatively charged because of deprotonation reaction and this leads to a decrease in the adsorption of the anionic IBU because of the strong repulsion forces between anions of IBU and the negatively charged surface of ZnO-SiO₂ (CTAB).

As shown in Figure 3.23(b) the removal efficiency of ibuprofen decreases when the alkalinity of the system increases (from 85.7% at pH=2 to 72.2% at pH=8), and a maximum adsorption of the IBU to ZnO-SiO₂ (CTAB) has been reached when pH is lower than the pK_a of IBP due to the presence of free –OH group at the surface of ZnO-SiO₂ (CTAB), leading to better adsorption of IBU by the H-bonding attraction phenomenon. While with increasing pH, the H-donor content of ZnO-SiO₂ (CTAB) will be decreased because of deprotonation. It was found that the removal efficiency of IBU increases by decreasing pH. Moreover, an increase in pH of the medium and the electrostatic interaction between the ionic charge of IBU molecules and surface charge of the adsorbent. Therefore, acidic pH values are more effective for the removal of anionic IBU. So the adsorption of IBU on ZnO-SiO₂ (CTAB) and Fe₃O₄-SiO₂ (CTAB) depend largely on pH.¹¹¹⁻¹¹⁴

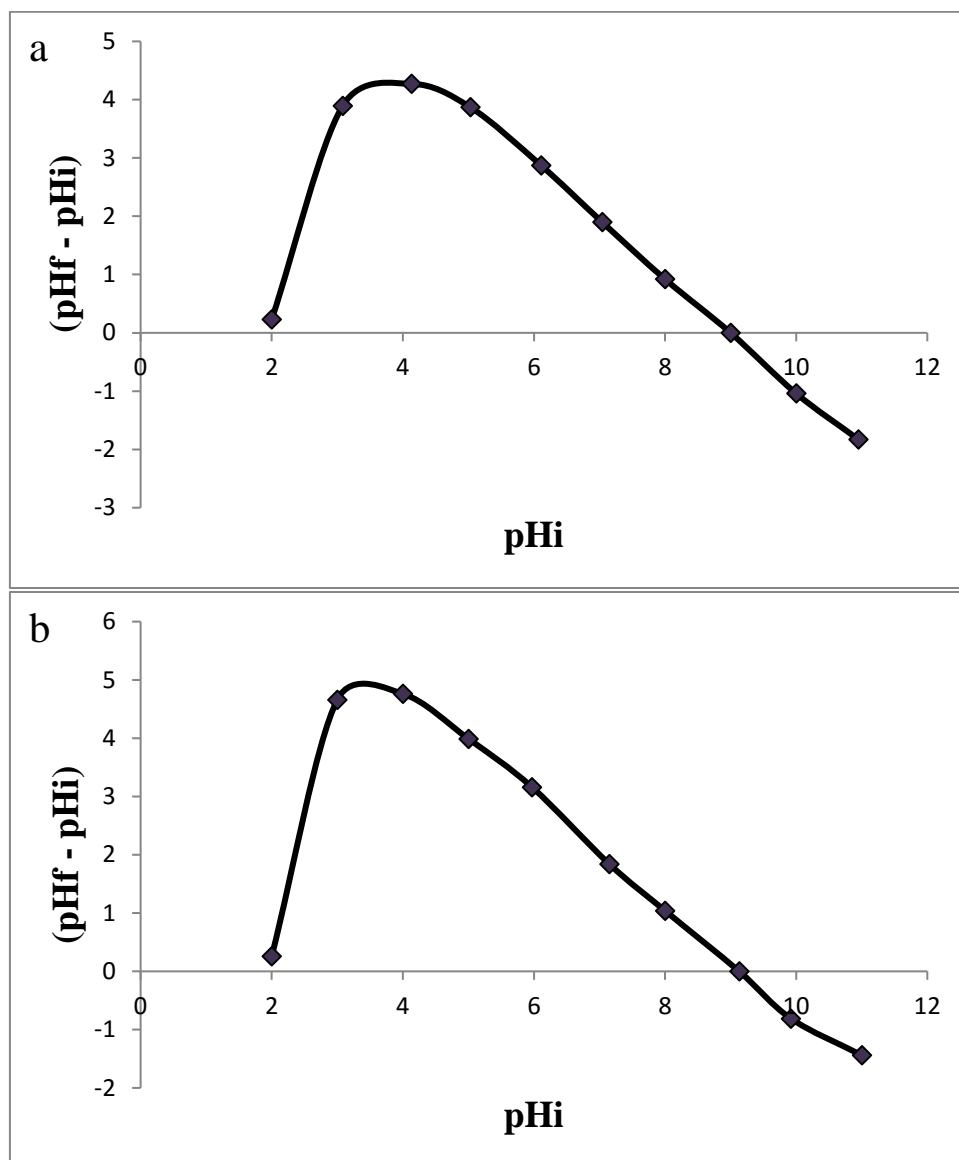


Figure 3.22: Evaluation of pH_{pzc} for: a) $Fe_3O_4-SiO_2$ (CTAB) NP's b) $ZnO-SiO_2$ (CTAB) NP's.

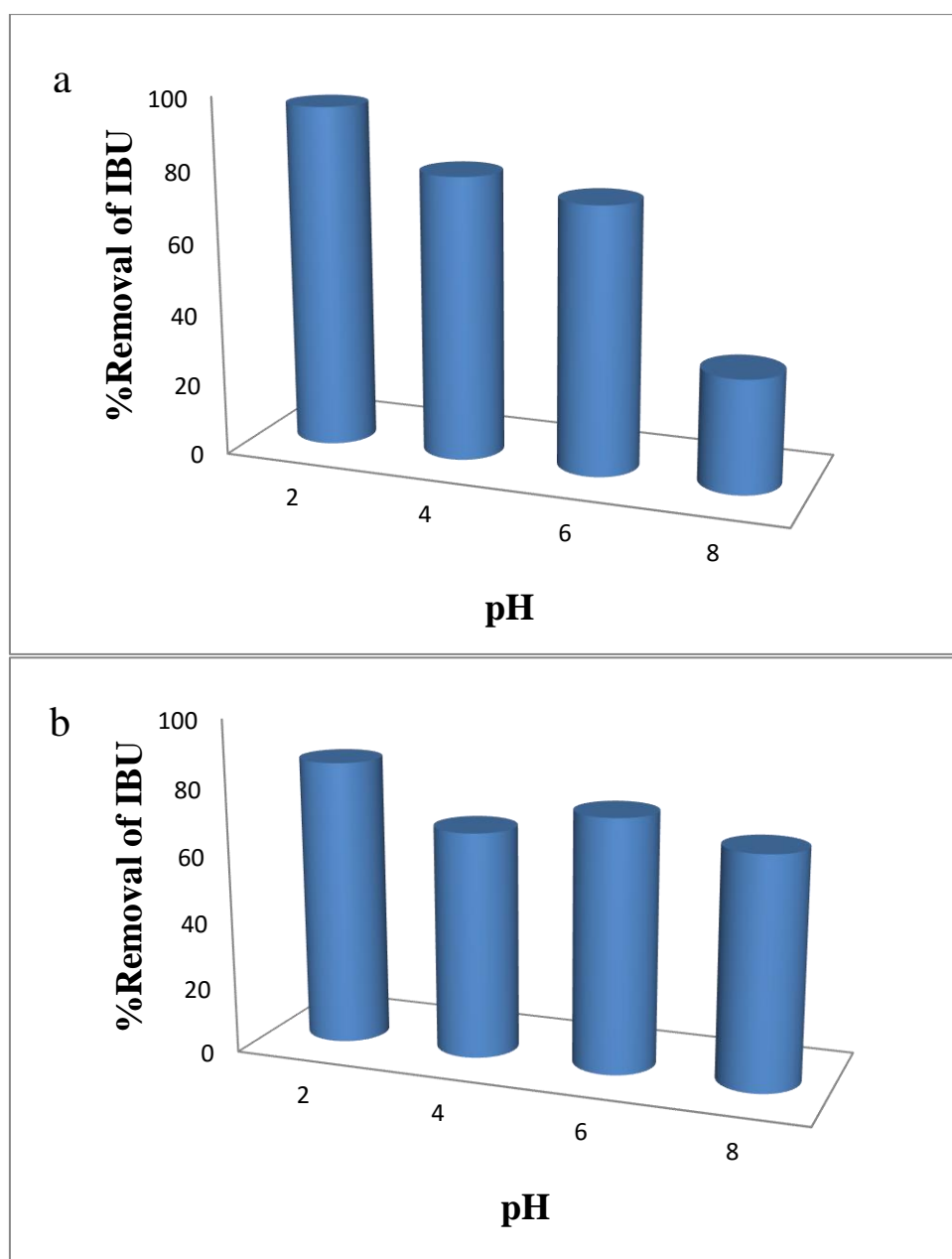


Figure 3.23: Effect of pH on the percentage removal of IBU using: a) Fe₃O₄-SiO₂ (CTAB) b) ZnO-SiO₂ (CTAB) NP's at 298 K.

3.7 Effect of temperature

The effect of temperature on the adsorption process was studied using $\text{Fe}_3\text{O}_4\text{-SiO}_2$ (CTAB) and ZnO-SiO_2 (CTAB) NP's at different initial IBU concentrations of 15, 25, and 35 mg/L. and the shaking speed was 150 rpm for 90 min.

The results of the adsorption of IBU on two type of NP's was studied at temperature 288, 298, and 318 K are shown in Table 3.9 and represented in Figure 3.24.

Figure 3.24 indicate clearly that the increase of the temperature affects negatively at the adsorption process, as temperature raises the adsorption capacity decreases. Obviously, the increase of temperature from 288 to 318 K induces a decrease of the adsorption capacity. The increasing of temperature confirms destabilization of the physical forces between IBU and adsorbent.

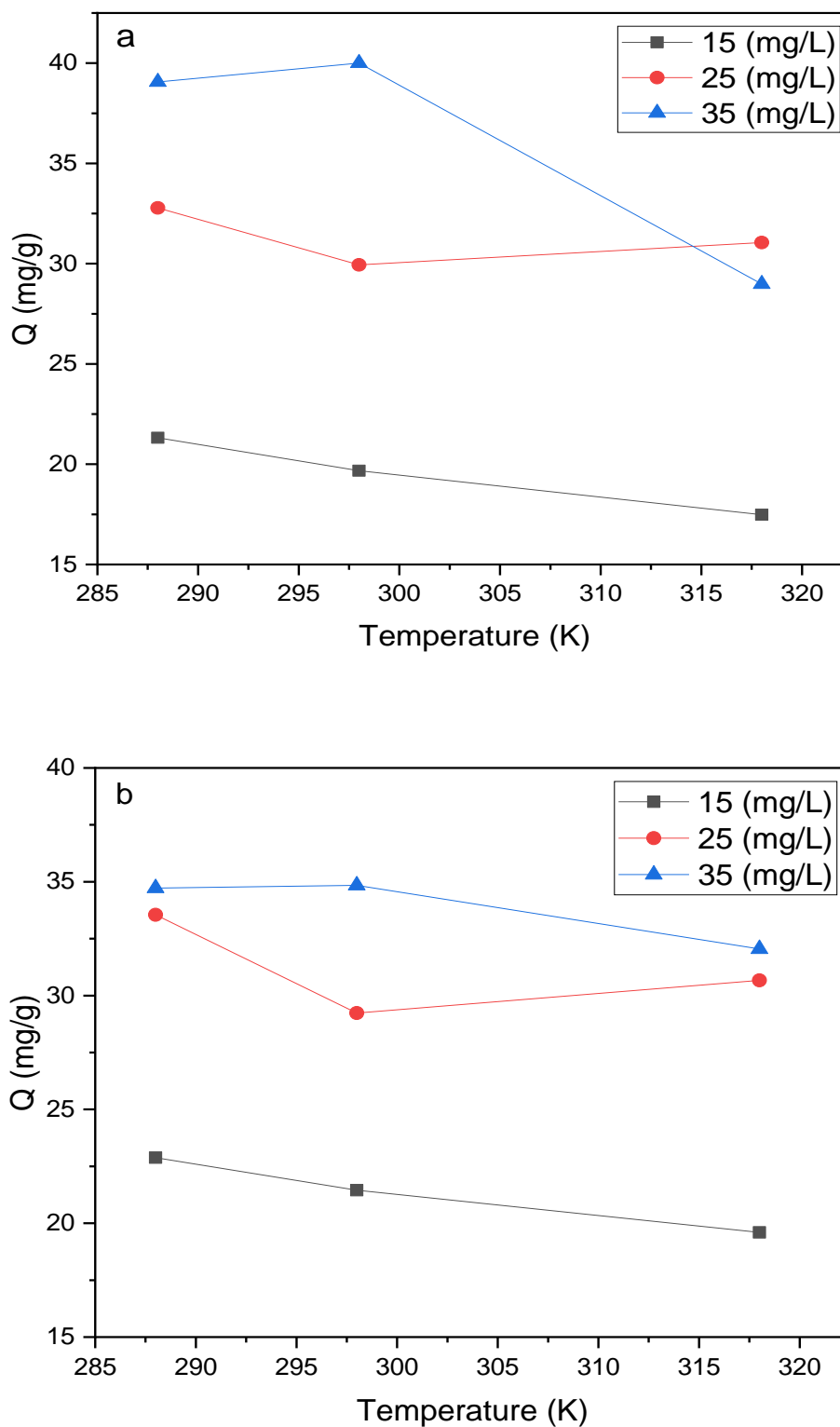


Figure 3.24: Effect of temperature on the adsorption of IBU onto: a) $\text{Fe}_3\text{O}_4\text{-SiO}_2$ (CTAB) NP's b) ZnO-SiO_2 (CTAB) NP's at different initial IBU concentration.

From data in Table 3.13 two main results were concluded; the amounts of IBU sorption on both nanoparticles decrease at the highest temperature due to the change in the equilibrium toward desorption, and when the initial IBU concentration increases Q value increases.¹¹⁵

Table 3.13: Amount of IBU adsorbed via Fe₃O₄-SiO₂ (CTAB) and ZnO-SiO₂ (CTAB) NP's at different temperatures using different initial IBU concentrations.

C ₀ (mg/L)	Q (mg/g)					
	288 K		298 K		318 K	
	Fe ₃ O ₄ -SiO ₂ (CTAB)	ZnO-SiO ₂ (CTAB)	Fe ₃ O ₄ -SiO ₂ (CTAB)	ZnO-SiO ₂ (CTAB)	Fe ₃ O ₄ -SiO ₂ (CTAB)	ZnO-SiO ₂ (CTAB)
15	21.3	22.9	19.7	21.4	17.5	19.6
25	32.8	33.5	29.9	29.2	31.05	30.7
35	39.06	34.72	40	34.8	28.9	32.05

From the kinetics data obtained at different temperatures the activation energy of adsorption IBU on Fe₃O₄-SiO₂ (CTAB) and ZnO-SiO₂ (CTAB) NP's were calculated using the Arrhenius equation: ¹¹⁶

$$\ln k_2 = \ln A - \frac{E_a}{R T} \dots \dots \dots (22)$$

Where k_2 is the rate constant of pseudo-second-order ($\text{g mg}^{-1} \text{min}^{-1}$).

A is the pre-exponential factor.

E_a is the activation energy (kJ mol^{-1}).

R is the gas constant ($8.314 \text{ J K}^{-1} \text{ mol}^{-1}$).

T is the absolute temperature (K).

The value of E_a was calculated from the slope of the linear plot of $\ln k_2$ versus $1/T$. as shown in Figure 3.25.

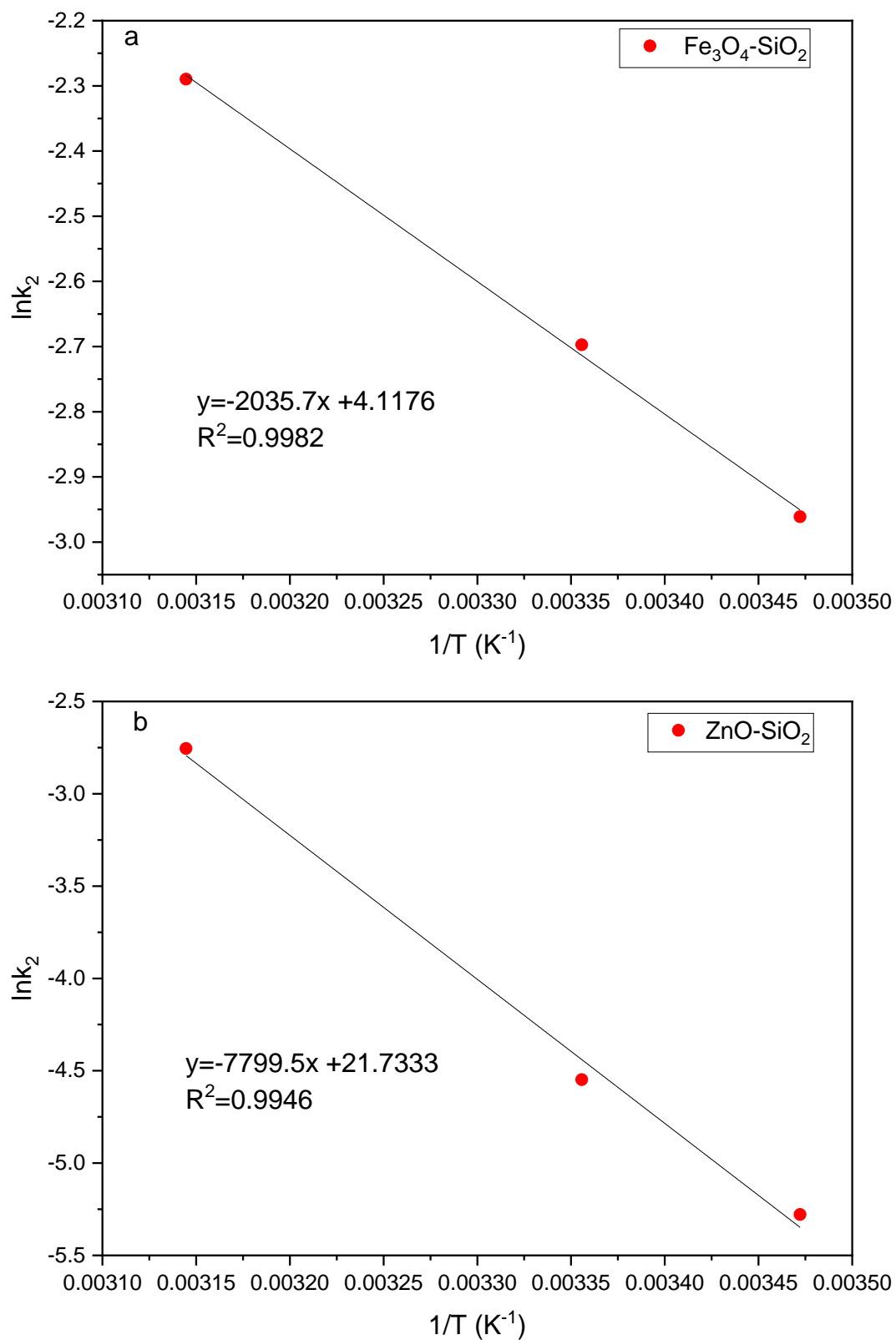


Figure 3.25: Arrhenius equation graph of IBU adsorption on: a) Fe₃O₄-SiO₂ (CTAB) NP's b) ZnO-SiO₂ (CTAB) NP's.

The magnitude of the activation energy can be used to indicate whether the adsorption mechanism is physisorption (in the range 5 to 40 kJ mol⁻¹) or chemisorption (in the range 40 to 800 kJ mol⁻¹).^{115, 117-}

118

As shown in Table 3.14 the value of activation energy barrier for adsorption IBU on to ZnO-SiO₂ (CTAB) NP's was calculated to be 64.8 (kJ mol⁻¹) indicating that the adsorption mechanism seems to be weak chemisorption, while the value of activation energy barrier in adsorption process of Fe₃O₄-SiO₂ (CTAB) NP's was calculated to be 16.9 (KJ mol⁻¹) this means that the adsorption is a physisorption process. Moreover, we conclude that the value of rate constant increases with decreasing the value of activation energy as shown in the Table 3.14, the rate constant values for adsorption of IBU on to Fe₃O₄-SiO₂ (CTAB) NP's are larger than that of the adsorption of IBU on to ZnO-SiO₂ (CTAB) NP's.

Table 3.14 : Activation energy and rate constant values of adsorbed IBU onto Fe₃O₄-SiO₂ (CTAB) and ZnO-SiO₂ (CTAB) NP at different temperature.

Temperature (K)	k_2 (g mg ⁻¹ min ⁻¹) Fe ₃ O ₄ -SiO ₂ (CTAB)	k_2 (g mg ⁻¹ min ⁻¹) ZnO-SiO ₂ (CTAB)
288	0.052	0.0051
298	0.068	0.010
318	0.101	0.064
E_a	16.9 kJ/mol	64.8 kJ/mol

3.8 Adsorption thermodynamics

In the previous section, the effect of temperature on the adsorption process was studied and the data were analyzed to determine the thermodynamic parameters including Gibbs free energy change (ΔG°), change in standard enthalpy (ΔH°), and change in standard entropy (ΔS°).

The ΔH° and ΔS° values were determined using van't Hoff equation:¹¹⁷

$$\ln K = \frac{\Delta S^\circ}{R} - \frac{\Delta H^\circ}{RT} \dots \dots \dots (23)$$

The value of Gibbs free energy change (ΔG°) was obtained from the following equations:

$$\Delta G^\circ = \Delta H^\circ - T\Delta S^\circ \dots \dots \dots (24)$$

$$\Delta G^\circ = -RT \ln K \dots \dots \dots (25)$$

Where ΔG° change in Gibbs free energy (kJ mol^{-1}), ΔH° change in enthalpy (kJ mol^{-1}), ΔS° change in entropy ($\text{kJ mol}^{-1} \text{K}^{-1}$), R is the

ideal gas constant (8.3145 J/mol K), T is the temperature in Kelvin, K is the apparent equilibrium constant expressed as $\left(\frac{Q_e}{C_e}\right)$.

The values of ΔH° and ΔS° were calculated from the slope and y-intercept obtained from the linear plot of $\ln K$ versus $1/T$ as shown in Figure 3.26. The thermodynamic parameters were calculated and are tabulated in Table 3.15 and Table 3.16.

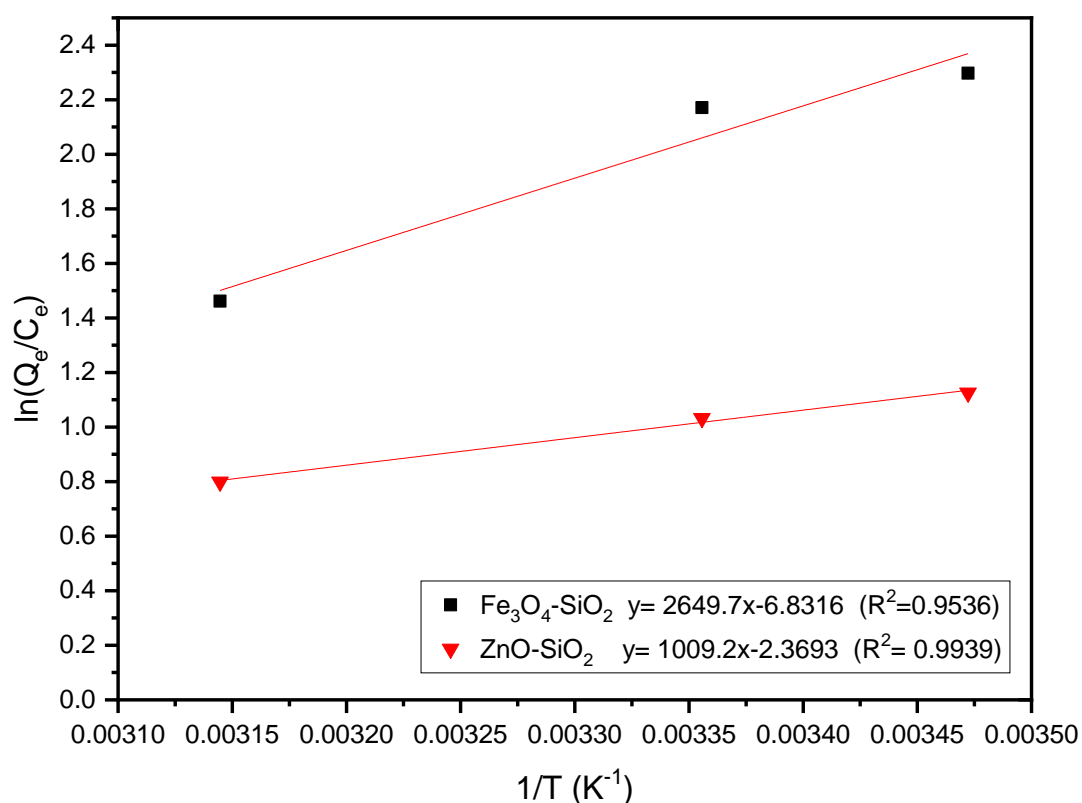


Figure 3.26: Determination of thermodynamic parameters of IBU adsorbed onto Fe₃O₄-SiO₂ (CTAB) and ZnO-SiO₂ (CTAB) NP's.

Table 3.15: Thermodynamic parameters of IBU adsorbed using Fe₃O₄-SiO₂ (CTAB).

ΔH° (kJ/mol)	ΔS° (J/mol.K)	ΔG° (kJ/mol)		
		288 K	298 K	318 K
-22.02	-56.8	-5.67	-5.10	-3.96

Table 3.16: Thermodynamic parameters of IBU adsorbed using ZnO-SiO₂ (CTAB).

ΔH° (kJ/mol)	ΔS° (J/mol.K)	ΔG° (kJ/mol)		
		288 K	298 K	318 K
-8.39	-19.7	-2.71	-2.52	-2.12

From the data in these tables, it is possible to conclude some information about the adsorption process. Through previous research^{105,119}, it was concluded that the negative value of Gibbs free energy (ΔG°) indicates that the adsorption process favors the products, and the increasing magnitude of ΔG° as temperature increase indicated that the adsorption process was more favorable at a higher temperature. In addition, the type of adsorption can be known by the

value of ΔG° , if it is in the range from -20 to 0 kJ mol^{-1} , it considered a physisorption process, while for chemisorption process has a range from -80 to -400 kJ mol^{-1} . Also, the value of ΔH° may give an indication about the type of adsorption if it lies in the range 2.1 to 20.9 kJ mol^{-1} and 80 to 200 kJ mol^{-1} Physical and chemical adsorption respectively. And the enthalpy value of the adsorption process can be used to distinguish between the exothermic and endothermic processes.^{101,120}

Based on Table 3.15 and Table 3.16, the adsorption process of IBU is exothermic due to the negative values of ΔH° . Also, the low values of enthalpy in both types of NP's indicate that this is a physical adsorption. The negative values of ΔS° indicate that the degree of disorderliness decreased at the interface between solid and liquid phases during IBU adsorption process. Moreover, Ibuprofen adsorption was spontaneous because the values of ΔG° were negative for the all studied temperatures.

4. Conclusions

In this study, the ZnO and Fe₃O₄ NP's were synthesized through ethanol-based precipitation and co-precipitation method respectively. Then the NPs were encapsulated with silica using a cationic surfactant CTAB as a templating agent. The adsorption behavior of IBU onto Fe₃O₄-SiO₂ (CTAB) and ZnO-SiO₂ (CTAB) NP's surface were investigated. It was found that the kinetic data correlates better with pseudo-second-order equation than with pseudo-first-order equation. The calculated value of activation energy shows that the Fe₃O₄-SiO₂ (CTAB) has a smaller activation barrier of IBU sorption than the ZnO-SiO₂ (CTAB) NP's and the value of rate constant increases with decreasing the value of activation energy, so the rate constant values for adsorption of IBU on to Fe₃O₄-SiO₂ (CTAB) NP's are larger than that of the adsorption of IBU on to ZnO-SiO₂ (CTAB) NP's. Moreover, the values of the maximum adsorption capacities of Fe₃O₄-SiO₂ (CTAB) are larger than those corresponding to ZnO-SiO₂ (CTAB) NP's.

Both the concentration and pH affected the adsorption of IBU using both $\text{Fe}_3\text{O}_4\text{-SiO}_2$ (CTAB) and ZnO-SiO_2 (CTAB) NP's. The removal efficiency of IBU from aqueous solution increases with a decrease in pH values of solutions. On the other hand, the amount of IBU adsorbed increases with the increase in the initial concentration of IBU.

In addition, the temperature change has an effect on the extent of the IBU removal process; the increasing in temperature leads to a decrease in the adsorbed amount of IBU at specific concentration.

Finally, thermodynamic results indicate that the adsorption of IBU via both $\text{Fe}_3\text{O}_4\text{-SiO}_2$ (CTAB) and ZnO-SiO_2 (CTAB) NP's is exothermic in both cases, and favors the products.

5. References

1. Tambe Patil, B.B. Wastewater Treatment Using Nanoparticles. *J. Adv. Chem. Eng.* **2015**.
2. Alrumman, A.S.; El-kott, F.A.; Keshk, S. M. A. S. Water Pollution: Source & Treatment. *Am. J. Environ. Eng.* **2016**, 6(3), 88-98.
3. Ladu, C. L. G.; Athiba, L.A.; Lako, V.T.S.; Alfred, L.M. Investigation on the Impact of Water Pollution on Human Health in Juba County, Republic of South Sudan. *J. Environ. Pollu. Hum. Health.* **2018**, 6, 89-95.
4. Yunus, S, I.; Harwin; Kurniawan, A.; Adityawarman, D.; Indarto, A. Nanotechnologies in water and air pollution treatment. *Environ. Techno. Reviews.* **2012**, 1, 136-148.
5. Haseena, M.; Malik, F.M.; Javed, A.; Arshad, S.; Asif, N.; Zulfiqar, S.; Hanif, J. Water pollution and human health. *Environ. Risk Assess Remediat.* **2017**, 1(3), 16-19.
6. Bartolomeu, M.; Neves, M.D. G. P. M. S.; Faustino, M. A.; Almeida, A. Wastewater chemical contaminants: remediation by Advanced Oxidation Processes. *Photochem. Photobiol. Sci.* **2018**.

7. Schwarzenbach, P.; Egli, T.; Hofstetter, T. B.; Gunten, U. Von; Wehrli, B. Global Water Pollution and Human Health. *Annu. Rev. Environ.* **2010**, *35* (1), 109-136.
8. Lapworth, D. J.; Baran, N.; Ward, R. S. Emerging Organic Contaminants in Groundwater : A Review of Sources , Fate and Occurrence.
9. Ziylan, A.; Ince, N. H. The Occurrence and Fate of Anti-Inflammatory and Analgesic Pharmaceuticals in Sewage and Fresh Water : Treatability by Conventional and Non-Conventional Processes. *J. Hazard. Mater.* **2011**, *187* (1–3), 24–36.
10. Jones, O. A. H.; Voulvoulis, N.; Lester, J. N. Human Pharmaceuticals in Wastewater Treatment Processes. *Environ.Sci.Techno.* **2005**, *35*(4), 401-427.
11. Hernando, M. D.; Mezcuca, M.; Fernández-Alba, A. R.; Barceló, D. Environmental Risk Assessment of Pharmaceutical Residues in Wastewater Effluents, Surface Waters and Sediments. *Talanta.* **2006**, *69* (2 SPEC. ISS.), 334–342.

12. Yang, X.; Flowers, R. C.; Weinberg, H. S.; Singer, P. C. Occurrence and Removal of Pharmaceuticals and Personal Care Products (PPCPs) in an Advanced Wastewater Reclamation Plant. *Water Res.* **2011**, *45* (16), 5218–5228.
13. Tiwari, B.; Sellamuthu, B.; Ouarda, Y.; Drogui, P.; Tyagi, R. D.; Buelna, G. Review on Fate and Mechanism of Removal of Pharmaceutical Pollutants from Wastewater Using Biological Approach. *Bioresour. Technol.* **2017**, *224*, 1–12.
14. Beere, W.; Mullet, S.; Wingstedt, E.; Berg, Ø.; Savoainen, S.; Lahti, T. Model-Based Condition Monitoring Techniques for Balance of Plant Analysis Using Tempo. *7th Int. Top. Meet. Nucl. Plant Instrumentation, Control. Human-Machine Interface Technol. 2010, NPIC HMIT 2010* **2010**, *3* (2), 1920–1924.
15. Tambosi, J. L.; Yamanaka, L. Y.; José, H. J.; De Fátima Peralta Muniz Moreira, R.; Schröder, H. F. Recent Research Data on the Removal of Pharmaceuticals from Sewage Treatment Plants (STP). *Quim. Nova* **2010**, *33* (2), 411–420.
16. Kalyva, M. Fate of Pharmaceuticals in the Environment -A Review. **2017**, No. March, 1–30.

17. Cunningham, V. L.; Binks, S. P.; Olson, M. J. Human Health Risk Assessment from the Presence of Human Pharmaceuticals in the Aquatic Environment. *Regul. Toxicol. Pharmacol.* **2009**, *53* (1), 39–45.
18. Farmacéuticos, P.; El, E. N.; Fuentes, A.; Riesgos, E. Y. Pharmaceutical products in the environment: sources, effects and risks. *Vitae.* **2012**, *19*, 93-108.
19. Celiz, D.M.; Tso, J.; Aga, S.D. Critical Review Pharmaceutical metabolites in the environment: analytical challenges and ecological risks. *Environ. Toxicol. Chem.* **2009**, *28* (12), 2473–2484.
20. Luo, Y.; Guo, W.; Hao, H.; Duc, L.; Ibney, F.; Zhang, J.; Liang, S.; Wang, X. C. Science of the Total Environment A Review on the Occurrence of Micropollutants in the Aquatic Environment and Their Fate and Removal during Wastewater Treatment. *Sci. Total Environ.* **2014**, *473–474*, 619–641.
21. Deblonde, T.; Cossu-Leguille, C.; Hartemann, P. Emerging Pollutants in Wastewater: A Review of the Literature. *Int. J. Hyg. Environ. Health* **2011**, *214* (6), 442–448.

22. Geissen, V.; Mol, H.; Klumpp, E.; Umlauf, G.; Nadal, M.; van der Ploeg, M.; van de Zee, S. E. A. T. M.; Ritsema, C. J. Emerging Pollutants in the Environment: A Challenge for Water Resource Management. *Int. Soil Water Conserv. Res.* **2015**, *3* (1), 57–65.
23. De Andrade, J. R.; Oliveira, M. F.; Da Silva, M. G. C.; Vieira, M. G. A. Adsorption of Pharmaceuticals from Water and Wastewater Using Nonconventional Low-Cost Materials: A Review. *Ind. Eng. Chem. Res.* **2018**, *57* (9), 3103–3127.
24. Yang, X.; Flowers, R. C.; Weinberg, H. S.; Singer, P. C. Occurrence and Removal of Pharmaceuticals and Personal Care Products (PPCPs) in an Advanced Wastewater Reclamation Plant. *Water Res.* **2011**, *45* (16), 5218–5228.
25. Adams, C.; Wang, Y.; Loftin, K.; Meyer, M. Removal of Antibiotics from Surface and Distilled Water in Conventional Water Treatment Processes. *J. Environ. Eng.* **2002**, *128* (3), 253–260.
26. Zwiener, C.; Frimmel, F. H. Oxidative Treatment of Pharmaceuticals in Water. *Water Res.* **2000**, *34* (6), 1881–1885.

27. Neyens, E.; Baeyens, J.; Dewil, R.; De, B. Advanced Sludge Treatment Affects Extracellular Polymeric Substances to Improve Activated Sludge Dewatering. *Journal of Hazardous Materials*. **2004**, 83–92.
28. Fazal, S.; Zhang, B.; Zhong, Z.; Gao, L.; Chen, X. Industrial Wastewater Treatment by Using MBR (Membrane Bioreactor) Review Study. *J. Environ. Prot. (Irvine,. Calif)*. **2015**, 06, 584–598.
29. Verma, A. K.; Dash, R. R.; Bhunia, P. A Review on Chemical Coagulation/Flocculation Technologies for Removal of Colour from Textile Wastewaters. *J. Environ. Manage*. **2012**, 93 (1), 154–168.
30. Amuda, O. S.; Alade, A. Coagulation / Flocculation Process in the Treatment of Abattoir Wastewater. *Desalination*. **2006**, 196, 22–31.
31. Teh, C. Y.; Budiman, P. M.; Shak, K. P. Y.; Wu, T. Y. Recent Advancement of Coagulation-Flocculation and Its Application in Wastewater Treatment. *Ind. Eng. Chem. Res*. **2016**, 55 (16), 4363–4389.
32. Kobya, M.; Demirbas, E.; Senturk, E.; Ince, M. Adsorption of Heavy Metal Ions from Aqueous Solutions by Activated Carbon Prepared from Apricot Stone. *Bioresour. Technol*. **2005**, 96 (13), 1518–1521.

33. Deegan, A. M.; Shaik, B.; Nolan, K.; Urell, K.; Oelgemöller, M.; Tobin, J.; Morrissey, A. Treatment Options for Wastewater Effluents from Pharmaceutical Companies. *Int. J. Environ. Sci. Technol.* **2011**, 8 (3), 649–666.
34. Ikehata, K.; Jodeiri Naghashkar, N.; Gamal El-Din, M. Degradation of Aqueous Pharmaceuticals by Ozonation and Advanced Oxidation Processes: A Review. *Ozone Sci. Eng.* **2006**, 28 (6), 353–414.
35. Beijer, K.; Björlenius, B.; Shaik, S.; Lindberg, H.R.; Brunström, B.; Brandt, I. Removal of pharmaceuticals and unspecified contaminants in sewage treatment effluents by activated carbon filtration and ozonation: Evaluation using biomarker responses and chemical analysis. *Chemosphere* **2017**.
36. Ternes, T. A.; Meisenheimer, M.; McDowell, D.; Sacher, F.; Brauch, H. J.; Haist-Gulde, B.; Preuss, G.; Wilme, U.; Zulei-Seibert, N. Removal of Pharmaceuticals during Drinking Water Treatment. *Environ. Sci. Technol.* **2002**, 36 (17), 3855–3863.
37. Ahammad, S. Z.; Gomes, J.; Sreekrishnan, T. R. Wastewater Treatment For production of H₂S-Free Biogas. *J. Chem. Technol. Biotechnol.* **2008**, 83, 1163–1169.

38. Dialynas, E.; Mantzavinos, D.; Diamadopoulos, E. Advanced Treatment of the Reverse Osmosis Concentrate Produced during Reclamation of Municipal Wastewater. *Water Res.* **2008**, *42* (18), 4603–4608.
39. Kurniawan, T. A.; Chan, G. Y. S.; Lo, W. H.; Babel, S. Physico-Chemical Treatment Techniques for Wastewater Laden with Heavy Metals. *Chem. Eng. J.* **2006**, *118* (1–2), 83–98.
40. Radjenović, J.; Petrović, M.; Ventura, F.; Barceló, D. Rejection of Pharmaceuticals in Nanofiltration and Reverse Osmosis Membrane Drinking Water Treatment. *Water Res.* **2008**, *42* (14), 3601–3610.
41. Ng, K. K.; Lin, A. Y. C.; Yu, T. H.; Lin, C. F. Tertiary Treatment of Pharmaceuticals and Personal Care Products by Pretreatment and Membrane Processes. *Sustain. Environ. Res.* **2011**, *21* (3), 173–180.
42. Van Hoof, S. C. J. M.; Hashim, A.; Kordes, A. J. The Effect of Ultrafiltration as Pretreatment to Reverse Osmosis in Wastewater Reuse and Seawater Desalination Applications. *Desalination* **1999**, *124* (1–3), 231–242.

43. Ali, I.; Gupta, V. K. Advances in Water Treatment by Adsorption Technology. *Nat. Protoc.* **2007**, *1* (6), 2661–2667.
44. Bhatnagar, A.; Hogland, W.; Marques, M.; Sillanpää, M. An Overview of the Modification Methods of Activated Carbon for Its Water Treatment Applications. *Chem. Eng. J.* **2013**, *219*, 499–511.
45. Babel, S.; Kurniawan, T. A. Low-Cost Adsorbents for Heavy Metals Uptake from Contaminated Water: A Review. *J. Hazard. Mater.* **2003**, *97* (1–3), 219–243.
46. Jiang, C.; Cui, S.; Han, Q.; Li, P.; Zhang, Q.; Song, J.; Li, M. Study on Application of Activated Carbon in Water Treatment. *IOP Conf. Ser. Earth Environ. Sci.* **2019**, *237* (2).
47. Delgado, N.; Capparelli, A.; Navarro, A.; Marino, D. Pharmaceutical Emerging Pollutants Removal from Water Using Powdered Activated Carbon: Study of Kinetics and Adsorption Equilibrium. *J. Environ. Manage.* **2019**, *236* (September 2018), 301–308.
48. Chauhan, A.; Sillu, D.; Agnihotri, S. Removal of Pharmaceutical Contaminants in Wastewater Using Nanomaterials: A Comprehensive Review. *Curr. Drug Metab.* **2018**, *20* (6), 483–505.

49. Qu, X.; Brame, J.; Li, Q.; Alvarez, P. J. J. Nanotechnology for a Safe and Sustainable Water Supply: Enabling Integrated Water Treatment and Reuse. *Acc. Chem. Res.* **2013**, *46* (3), 834–843.
50. Kunduru, K.; Nazarkovsky, M.; Farah, S.; Pawar, R.; Basu, A.; Domb, A. nanotechnology for water purification: applications of anotechnology methods in wastewater treatment. *Nanotechnology for Water Filter*.**2011**.
51. Theron, J.; Walker, J. A.; Cloete, T. E. Nanotechnology and Water Treatment: Applications and Emerging Opportunities. *Crit. Rev. Microbiol.* **2008**, *34* (1), 43–69.
52. Jiménez-Silva, V. A.; Santoyo-Tepole, F.; Ruiz-Ordaz, N.; Galíndez-Mayer, J. Study of the Ibuprofen Impact on Wastewater Treatment Mini-Plants with Bioaugmented Sludge. *Process Saf. Environ. Prot.* **2019**, *123*, 140–149.
53. Davarnejad, R.; Soofi, B.; Farghadani, F.; Behfar, R. Ibuprofen Removal from a Medicinal Effluent: A Review on the Various Techniques for Medicinal Effluents Treatment. *Environ. Technol. Innov.* **2018**, *11*, 308–320.

54. Filippa, M. A.; Gasull, E. I. Ibuprofen Solubility in Pure Organic Solvents and Aqueous Mixtures of Cosolvents: Interactions and Thermodynamic Parameters Relating to the Solvation Process. *Fluid Phase Equilib.* **2013**, *354*, 185–190.
55. Langenhoff, A.; Inderfurth, N.; Veuskens, T.; Schraa, G.; Blokland, M.; Kujawa-Roeleveld, K.; Rijnaarts, H. Microbial Removal of the Pharmaceutical Compounds Ibuprofen and Diclofenac from Wastewater. *Biomed Res. Int.* **2013**, *2013*.
56. <https://www.usetute.com.au/ibuprofen.html> (accessed Mar 27th , 2020)
57. <https://www.news-medical.net/health/Ibuprofen-Chemistry.aspx>. (accessed Mar 26th , 2020)
58. Buser, H. R.; Poiger, T.; Muller, M. D. Occurrence and Environmental Behavior of the Chiral Pharmaceutical Drug Ibuprofen in Surface Waters and in Wastewater. *Environ. Sci. Technol.* **1999**, *33* (15), 2529–2535.
59. Siódmiak, J.; Siódmiak, T.; Tarczykowska, A.; Czirson, K.; Dulęba, J.; Marszałł, M. P. Metabolic Chiral Inversion of 2-Arylpropionic Acid Derivatives (Profens). *Med. Res. J.* **2017**, *2* (1), 1–5.

60. Rainsford, K. D. Ibuprofen: Pharmacology, Efficacy and Safety. *Inflammopharmacology*. **2009**, *17* (6), 275–342.
61. Li, W.; Zhao, D. Extension of the Stöber Method to Construct Mesoporous SiO₂ and TiO₂ Shells for Uniform Multifunctional Core-Shell Structures. *Adv. Mater.* **2013**, *25* (1), 142–149.
62. Iida, H.; Takayanagi, K.; Nakanishi, T.; Osaka, T. Synthesis of Fe₃O₄ Nanoparticles with Various Sizes and Magnetic Properties by Controlled Hydrolysis. *J. Colloid Interface Sci.* **2007**, *314* (1), 274–280.
63. Zandipak, R.; Sobhan Ardakani, S.; Shirzadi, A. Synthesis and Application of Nanocomposite Fe₃O₄@SiO₂ as a Novel Adsorbent for Removal of Cyclophosphamide from Water Samples. *Sep. Sci. Technol.* **2020**, *55* (3), 456–470.
64. Nassar, N. N. Rapid Removal and Recovery of Pb(II) from Wastewater by Magnetic Nanoadsorbents. *J. Hazard. Mater.* **2010**, *184* (1–3), 538–546.
65. Afkhami, A.; Saber-Tehrani, M.; Bagheri, H. Modified Maghemite Nanoparticles as an Efficient Adsorbent for Removing Some Cationic Dyes from Aqueous Solution. *Desalination* **2010**, *263* (1–3), 240–248.

66. Wei, Y.; Han, B.; Hu, X.; Lin, Y.; Wang, X.; Deng, X. Synthesis of Fe₃O₄ Nanoparticles and Their Magnetic Properties. *Procedia Eng.* **2012**, *27* (2011), 632–637.
67. Popescu, R. C.; Andronescu, E.; Vasile, B. S. Recent Advances in Magnetite Nanoparticle Functionalization for Nanomedicine. *Nanomaterials* **2019**, *9* (12), 1–31.
68. Rahmawati, R.; Taufiq, A.; Sunaryono, S.; Fuad, A.; Yulianto, B.; Suyatman, S.; Kurniadi, D. Synthesis of Magnetite (Fe₃O₄) Nanoparticles from Iron Sands by Coprecipitation-Ultrasonic Irradiation Methods. *J. Mater. Environ. Sci.* **2018**, *9* (1), 155–160.
69. Karimzadeh, I.; Aghazadeh, M.; Doroudi, T.; Ganjali, M. R.; Kolivand, P. H. Superparamagnetic Iron Oxide (Fe₃O₄) Nanoparticles Coated with PEG/PEI for Biomedical Applications: A Facile and Scalable Preparation Route Based on the Cathodic Electrochemical Deposition Method. *Adv. Phys. Chem.* **2017**.
70. Khoshnevisan, K.; Barkhi, M.; Zare, D.; Davoodi, D.; Tabatabaei, M. Preparation and Characterization of CTAB-Coated Fe₃O₄ Nanoparticles. *Synth. React. Inorganic, Met. Nano-Metal Chem.* **2012**, *42* (5), 644–648.

71. Liu, H.; Ji, S.; Yang, H.; Zhang, H.; Tang, M. Ultrasonics Sonochemistry
Ultrasonic-Assisted Ultra-Rapid Synthesis of Monodisperse Meso -SiO₂ @
Fe₃O₄ Microspheres with Enhanced Mesoporous Structure. *Ultrasonics
Sonochemistry*. **2013**.
72. Chithra, M. J.; Sathya, M.; Pushpanathan, K. Effect of PH on Crystal Size
and Photoluminescence Property of Zno Nanoparticles Prepared by
Chemical Precipitation Method. *Acta Metall. Sin. (Engl. Lett.)* **2015**, 28
(3), 394–404.
73. Hariharan, C. Photocatalytic Degradation of Organic Contaminants in
Water by ZnO Nanoparticles : Revisited. *Applied Catalysis A: General*.
2006, 304, 55–61.
74. Musat, V.; Fortunato, E.; Petrescu, S.; Botelho, A. M. Pss Solidi.
ZnO/SiO₂ nanocomposite thin films by sol–gel method. *phys. stat. sol.*
2008, 2079 (8), 2075–2079.
75. Kolodziejczak-Radzimska, A.; Jesionowski, T. Zinc Oxide-from Synthesis
to Application: A Review. *Materials (Basel)*. **2014**, 7 (4), 2833–2881.

76. Zhai, J.; Tao, X.; Pu, Y.; Zeng, X. F.; Chen, J. F. Core/Shell Structured ZnO/SiO₂ Nanoparticles: Preparation, Characterization and Photocatalytic Property. *Appl. Surf. Sci.* **2010**, *257* (2), 393–397.
77. Kumar, V. B.; Annamanedi, M.; Prashad, M. D.; Arunasree, K. M.; Mastai, Y.; Gedanken, A.; Paik, P. Synthesis of Mesoporous SiO₂-ZnO Nanocapsules: Encapsulation of Small Biomolecules for Drugs and “SiOZO-Plex” for Gene Delivery. *J. Nanoparticle Res.* **2013**, *15* (9).
78. Hao, Y.; Xu, L.; Lei, J.; Cui, F.; Cui, T.; Qu, C. Self-Catalytic Synthesis of ZnO Nanoparticles@SiO₂ Composites with Controllable Fluorescence. *Chem. Lett.* **2017**, *46* (4), 426–429.
79. Tang, X.; Choo, E. S. G.; Li, L.; Ding, J.; Xue, J. Synthesis of ZnO Nanoparticles with Tunable Emission Colors and Their Cell Labeling Applications. *Chem. Mater.* **2010**, *22* (11), 3383–3388.
80. Ali, A. M.; Ismail, A. A.; Najmy, R.; Al-Hajry, A. Preparation and Characterization of ZnO-SiO₂ Thin Films as Highly Efficient Photocatalyst. *J. Photochem. Photobiol. A Chem.* **2014**, *275*, 37–46.

81. Zhong, J. B.; Li, J. Z.; Xiao, Z. H.; Hu, W.; Zhou, X. B.; Zheng, X. W. Improved Photocatalytic Performance of ZnO Prepared by Sol-Gel Method with the Assistance of CTAB. *Mater. Lett.* **2013**, *91*, 301–303.
82. Stanley, R.; J, A. J.; S, M. V. Enhanced Sunlight Photocatalytic Degradation of Methylene Blue by Rod-like ZnO-SiO₂ Nanocomposite. *Optik (Stuttg)*. **2019**, *180*, 134–143.
83. Faraji, M.; Yamini, Y.; Tahmasebi, E.; Saleh, A.; Nourmohammadian, F. Cetyltrimethylammonium Bromide-Coated Magnetite Nanoparticles as Highly Efficient Adsorbent for Rapid Removal of Reactive Dyes from the Textile Companies' Wastewaters. *J. Iran. Chem. Soc.* **2010**, *7* (2), 130–144.
84. Volentiru, E.; Nyári, M.; Szabó, G.; Hórvölgyi, Z.; Murçan, L. M. Silica Sol - Gel Protective Coatings against Corrosion of Zinc Substrates. *Period. Polytech. Chem. Eng.* **2014**, *58*, 61–66.
85. Ma, C.; Li, C.; He, N.; Wang, F.; Ma, N.; Zhang, L.; Lu, Z.; Ali, Z.; Xi, Z.; Li, X.; et al. Preparation and Characterization of Monodisperse Core-Shell Fe₃O₄-SiO₂ (CTAB)Microspheres and Its Application for Magnetic Separation of Nucleic Acids from E. Coli BL21. *J. Biomed. Nanotechnol.* **2012**, *8* (6), 1000–1005.

86. Asmaly, H. A.; Ihsanullah; Abussaud, B.; Saleh, T. A.; Laoui, T.; Gupta, V. K.; Atieh, M. A. Adsorption of Phenol on Aluminum Oxide Impregnated Fly Ash. *Desalin. Water Treat.* **2016**, *57* (15), 6801–6808.
87. Ira N. Levine. PHYSICAL CHEMISTRY; Brooklyn, New York, 2009; PP1-967.
88. Liu, L.; Lin, Y.; Liu, Y.; Zhu, H.; He, Q. Removal of Methylene Blue from Aqueous Solutions by Sewage Sludge Based Granular Activated Carbon: Adsorption Equilibrium, Kinetics, and Thermodynamics. *J. Chem. Eng. Data* **2013**, *58* (8), 2248–2253.
89. Alebachew, N.; Yadav, O. P.; . L. Removal of Phenol Red Dye From Contaminated Water Using Barley (*Hordeum Vulgare L.*) Husk-Derived Activated Carbon. *Sci. Int.* **2017**, *5* (1), 7–16.
90. Limousin, G.; Gaudet, J. P.; Charlet, L.; Szenknect, S.; Barthès, V.; Krimissa, M. Sorption Isotherms: A Review on Physical Bases, Modeling and Measurement. *Appl. Geochemistry* **2007**, *22* (2), 249–275.
91. Hashemian, S.; Ardakani, M. K.; Salehifar, H. Kinetics and Thermodynamics of Adsorption Methylene Blue onto Tea Waste/CuFe₂O₄ Composite. *Am. J. Anal. Chem.* **2013**, *04* (07), 1–7.

92. Allen, S. J.; Gan, Q.; Matthews, R.; Johnson, P. A. Comparison of Optimised Isotherm Models for Basic Dye Adsorption by Kudzu. *Bioresour. Technol.* **2003**, *88* (2), 143–152.
93. Bulut, Y.; Aydin, H. A Kinetics and Thermodynamics Study of Methylene Blue Adsorption on Wheat Shells. *Desalination* **2006**, *194* (1–3), 259–267.
94. Badhai, P.; Kashyap, S.; Behera, S. K. Adsorption of Phenol Red onto GO-Fe₃O₄ Hybrids in Aqueous Media. *Environ. Nanotechnology, Monit. Manag.* **2020**, *13* (October 2018), 100282.
95. Al-Jabari, M. H.; Sulaiman, S.; Ali, S.; Barakat, R.; Mubarak, A.; Khan, S. A. Adsorption Study of Levofloxacin on Reusable Magnetic Nanoparticles: Kinetics and Antibacterial Activity. *J. Mol. Liq.* **2019**, *291*, 111249.
96. Tang, X.; Choo, E. S. G.; Li, L.; Ding, J.; Xue, J. Synthesis of ZnO Nanoparticles with Tunable Emission Colors and Their Cell Labeling Applications. *Chem. Mater.* **2010**, *22* (11), 3383–3388.
97. Al-Jabari, M. H.; Sulaiman, S.; Khalid, I.; Alawi, I.; Shilo, J. Synthesis, Characterization, Kinetic and thermodynamic investigation of silica nanoparticles and their application in mefenamic acid removal from aqueous solution. *Desalination and Water Treatment.* **2018**, *129*, 160-167.

98. Galedari, N. A.; Rahmani, M.; Tasbihi, M. Preparation, Characterization, and Application of ZnO-SiO₂ (CTAB) Core–Shell Structured Catalyst for Photocatalytic Degradation of Phenol. *Environ. Sci. Pollut. Res.* **2017**, *24* (14), 12655–12663.
99. Wang, P.; Wang, X.; Yu, S.; Zou, Y.; Wang, J.; Chen, Z.; Alharbi, N. S.; Alsaedi, A.; Hayat, T.; Chen, Y.; et al. Silica Coated Fe₃O₄ Magnetic Nanospheres for High Removal of Organic Pollutants from Wastewater. *Chem. Eng. J.* **2016**, *306*, 280–288.
100. Thilagan, J.; Gopalakrishnan, S.; Kannadasan, T. A Study on Adsorption of Copper (II) Ions in Aqueous Solution by Chitosan - Cellulose Beads Cross Linked by Formaldehyde. *International journal of pharmaceutical and chemical sciences.* **2013**, *2* , 1043–1054.
101. M. Dharmendirakumar, G.Vijayakumar, R. T.; Vijayakumar, G.; Tamilarasan, R.; Dharmendirakumar, M. Adsorption, Kinetic, Equilibrium and Thermodynamic Studies on the Removal of Basic Dye Rhodamine-B From. *J. Mater. Environ. Sci.* **2015**, *3*, 157–170.
102. Shahwan, T. Sorption Kinetics : Obtaining a Pseudo-Second Order Rate Equation Based on a Mass Balance Approach. *Environ.chem.Eng.* **2014**, 1001–1006.

103. Zhao, G.; Li, J.; Ren, X.; Chen, C.; Wang, X. Few-Layered Graphene Oxide Nanosheets As Superior Sorbents for Heavy Metal Ion Pollution Management. *Environ. Sci. Technol.* **2011**, 10454–10462.
104. Khadir, A.; Motamedi, M.; Negarestani, M.; Sillanpää, M.; Sasani, M. *JoUrOf.Int.J.Biol.Macromol.* **2020**.
105. Husein, D. Z.; Hassanien, R.; Al-hakkani, M. F. Heliyon Green-Synthesized Copper Nano-Adsorbent for the Removal of Pharmaceutical Pollutants from Real Wastewater Samples. *Heliyon* **2019**, 5 (August), e02339.
106. Gu, Y.; Yperman, J.; Carleer, R.; Haen, J. D.; Maggen, J.; Vanderheyden, S.; Vanreppelen, K.; Machado, R. Chemosphere Adsorption and Photocatalytic Removal of Ibuprofen by Activated Carbon Impregnated with TiO₂ by UV e Vis Monitoring. *Chemosphere* **2019**, 217, 724–731.
107. Banerjee, P.; Das, P.; Zaman, A.; Das, P. Application of Graphene Oxide Nanoplatelets for Adsorption of Ibuprofen from Aqueous Solutions : Evaluation of Process Kinetics And. *Process Saf. Environ. Prot.* **2016**, 101, 45–53.

108. Al-khateeb, L. A.; Hakami, W.; Salam, M. A. Removal of Non-Steroidal Anti-Inflammatory Drugs from Water Using High Surface Area Nanographene: Kinetic and Thermodynamic Studies Removal of Non-Steroidal Anti-inflammatory Drugs from Water Using High Surface Area Nanographene: Kinetic and Thermodynamic Studies. *J. Mol. Liq.* **2017**, *241* (June), 733–741.
109. Khazri, H.; Ghorbel-abid, I.; Trabelsi-ayadi, R. K. M. Removal of Ibuprofen, Naproxen and Carbamazepine in Aqueous Solution onto Natural Clay: Equilibrium, Kinetics, and Thermodynamic Study. *Appl. Water Sci.* **2016**, No. 1 M.
110. Mzukisi, L.; Chimuka, L. Journal of Environmental Chemical Engineering Synthesis, Adsorption and Selectivity Studies of a Polymer Imprinted with Naproxen, Ibuprofen and Diclofenac. *Biochem. Pharmacol.* **2016**, *4(4)*, 4029–4037.

111. Chham, A.; Khouya, E. H.; Oumam, M.; Abourriche, A.; Gmouh, S.; Mansouri, S.; Elhammoudi, N.; Hanafi, N.; Hannache, H. The Use of Insoluble Mater of Moroccan Oil Shale for Removal of Dyes from Aqueous Solution The Use of Insoluble Mater of Moroccan Oil Shale for Removal of Dyes from Aqueous Solution. **2018**, No. January.
112. Bhadra, B. N.; Ahmed, I.; Kim, S.; Jhung, S. H. Adsorptive Removal of Ibuprofen and Diclofenac from Water Using Metal-Organic Framework-Derived Porous Carbon. *Chem. Eng. J.* **2016**.
113. Song, J. Y.; Bhadra, B. N.; Jhung, S. H. SC. *Microporous Mesoporous Mater.* **2017**.
114. Martínez, Y. V.; Caravaca, M.; Meca, A. S.; González, R. S. Magnetic Core - Modified Silver Nanoparticles for Ibuprofen Removal: An Emerging Pollutant in Waters. *Sci. Rep.* **2020**, 1–10.
115. Cottet, L.; Almeida, C. A. P.; Naidek, N.; Viante, M. F.; Lopes, M. C.; Debacher, N. A. Applied Clay Science Adsorption Characteristics of Montmorillonite Clay Modified with Iron Oxide with Respect to Methylene Blue in Aqueous Media. *Appl. Clay Sci.* **2014**, 95, 25–31.(104)

116. Boruah, P. K.; Sharma, B.; Hussain, N.; Das, M. R. Chemosphere Magnetically Recoverable Fe₃O₄ / Graphene Nanocomposite towards Efficient Removal of Triazine Pesticides from Aqueous Solution : Investigation of the Adsorption Phenomenon and Specific Ion Effect. *Chemosphere*. **2016**, 1–10.(103)
117. Mahmoud, M. A. ScienceDirect Kinetics and Thermodynamics of Aluminum Oxide Nanopowder as Adsorbent for Fe (III) from Aqueous Solution. *Beni-Suef Univ. J. Basic Appl. Sci.* **2015**, 4 (2), 142–149.
118. Anirudhan, T. S.; Suchithra, P. S. Journal of Industrial and Engineering Chemistry Humic Acid-Immobilized Polymer / Bentonite Composite as an Adsorbent for the Removal of Copper (II) Ions from Aqueous Solutions and Electroplating Industry Wastewater. **2010**, 16, 130–139.
119. Húmpola, P. D.; Odetti, H. S.; Fertitta, A. E.; Vicente, J. L. thermodynamic analysis of adsorption models of phenol in liquid phase on different activated carbons. **2013**, 1, 1541–1544. (118)
120. Yu, Y.; Zhuang, Y.; Wang, Z. Adsorption of Water-Soluble Dye onto Functionalized Resin. *Journal of Colloid and Interface Science*. **2001**, 293, 288–293. (119)

Appendix

Ibuprofen calibration curve

